

This is to certify that the
dissertation entitled
Technology & Electronic Properties
of CVD Diamond Film Microsensors
for Thermal Signals

presented by

Ashraf Masood

has been accepted towards fulfillment
of the requirements for

Ph.D. degree in EE


Major professor

Date 11/20/52

LIBRARY
Michigan State
University

PLACE IN RETURN BOX to remove this checkout from your record.
 TO AVOID FINES return on or before date due.

DATE DUE	DATE DUE	DATE DUE
MAR 29 2000	10 08 04	_____
JUN 05 2000	APR 08 2005	_____
DEC 07 2001	_____	_____
NOV 09 2002	_____	_____
JUN 04 2003	_____	_____
_____	_____	_____
_____	_____	_____

MSU is An Affirmative Action/Equal Opportunity Institution

c:\circ\date\due.pn3-p.1

**TECHNOLOGY AND ELECTRONIC PROPERTIES OF
DIAMOND FILM MICROSENSORS FOR
THERMAL SIGNALS**

By

Ashraf Masood

A DISSERTATION

Submitted to
Michigan State University
in partial fulfilment of the requirement
for the degree of

DOCTOR OF PHILOSOPHY

Department of Electrical Engineering

1992

ABSTRACT

TECHNOLOGY AND ELECTRONIC PROPERTIES OF DIAMOND FILM MICROSENSORS FOR THERMAL SIGNALS

By

Ashraf Masood

Microsensors based on boron doped polycrystalline CVD diamond films for thermal signals in the temperature range of 77 K to 1273 K were developed. New techniques for boron doping, nucleation, patterning and metallization of diamond films were developed. A test chip was designed and fabricated for electrical characterization of diamond films and acquisition of thermal sensing parameters.

The diamond films were synthesized by hot filament chemical vapor deposition (HFCVD). In situ boron doping was implemented by using an accurately measured quantity (0.1-2.6 mg) of high purity amorphous boron powder through a specially designed holder. The quality of the diamond films as determined from Raman spectroscopy and SEM was not affected by boron doping in the useful range of boron concentration (up to 10^{19} cm^{-3}). SIMS depth profile showed uniform boron concentration throughout the thickness of the films. The measured resistivity and Hall concentration of diamond films doped by using 0.1-2.6 mg of boron powder were in the range of $0.3\text{-}64 \text{ }\Omega\text{-cm}$ and $2 \times 10^{15}\text{-}9 \times 10^{18} \text{ cm}^{-3}$, respectively.

A test microchip containing several devices was designed and fabricated. Three IC compatible techniques for diamond film patterning based on selective deposition and selective etching were developed. The diamond photoresist (DPR) patterning technique based on mixing diamond powder in photoresist is especially advantageous in terms of selectivity, resolution and ease and flexibility of implementation. In case of

Ashraf Masood

metallization, the stringent requirement of providing ohmic contacts on diamond films, and of stability and good adhesion on diamond as well as SiO₂ surfaces simultaneously accomplished by a two layer structure of Pt(8000°A)/Ti(100°A).

Resistivity, Current-voltage measurement, carrier type, Hall concentration and Hall mobility were directly measured. The resistivity and Hall mobility were in the range of 0.3-64 Ω-cm and 2-48 cm²V⁻¹s⁻¹ respectively. The dopant activation energies, as computed from the resistivity versus temperature curves (up to 300°C), were in the range of 0.38-0.11 eV corresponding to Hall concentration in the range of 2×10¹⁵-9×10¹⁸cm⁻³ and boron concentration in the range of 10¹⁷-10²³cm⁻³. The annealing behavior of doped diamond films was investigated for the first time.

The static temperature response of diamond film thermal sensors was measured over the temperature range of 77-1273 K for the first time. The change in resistivity with temperature was monotonic with a sensitivity given by temperature coefficient at ~ 0.07 K⁻¹ at all doping levels over the entire temperature range. This is the largest temperature range ever covered by a single semiconductor temperature measuring device either in absolute or relative terms. The dynamic temperature response time constant for the diamond film sensors on oxidized silicon was determined experimentally to be about 25 μs. This is smaller than any known solid state temperature sensor. As a heat flux sensor, diamond film thermistor is shown qualitatively to outperform conventional Pt sensors for shock tunnel applications.

**to
my parents
and
my family**

ACKNOWLEDGEMENT

All praises be to Allah (SWT), the creator and sustainer of the universe, for providing me with the ability and opportunity to complete this research.

I am grateful for the financial support from Government of Pakistan during my studies. Without this support, this research effort would not have been possible.

I would like to express my sincere gratitude to my advisor, Dr. Mohammad Aslam for his inspiration, guidance and professional support throughout my graduate studies. His help, able guidance and understanding were key to my academic and professional growth. I owe thanks to Dr. Donnie Reinhard, Dr. Jes Assmussen, Dr. T. J. Pinnaviah, Dr. Ronald Fredricks and especially Dr. M. A. Tamor for their valuable guidance throughout this research. I am also grateful to the staff of Ford Scientific Research Laboratory especially Mr. T. J. Potter for the help and cooperation they extended during my experiments.

I wish to express my sincere thanks to my family and my wife's family for their continued support, prayers, patience and encouragement. My wife Perveen and daughters Naveeda and Sadaf deserve special thanks for their understanding and support throughout this research effort.

TABLE OF CONTENTS

LIST OF TABLES	ix
LIST OF FIGURES	x
Chapter 1. INTRODUCTION	
1.0 Research Motivation	1
1.1 Research Approach	3
1.2 Dissertation Organization	5
Chapter 2. BACKGROUND	
2.0 Introduction	7
2.1 Development of Sensors	8
2.2 Sensors for Thermal Signals	8
2.2.1 Thermocouples	10
2.2.2 Resistance Temperature Detectors	14
2.2.3 Other Devices	15
2.2.4 Thermistors	16
2.2.5 CVD Diamond Films as Temperature Sensors	19
2.3 Theoretical Analysis of Thermistors	21
2.4 Properties of Diamond	27
2.5 Chemical Vapor Deposition of Diamond	28
2.6 Hot-Filament CVD	31
2.6.1 The Deposition System	31
2.6.2 Effect of Gas Composition	32
2.6.3 Effect of C-H-O Ratio	32
2.6.4 Effect of Oxygen	34
2.6.5 Effect of Substrate Temperature	34
2.7 Analysis Tools	35
2.7.1 Raman Spectroscopy	35

2.7.2 Scanning Electron Microscope	36
2.7.3 Secondary Ion Mass Spectroscopy	37
2.7.4 Surface Profiler	38
2.8 Electronic properties	39
2.9 Film and Bulk Properties	42
2.10 Device Fabrication technologies	45
 Chapter 3. SEMICONDUCTING DIAMOND FILM SYNTHESIS AND CHARACTERIZATION	
3.0 Introduction	48
3.1 The Deposition System	51
3.2 The Nucleation Methods	52
3.2.1 Ultrasonic Treatment	52
3.2.2 Diamond-Photoresist Seeding	52
3.2.3 Comparative Analysis	56
3.3 Diamond Deposition Processing Parameters	57
3.3.1 Reactant Gas Composition	59
3.3.2 System Pressure	59
3.3.3 Substrate Temperature	59
3.3.4 System Operation	63
3.4 Boron Doping	64
3.5 Silicon Dioxide Etching	75
3.6 Summary	77
 Chapter 4. TEST MICRO-CHIP FABRICATION	
4.0 Introduction	78
4.1 Test Microchip Design	78
4.2 Diamond Film Patterning	82
4.2.1 Selective Etching	84
4.2.2 Selective Deposition	88
4.2.2.1 Ultrasonic Treatment Patterning	90
4.2.2.2 Diamond-Photoresist Patterning	93
4.3 Metallization	106
4.3.1 Problem Analysis	106
4.3.2 Experimental Results	108
4.4 Fabrication of Heat Flux Sensors	119
4.5 Summary	120
 Chapter 5. ELECTRICAL CHARACTERIZATION	
5.0 Introduction	123
5.1 Preliminary Annealing study	124
5.2 Electrical Measurements	130

5.2.1 Overview	130
5.2.2 Current-Voltage Measurements	130
5.2.3 Conduction Type Measurements	134
5.2.3 Resistivity Measurements	136
5.2.4 Hall Measurements	141
5.3 Computed Parameters	144
5.5 Summary	151
Chapter 6. CVD DIAMOND FILM SENSORS FOR THERMAL SIG-	
NALS	
6.0 Introduction	152
6.1 Static Response of Temperature Sensors	152
6.2 High Temperature Effects	160
6.3 Dynamic Response of Temperature Sensors	162
6.4 On-chip Signal Processing	173
6.5 Summary	176
Chapter 7. CONCLUSION	
7.1 Summary of Present work	178
7.2 Future Research	181
Appendix A. DIAMOND FILM DEPOSITIONS	183
BIBLIOGRAPHY	191

LIST OF TABLES

2.1 Comparison of principle parameters of main temperature sensing devices [12]	11
2.2 Comparison of semiconductor properties of diamond with SiC, Si, and GaAs [86].	43
4.1 Sample preparation for optimization of diamond film thickness and surface smoothness study. (Photoresist quantity = 42 ml)	96
5.1 The organization of electrical measurements for the characterization of p-type diamond films.	131
6.1 Thermal properties of Si, SiO ₂ , Pt and Cu [160,47,169].	170

LIST OF FIGURES

2.1 Temperature response curves of typical (a) thermocouples, (b) RTDs, (c) NTC and PTC thermistors. (the Pt resistor curve has been given for sensitivity comparison only) [3]	12
2.2 Static temperature response curves of thermistors made of semiconducting (a) natural and synthetic crystalline diamonds [38] (b) CVD diamond films with various doping levels [39].	20
2.3 (a) Electrical resistivity of a semiconductor similar to Ge as a function of temperature on logarithmic scales [44] (b) \log_e resistance of two commercial thermistors plotted against reciprocal of temperature in region III of curve given in (a).	23
2.4 (a) Influence of C-H-O ratio on the morphology of CVD deposited diamond films [71] (b) Atomic C-H-O diamond deposition phase diagram with the diamond growth domain [72].	33
2.5 Comparison of thermal conductivity of (a) natural diamond with several other solids as a function of temperature [116] (b) CVD diamond films using different methane concentrations with natural diamonds, Ag and Cu [88].	40
3.1 A simplified schematic diagram of diamond HFCVD system.	50
3.2 Raman spectra of diamond films on oxidized silicon substrates seeded by UT and DPR nucleation methods.	53
3.3 SEM micrographs of diamond films on oxidized silicon substrates seeded by (a) UT and (b) DPR nucleation methods.	55
3.4 Raman spectra of diamond films deposited by using methane, acetylene, acetone and methanol as carbon source.	58
3.5 Raman spectra of the diamond films deposited with and without CO.	60
3.6 Effect of system pressure on the (a) quality (sp^3/sp^2) ratio and (b)	

growth rate of the diamond films.	61
3.7 Effect of substrate temperature on the (a) quality (sp^3/sp^2) ratio and (b) growth rate of the diamond films.	62
3.8 SIMS depth profile of a diamond film deposited on oxidized silicon	66
3.9 Measured Hall concentration at room temperature against the quantity of boron powder used for the doping of diamond films during deposition.	67
3.10 Raman spectra of the diamond films deposited on oxidized silicon substrate using various amounts of boron powder quantity.	68
3.11 Raman spectra of the diamond films deposited on undoped diamond films deposited on oxidized silicon substrate using various amounts of boron powder quantity.	69
3.12 Comparison of the effect of boron powder quantity on the purity of diamond films deposited on (a) oxidized silicon and (b) undoped diamond films.	70
3.13 Raman spectra of the diamond films deposited on various surface orientation of single crystal diamond and oxidized silicon substrates.	72
3.14 A short range high resolution Raman spectrum of a doped diamond film deposited on undoped diamond films.	73
3.15 SEM micrographs of (a) undoped and (b) doped diamond films.	74
3.16 SEM micrographs of presumably heavily doped films on oxidized silicon.	75
3.17 The effect of pre-deposition SiO_2 thickness on the etch rate of SiO_2 during diamond deposition.	76
4.1 Composite mask layout of test micro-chip.	80
4.2 Test chip masks for (a) diamond, (b) Interconnect metallization, (c) passivation/ gate insulator and (d) gate metallization.	81
4.3 The hierarchal layout of diamond film patterning techniques.	83
4.4 Undoped diamond films on silicon etched in RTP at $700^\circ C$ for (a) 40 seconds, (b) 80 seconds, (c) 120 seconds and (e) 220 seconds. The cross-section view of films shown in in (c) and (e) are shown in (d) and (f) respectively.	85
4.5 The plot of etched thickness against etching time of diamond film thick-	

ness in RTP at 700°C under an oxygen flow of 40 sccm. The increasing size of error bar is indicative of highly non-uniform etching.	86
4.6 The schematic diagram of diamond film patterning technique through selective etching in RTP.	87
4.7 Diamond films patterned by selective etching at 700°C in RTP. The patterns in (b) is close up view of (a).	89
4.8 Schematic diagrams of selective diamond nucleation technique by UT using (a) Pre-treatment masking and (b) Post-treatment masking.	91
4.9 SEM micrographs of diamond films patterned by UT method using pre-treatment masking. The masks used were (a) Al film (1.1 μm) and (b) thermal SiO_2 (0.88 μm).	92
4.10 SEM micrographs of diamond films patterned by UT method using post-treatment masking. The masks used were (a) Ni film (4000 $^\circ\text{A}$), (b) CVD SiO_2 (4400 $^\circ\text{A}$).	94
4.11 SEM micrographs of diamond films deposited on substrates coated with DPR suspension of (a) 41.7 mg, (b) 122.6 mg and (c) 142.6 mg of diamond powder in 42 ml of photo-resist.	98
4.12 The cross-sectional view of a diamond film grown after thickness uniformity and surface smoothness optimization study.	99
4.13 The effect of diamond film thickness on the surface roughness.	99
4.14 Schematic diagrams of DPR methods of diamond film patterning.	100
4.15. SEM micrographs of the diamond films patterned by DPR method.	101
4.16 SEM micrograph of the diamond film line parallel to the main pattern shown in Fig. 4.15(b). The image was taken in the early part of growth.	102
4.17 SEM micrographs of the diamond film scratched with knife edge. The picture shown in (b) is the higher resolution image of upper portion of pattern shown in (a).	104
4.18 Micrographs of test micro-chip after diamond deposition using DPR patterning at various resolution.	105
4.19 Test micro-chip metallization. The patterns on was generated by using shadow mask. The pictures in (b) and (c) are higher magnification images of (b). The diamond pattern in (c) on the left is 160 μm	109

4.20 (a) Diamond film pattern on test chip with as deposited metal Pt (3000°A)/ Ti (500°A). (b) The top view of metallized diamond film surface in (a).	110
4.21 SEM micrographs of the metallization (Pt (3000°A)/ Ti (500°A) on test chip heat treated at 1000°C.	112
4.22. Resistance of a metallized diamond resistor with time during annealing at 600°C.	114
4.23 SEM micrographs of metallization Pt (1.2 μm/ Ti (100°A) on test micro-chip after annealing at 1000°C. (a) The top view with diamond pattern in left half, (b) stray diamond crystals and (c) a 60° view around a metal contact on diamond.	116
4.24 SEM micrographs of metallization Pt (8000°A/ Ti (100°A) on test micro-chip after annealing at 1000°C. (a) a 60° view around a metal contact on diamond and (b) stray diamond crystal.	117
4.25 Gold wire bonding on the test chip bonding pad composed of Pt (8000°A/ Ti (100°A).	118
4.26 Mask set for diamond film heat flux sensors. (a) diamond and (b) metallization mask.	121
4.27 SEM micrographs of diamond film heat flux sensors on silicon rod. (b) is a high magnification images of (a).	122
5.1 Schematic diagram of the experimental set up for resistivity measurements at high temperature.	125
5.2 The temperature response of resistivity of diamond films sensor annealed at different temperatures. The annealing temperature is also indicated.	125
5.3 The reproducibility of temperature response of resistivity of unannealed diamond temperature sensor over a temperature range of 300-573 K.	127
5.4 The reproducibility of temperature response of resistivity after annealing in temperature range (a) 300-1273 K and (b) 77-300 K.	128
5.5 The time response of resistivity of two diamond film resistors during annealing at 1000°C. The measured Hall concentration for each sample is also indicated.	129
5.6 Schematic diagram of the high temperature characterization system.	132
5.7 I-V characteristics of a test chip at selected temperatures in the temperature range 77-300 K (a) before and (b) after annealing at 1000°C.	133

5.8 I-V characteristics of (a) discrete and (b) test chip samples over temperature range 300-573 K and 300-1273 K respectively.	135
5.9 The contact designation at Van der Pauw pattern on the test chip.	137
5.10 The room temperature resistivity vs quantity of boron powder used for the doping of diamond films during deposition.	139
5.11 The temperature response of resistivity of discrete samples over temperature range of 300-573 K. The room temperature Hall concentration of each sample is also indicated.	139
5.12 The temperature response of resistivity of test chips before and after annealing over temperature range of (a) 300-1273 K ($p=2\times 10^{15} \text{ cm}^{-3}$) and (b) 77-300 K ($p=1.7\times 10^{16}$).	140
5.13 The room temperature (a) resistivity and (b) Hall mobility vs measured Hall concentration of the two types of samples.	143
5.14 The temperature response of (a) Hall concentration and (b) Hall mobility in the temperature range of 77-300 K.	145
5.15 The plots of computed boron (a) activation energy and (b) concentration against measured Hall concentration for two types of samples.	148
5.16 The plots of computed boron activation energy of test chips before (assuming no compensation) and after annealing (assuming compensation) against Hall concentration measured at room temperature.	150
6.1 The temperature response of the (a) resistivity and (b) sensitivity in terms of $\Delta\rho/\Delta T$, of diamond film thermal sensors. The Hall concentration of each sensor is also indicated.	153
6.2 The plots of temperature coefficient α versus temperature for diamond film thermal sensors. The Hall concentration of each sensor is also indicated.	155
6.3 The sensitivity of diamond film thermal sensors in terms of W as defined by Eq. 6.2 against measured Hall concentration.	157
6.4 The plots of fitted curves along with measured data for (a) temperature and (b) reciprocal of temperature against \ln resistivity. ($p=2\times 10^{15}$)	159
6.5 The temperature response of the resistance of (a) 1.1 μm -thick thermal SiO_2 layer and (b) metal conducting lines (see text for experimental set up).	161
6.6. Raman spectra of diamond film thermal sensors before and after heat treatment at 1000°C for a total of 14 minutes in four cycles at a pressure of	

10 ⁻⁷ torr at two scan ranges.	163
6.7 SEM micrographs of diamond film thermal sensor after heat treatment at 1000°C for a total of 14 minutes in four cycles at a pressure of 10 ⁻⁷ torr. (a) normal view and (b) view at 60° angle.	164
6.8 SEM micrographs of diamond film thermal sensors after two minutes of heat treatment at (a) 1249°C at 10 ⁻⁷ torr and (b) 1000°C at 100 mtorr.	165
6.9 Storage scope trace of voltage once a current step of 100 μA was applied to the diamond film thermal sensor with room temperature resistance of 165.5 kΩ.	167
6.10 The steady state resistance of diamond film thermal sensor against current flowing through it. The rise time of the voltage across the respective sensor with the applied current step is also shown.	168
6.11 The one-dimensional heat conduction model for thin film heat flux sensors on thermal insulator [124].	172
6.12 (a) The implementation of NAND logic with two p-channel depletion mode diamond MESFETs and a diamond resistor. (b) The block diagram of the proposed analog multiplexer circuit using all diamond based NAND gates shown in (a).	175

INTRODUCTION

1.0 RESEARCH MOTIVATION

With increasing automation of machinery and process control, the demands on the accuracy, stability, range and dynamic response of the temperature sensors is also becoming more and more stringent. Many applications require the operation of sensors under physically and chemically hazardous environment and present day sensors are unable to meet these demand successfully.

Among various kinds of temperature sensors used today, thermistors, thermocouples (TC), resistive temperature detectors (RTD), and integrated circuit (IC) sensors are most popular. They all have one or more limitations among limited temperature range, non-linearity, self heating, poor sensitivity, large response time, poor accuracy and incompatibility with harsh environment which make them unsuitable for modern application. While most kinds of sensors have intrinsic drawbacks, thermistor's shortcomings primarily come from the properties of material it is made from. Hence, a material with desirable properties which can withstand harsh physical and chemical environment can alleviate its vital drawbacks such as limited temperature range and instability under harsh environment, and fulfill today's tough demands. Diamond with remarkable

combination of physical, chemical and thermal properties appears to be an ideal choice.

The discovery of semiconduction in natural diamond revealed its excellent electronic properties in addition to its already known unrivaled physical properties. This created a new opportunity for utilizing semiconducting diamond in thermistor applications. The successful manufacture of synthetic diamond further enhanced the possibility of semiconducting diamond devices with extraordinary characteristics. In 1969, a patent was granted to General Electric for producing synthetic diamond thermistors. However, due to the cost and several technological problems including reproducibility in semiconducting properties and sensing parameters with synthetic diamond thermistor stayed in the laboratory for over three decades.

Recent developments in the process of growing thin diamond films by various chemical vapor deposition (CVD) techniques has led to a renewed interest in developing "low cost" diamond devices. However, the potential applications of thin diamond films greatly depends on their crystalline structure which in turn depends on the growth conditions. The CVD diamond films on non-diamond substrates are typically polycrystalline that cannot be used for most high performance active electronic devices. However, it seems to be an excellent material for passive electronic components and microsensors with performance that is significantly better than their counterparts made from other semiconductors.

In case of a temperature sensor, diamond's wide energy band gap (5.45eV) can extend its measuring range from cryogenic (77 K) to beyond gold point (1337 K), never possible before by any single temperature measuring device. Its high thermal conductivity (20 W/cm/K at 300K) and possibility to fabricate extremely small size sensors (feature size \approx few microns) can lead to unprecedented high speed (response time constant \approx few μ sec) operation. Its chemical inertness (except to oxidizing agents at temperatures $>650^{\circ}\text{C}$) and radiation immunity can permit highly stable operation

under extremely hostile environment. The relatively high resistivity as compared to other semiconductors at useful doping levels (10^{15} – 10^{18} cm⁻³) can lead to a simple two wire resistance measurement which is impracticable for RTDs.

Since the physical and electronic properties of thin polycrystalline diamond films may considerably differ from single crystal bulk diamond, it is very interesting to look into the feasibility of their utilization for sensing thermal signals. It is advantageous since film properties can be tailored by adjusting deposition parameters and doping concentration. The challenge, however, is to (i) synthesize high quality diamond films on non-diamond substrates, (ii) develop a reproducible, IC technology compatible and economical fabrication technology including doping, patterning, metallization and passivation processes, fabrication processes, (iii) gain an understanding the electronic behavior of the thin diamond films and their correlation to the nucleation and deposition conditions and (iv) characterize the diamond sensors for the intended application.

The object of this research was primarily to meet these challenges and develop diamond sensors for thermal signals with properties superior to all kinds of existing temperature sensors.

1.1 RESEARCH APPROACH

The work performed for the achievement of the objective is highly experimental in nature. It consists of four main subjects. The deposition of high quality semiconducting diamond films, development of technology for fabrication of a test microchip, characterization of semiconducting diamond films and characterization of microsensors for thermal signals.

Semiconducting diamond films were synthesized using hot-filament chemical vapor deposition (HFCVD) in a reactor designed and built at Ford Scientific Research Laboratory Dearborn, MI. Since the diamond deposition at low pressure is thermodynamically metastable, it is crucial to control associated parameters such as gas

composition, gas flow rates, chamber pressure, filament and substrate temperatures appropriately to ascertain the proper diamond phase. The experimental parameter such as reactant gases and their flow rates, chamber pressure, substrate and filament temperatures were optimized to synthesize high quality diamond films in terms of their purity, morphology, homogeneity, uniformity, and growth rate. The deposited diamond films were characterized by scanning electron microscope (SEM), Raman spectroscopy and surface profiler. A new nucleation technique was developed to achieve optimum grain size, film thickness uniformity and surface smoothness. Boron is used as p-type dopant in diamond. A method, using solid boron powder source, compatible with diamond CVD process, was developed to incorporate boron into diamond films in a controlled quantity without affecting the quality of diamond itself. The suitability of this doping method was evaluated experimentally through electrical measurements and secondary ion-mass spectroscopy (SIMS).

A test chip containing several resistors of varying sizes and orientation, a rectangular pattern for Hall measurements, and a couple of MOSFET structures was designed with four mask process. Fabrication process concentrated on film patterning and metallization. Three methods of diamond film patterning were developed. In case of metallization, the stringent requirement of providing ohmic contacts on diamond films, stability and good adhesion on diamond as well as SiO₂ surfaces simultaneously was extremely demanding. This task was accomplished by two layer structure of Pt/Ti based on experimental results of this research and previous work on high temperature metallization of silicon ICs using silicides.

The electrical characterization of diamond films as a semiconductor was carried out over a temperature range of 77-1273 K. Resistivity, Current-voltage measurement, carrier type, concentration and mobility were directly measured. For these measurements, a special vacuum chamber equipped with a high performance heater and a computer controlled data acquisition system was designed and built. The information

obtained through the measurements were analyzed to estimate the impurity concentration, dopant and hopping conduction activation energies.

The diamond film sensors for thermal signals were characterized for their static and dynamic temperature response. The static temperature response over a temperature range of 77-1273 K was done in two parts. The measurements below room temperature were made in a commercial system equipped with miniature cryogenic refrigerator. Measurements above room temperature were made in the above mentioned high temperature characterization system. The dynamic response was acquired by applying a temperature step function using a programmable current source and recording the sensor response on a storage scope in a single trace mode. The experimental results were compared with the existing sensors for temperature and heat flux measurements.

1.2 DISSERTATION ORGANIZATION

This dissertation is divided into five subjects. These are (1) literature review, (2) synthesis of semiconducting diamond films and their physical characterization, (3) development of diamond electronic device technology and fabrication of test microchip, (4) electrical characterization of diamond films and (5) properties of diamond film sensors for thermal signals.

These subjects have been covered in seven chapters. After an introduction in first chapter, all the review material is placed in chapter 2. Chapter 3 describes the synthesis of semiconductor diamond film with an emphasis on optimization of experimental parameters, boron doping and nucleation methods. Chapter 4 contains the development of device technology including, patterning, metallization, and passivation. The design and fabrication of test microchip and heat flux sensors is also included in this chapter. The measurement of fundamental semiconducting properties such as resistivity, carrier concentration are described in chapter 5. An analysis of these properties leading to evaluation of activation energies and impurity concentration is also included.

Chapter 6 explains the properties of diamond film temperature and heat flux sensors. In addition to their static and dynamic temperature response, an on chip analog multiplexer circuit is suggested. Chapter 7 concludes this research with a summary of important results and suggestions for future research.

BACKGROUND

2.0 INTRODUCTION

In this chapter an overview of two distinct subjects is presented: sensors for thermal signals, and synthesis and electronic properties of CVD diamond films. After a brief review of sensor development, at the beginning, a comparative description of major temperature sensing devices namely thermocouples, RTDs, thermistors and ICs is given. Available literature on semiconducting CVD diamond films as temperature sensors is also reviewed. Following this, a generic semiconductor is theoretically analyzed from the perspective of being able to understand and predict its performance as a temperature sensor in terms of range, sensitivity and linearity. In the second major part of this chapter, after brief mention of physical properties of diamond, various approaches of its synthesis with an emphasis on hot-filament CVD with respect to deposition parameters are discussed. This follows the discussion on characterization, electronic properties and fabrication technologies of diamond devices in comparison with other conventional semiconductors with a view point of looking into the feasibility of their application in active electronic devices and temperature sensors.

2.1 DEVELOPMENT OF SENSORS

Sensors are devices used to acquire physical informations and transform them into usable form. In general most sensors are mechanical or electronic devices which produce analog electrical signals as their output. Most electronic sensors are based on elements of which one of the parameters such as resistivity, dielectric constant, Hall voltage, junction voltage or signal frequency displays a small change in response to one or more measurands [1]. The sensor output is processed by a signal conditioning circuit which performs one or more of the functions including amplification, linearization, calibration, compensation, comparison and switching. This signal is then converted into digital output for display, control, recording or digital signal processing purposes. The sensors and signal conditioning interface circuits are usually separate units. While more and more sensors are being fabricated from conventional semiconductors, it is possible to integrate them with interface circuit on a monolithic or hybrid chip [2]. Such device is usually referred to as a smart sensor. The development of planar semiconductor technology has made this integration of sensor elements and interface signal conditioning economically feasible. This approach will eventually lead to a microprocessor-compatible output which can be applied to a bus organized data acquisition system [3]. A fully integrated sensor can offer significant advantage over others by employing additional features such as self testing, auto-calibration, and digital compensation to improve system reliability and performance while reducing overall cost [2].

2.2 SENSORS FOR THERMAL SIGNALS

All sensors employed in any application of detection and measuring thermal signals are primarily the temperature sensors. Most applications other than the basic temperature measurements, in effect, are special configurations of a single or multiple sensor elements along with transformation of their output signal to represent other

physical measurands. For example, the thermal vacuum sensor such as the Pirani gauge is basically an array of thermistor elements [4]. The device operation is based on the principle of measuring heat transfer between two adjacent sensor elements by the gas molecules. Therefore, while looking for a new sensor for any application involving measurement of thermal signals, it is sufficient to explore its fundamental characteristics as a basic temperature sensor. This knowledge can then be used for any other specific thermal measurement application through well known transformation functions and sensor structures. Hence, following review will contain the discussion about the basic kinds of temperature sensors and their typical temperature responses only.

Temperature sensors are frequently used to measure measurands other than temperature itself. For example, an air flow velocity sensor based on measurement of difference of temperature between individual thermistor elements of an array is reported [5]. Also transducers for radiation, pressure, position, level, vacuum, radiation and chemical reaction can be constructed on the basis of absolute temperature or temperature difference [4,6,7]. They are also frequently used in the measurement of velocity, thermodilution flow, power, level control and thermal conductivity [3]. Once these sensors are fabricated from semiconducting material, they can be integrated into the electronic circuit on a monolithic or hybrid chip. This arrangement is frequently applied for the temperature compensation of electronic circuits to offset the errors caused by the undesired temperature changes [3,8,9].

Lately, there is a trend towards integrated multi-functional sensors [10]. It includes temperature sensors for several physical variables along with optional interface circuitry. For instance, an integrated multi-function sensor for temperature, vacuum and flow velocity based on heat transfer at a constant chip temperature has been fabricated [5]. Another sensor capable of measuring the wall shear stress (the friction force that fluid flow exerts on the surface of an object) has been reported [11]. The sensor is comprised of an integrated thermopile which measures the relation

between flow rate and the heat loss as well as the temperature difference on the chip in the direction of flow to acquire the wall shear stress.

Temperature sensors can be divided into two main categories: self generating and modulating sensors [4]. The self generating sensors are thermocouples which do not require any source of power for their operation. Temperature sensors based on thermal modulation of electric energy supplied by an auxiliary source are metallic and semiconductor thermoresistors, diodes and transistors. More recently, integrated circuit (IC) temperature sensors have also been developed. Since it is difficult to compare the properties of all these devices descriptively, their relative merits with respect to some common parameters have been summarized in Table 2.1 [12].

2.2.1 Thermocouples

When the junction of two wires of dissimilar metals is heated, a voltage commonly known as Seebeck voltage develops across the open terminals of the wires. This phenomenon is known as the thermo-electric effect. The fact that Seebeck voltage is a direct function of junction temperature, a voltage reading by a voltmeter represents the temperature of the junction. This is precisely the principle of thermocouple operation. Although all dissimilar metals exhibit this effect to a varying degree of sensitivity, only certain metals/metal alloy combinations are suitable for use as thermocouples. Fig. 2.1(a) shows the temperature response curves of commonly used standard thermocouple types [3].

The output voltage and voltage variations with temperature of all thermocouples are in terms of mV and $\mu\text{V}/^\circ\text{C}$ respectively. Such small voltages definitely need very sensitive and precision instruments. The output voltage of thermocouples is somewhat non-linear and, therefore, several curve fitted equations and look up tables have been developed and in some cases implemented in hardware of the readout instruments. In addition, the cold junction (where thermocouple wire is connected to dissimilar metal

Table 2.1 Comparison of principle parameters of main temperature sensing devices [12].

Parameter	Pt RTDs		Thermis- tors	Thermo- couples	ICs
	100 Ω	2000 Ω			
Temperature range	wide -240C to +650C	short -75C to +200C	short- medium -75C to +260C	very wide -240C to +2300C	very short -50 C to +135C
Interchangeability	Excellent	Fair	Poor- Fair	Good	Fair
Long term stability	Good	Fair	Poor	Poor to Fair	Good to Fair
Accuracy	High	Low	Medium	Medium	Medium
Repeatability	Excellent	Fair	Fair to Good	Poor to Fair	Good
Sensitivity	Low	High	Very High	Low	High
Response time	Medium	Medium	Fast	Medium	Medium to Fast
Linearity	Good	Fair	Poor	Excellent	Good
Self heating	Very Low to Low	Medium	High	High	Low
Point end sensitivity	Fair	Poor	Good	Excellent	Good
Lead Effect	Medium	Low	Very Low	High	Low
Physical size/ packaging	Medium	Large	Small	Small to Large	Small to Medium
Cost	High	Medium	Low	Low	Medium

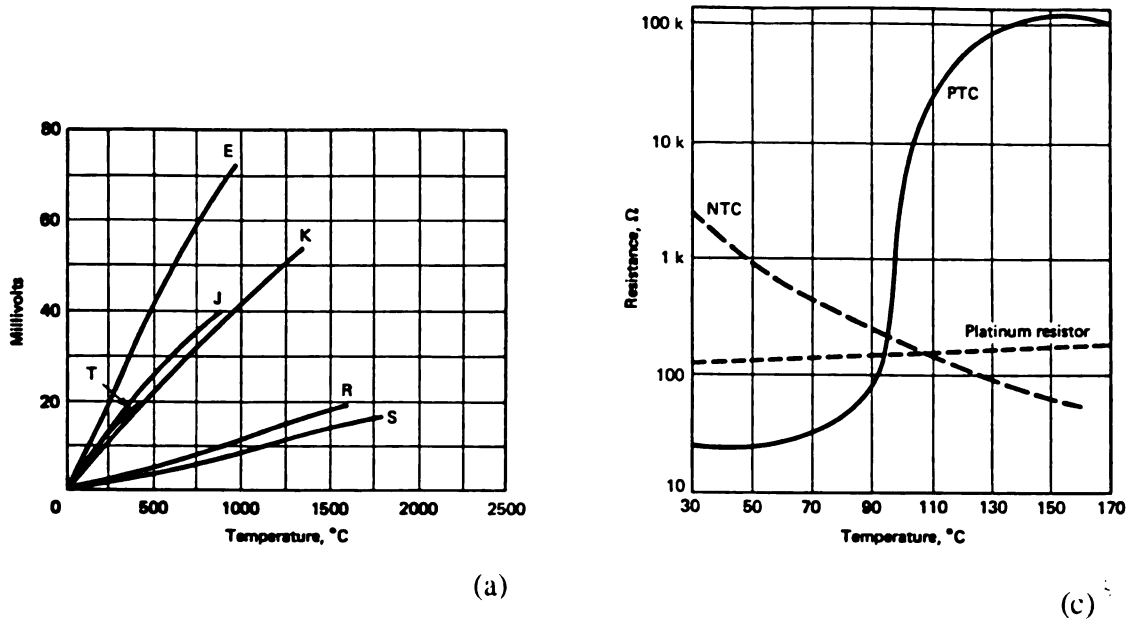


Figure 2.1 Temperature response curves of typical (a) thermocouples, (b) RTDs, (c) NTC and PTC thermistors. (the Pt resistor curve has been given for sensitivity comparison only) [3]

connectors of the voltmeter or display instrument) voltage and voltage drop across finite resistance of the lead wires cause undesirable error in measurements and which is required to be compensated for. Both manual and automatic instrumental compensations are available but it is never precise over the entire temperature range. Hence, an error in measurement is usually large especially at high temperatures. For example, an error of greater of 2.2°C or 0.75% of the actual temperature is specified for type K thermocouple (which is $\pm 7.5^{\circ}\text{C}$ at 1000°C) and it is a typical of any thermocouple.

Another frequent source of error is drift with time. Even though high temperature thermocouples are made of refractory metal alloys, their properties undergo a permanent change during long term exposure to high temperatures. Most thermocouples are not suitable for all environments especially for oxidizing, reactive and high vacuum applications. Such effects, in addition to precision, degrade the repeatability of thermocouples. The response time, by virtue of their size, generally exceeds several seconds which is too large for certain applications. Due to all these drawbacks, thermocouples are unsuitable for high speed precision temperature measurements. Despite this fact, their enormous temperature range i.e., -240°C to 2300°C , largest of all kinds of temperature measurement devices makes them popular for most conventional applications such as in furnaces, heaters, industrial plants and controlled environment chambers. However, the inherent design prohibits them from taking advantage of planar processing technology or integration with sensors of other measurands or signal conditioning circuitry. Lately, a unique thermocouple made of narrow bandgap compound semiconductor pair, i.e., Bi_2Te_3 and Sb_2Te_3 , has shown tremendous improvement in sensitivity over classical thermocouples [6]. This sensor has successfully been used in the measurement of laser radiation and super high frequency (SHF) powers.

2.2.2 Resistance Temperature Detectors

The resistance of most materials change with temperature. Hence, passing a known constant current will cause a voltage drop which is proportional to the temperature. Two types of modulating transducers use this phenomenon for temperature measurement namely resistance temperature detectors (RTDs) and thermistors. The difference between the two is the base material they are made from. RTDs use metallic sensing elements whereas thermistors are usually semiconductors. Due to their simplicity, these devices are increasingly replacing thermocouples in many applications since they do not need special wires or cold junction compensation.

RTDs are made from several metals or metal alloys such as Ni, Ni-Fe, Cu and Pt [12]. Platinum is usually preferred over the others due to its relatively high resistivity and linearity over the temperature range as shown in Fig. 2.1(b) [3]. Moreover, it is malleable and resists corrosion. Regardless of the base material, all RTDs are positive temperature coefficient of resistance (PTC) devices. Typically RTDs consists of a wound metal wire inside a glass or stainless steel package. To achieve a reasonably moderate resistance, long sensing wire is wrapped around a bobbin. In spite of this, the ultimate resistance is so low that special arrangements (e.g., bridge circuits) must be made to offset the lead effect [12]. A more rugged design is thin film type. The metal slurry is screened onto a ceramic substrate. The film is sealed after curing and laser trimming for calibration [13,14].

The packaging considerations of RTDs are very important for their operation. At elevated temperatures ($>400^{\circ}\text{C}$) small amounts of iron impurities can leach out the conventional stainless steel package and corrode the platinum [12]. Using other sheaths such as quartz drastically increases the response time. Above 550°C , the hydrogen poisoning can cause problem. Platinum elements breath through the seal and absorb the hydrogen atoms provided by the dissociation of ambient water molecules. This causes the platinum resistance to increase. In spite of these problems, RTDs are very

popular for their impressive stability, accuracy and speed compared to other temperature sensors. They generally have quoted accuracy of about 0.1% with typical drift of $<0.1^{\circ}\text{C}$ per year. RTDs are particularly well suited for temperature measurements in the laboratory due to their precision, wide temperature range and fast response.

2.2.3 Other Devices

Junction semiconductor devices such as diodes and transistors are frequently used for temperature sensing applications. However, junction voltage, instead of resistance, is temperature sensitive variable. PN junction diodes find useful applications as thermometers in cryogenic range. Si diodes, in particular, are very popular for temperatures below 30 K due to their high sensitivity and linearity [15]. Recently, sophisticated modification of transistor sensors is provided as a two terminal monolithic integrated circuit (AD590) [16]. They supply an output current or voltage that is linearly proportional to absolute temperature. Typical values are $1\mu\text{A/K}$ and 10mV/K . However, the concept of integration of temperature sensors and accompanying electronics is fairly innovative and provides a motivation for developing diamond based IC sensors with superior characteristics.

A number of temperature sensors based on non-conventional physical principles have been developed. For example a fiber optic temperature sensor and a quartz temperature sensor have been reported [17]. The former is a non-contact device which detects the intensity of emission of a particular wavelength from a hot surface whereas the later utilizes the temperature dependence of the natural resonance frequency of a quartz crystal for measuring temperature. Nuclear quadrupole resonance (NQR) thermometry has developed to the point where temperatures in the range of 90 K to 398 K can be measured with a resolution of $\sim 2\text{mK}$ [14]. At least one report describes a thermometry utilizing the rather complex temperature dependence of ferrites [18]. However, the present interest is limited to semiconducting resistance thermometry and this

brief description of junction and other devices is given for completeness only.

2.2.4 Thermistors

All semiconductors exhibit some degree of resistivity variation with temperature [8]. However, for temperature measurement purposes, special semiconductor resistors known as thermistors are fabricated which show large variations in their resistance in a predictable way as temperature is changed. They may be 10^3 to 10^6 times more sensitive than conventional Pt RTDs [19]. However, thermistors are less stable and operate in limited temperature range due to their high non-linearity (see Fig. 2.1(c) for curves of typical thermistors [3]). This non-linearity has practically prevented the manufacturers from standardizing their response curves to the same extent as those of RTDs. They are mostly employed for less precise temperature control, and for switching in the temperature range from -100 to 500°C [9]. They are usually made from compound semiconductors in ceramic composition in which solid solutions of transition metal oxides are used [8,20]. The first commercial thermistors were produced in 1930's from UO_2 , CuO or SiC . The elemental semiconductor based thermistors are, in particular, widely used for temperature compensation of electronic circuits. They are very popular for temperature measurements in the cryogenic range [15,21]. However, due to inherent material and electronic properties, they are unsuitable for high temperature measurements. Though there are thermistors with positive temperature coefficient (PTC) of resistance, most of the thermistors have negative temperature coefficient (NTC) of resistance.

The advantage of semiconductors is relatively higher resistivity than metals. This allows the resistance of thermistors to be in the range of several $\text{k}\Omega$ to few $\text{M}\Omega$ which in turn boosts the temperature sensitivity. Such large changes in resistance are easily measurable using a simple two wire resistance measurements. The problems associated with lead effect, contact resistance and cross sensitivity from stress in the sensing

elements, as faced by RTDs, are significantly reduced [19]. The real advantage of thermistors results from their inherent structural difference. Thermocouples and RTDs can be constructed from only a limited number of materials, and shape and size are restricted. Thermistors on the other hand can be fabricated from a variety of semiconductor materials and composition can be modified through introduction of impurities to meet specific application requirements. Moreover, considerable latitude is possible in sensor size and shape.

Thermistors are available in a variety of shapes including rods, films, flakes, disks, washers etc. But beads and chips are more popular for common applications particularly where space is limited or where minimal disturbance of the monitored medium by the sensor is required [9,12]. Bead thermistors have been particularly effective as sensors in gas chromatographs and thermal conductivity analyzers. Thermistor chips are especially well suited for direct surface mounting in hybrid and other circuits. One important application is an on board sensor for temperature compensated quartz crystal oscillators in microwave equipment. They are usually fired on Pt, Ag, or Au wires for external connections, and are encapsulated in glass, epoxy, or a ceramic sheath [20]. They are available in a wide range of tolerances from 1% to 20% of nominal resistance at some reference temperature (usually 25°C). Individual sensing elements, due to variety of reasons, cover only a narrow range of temperature [9]. However, in recent years, they are evolving most effectively to meet the stringent demands for improved stability, miniaturization, lower cost, close tolerance and interchangeability [14]. The largest emphasis has been to reduce non-linearity of the sensors either by making structural changes (through doping [22], combining PTC and NTC elements [23]) or through signal conditioning circuits [9,24].

There have been several reports about thermistors with unusual materials and properties. In 1971, a thermistor made of graphite powder mixed in melted mixture of paraffine and polythene was reported to have an anomalously large PTC in a limited

temperature range (20°C to 85°C) [25]. The reported resistivity change of about six orders of magnitude was monotonic but highly non-linear. Another thermistor used polysilicon as base material [26]. Its temperature response has been described to be fairly stable and linear on reciprocal temperature scale in the range of 300-900°C. Its applications as multifunction sensor have also been investigated [10]. Similar studies have been carried out on SiC thermistors in a temperature range below 300°C [27,28]. Furthermore, several non-conventional semiconductors including Bi [29,30], ruthenium oxide [31], compound ceramics [32], InSb(Mn) [33] and (Ba, Sr)TiO₃ [34] have also been investigated for varying applications involving temperature measurements.

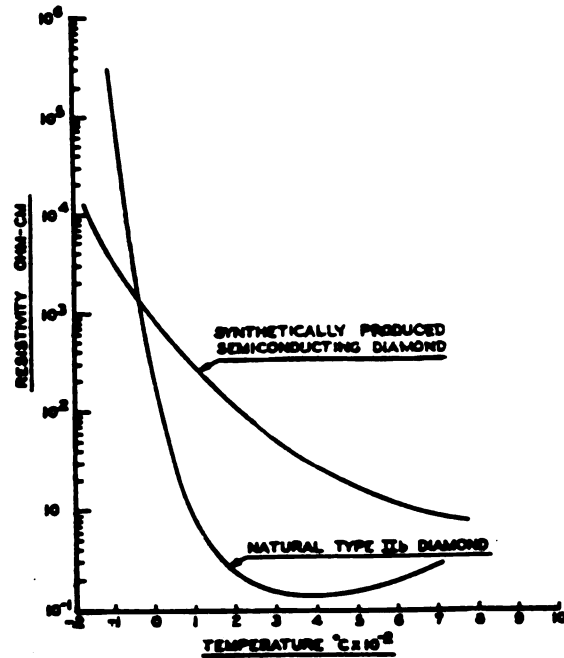
The dynamic temperature response of thermal sensors is a parameter important in certain applications where measurement of fast temperature changes is required [21,35,36]. An improvement in the dynamic response of a sensor requires, among other parameters, a reduction in its thermal mass. Doing this decreases the upper limit of temperature range the sensor can physically withstand. Hence, widening the temperature range and reducing the dynamic response are contradictory requirements for a sensor design. For example, type K thermocouple with response time of 1.8 seconds can go up to 668°C. To reach the specified limit of this thermocouple i.e., 1200°C, the wire size has to be increased which increases its response time up to 110 seconds [14]. Similar effect prevails in RTDs. A 100Ω Pt RTD has 1.5 seconds response time with upper temperature limit of 365°C. The same unit manufactured to reach 800°C has the response time of 54 seconds [14]. Though thermistors also show similar effect, but it is much less than thermocouples and RTDs. Moreover, their intrinsic response time is so short (fraction of a second) that manufacturers usually do not specify it [14]. Additionally, the inherent flexibility in their design is also, some times, used to improve their dynamic response significantly [35].

2.2.5 CVD Diamond Temperature Sensors

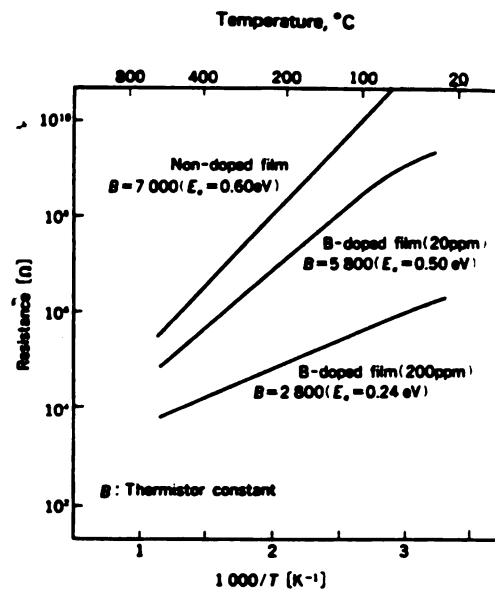
When first diamond based thermistors were made of natural semiconducting diamonds, their remarkable features were pointed out [37]: corrosion and abrasion resistance, low specific heat and excellent thermal conductivity. Additionally they could operate at temperatures > 600 K. Later on, a patent [38] was granted to G. E. for producing synthetic diamond thermistors. These thermistors were nominally doped with 0.001-0.15% B during synthesis and sealed into a glass envelop. They were said to be superior to natural diamonds, since they did not exhibit the resistivity increase with temperature between 700 and 800 K as shown in Fig. 2.2(a) [38]. These sensors were, however, never produced commercially due to high production cost and several technological problems especially reproducibility of size, shape and doping concentration which resulted in high tolerance in resistance ($\approx 20\%$) and sensitivity ($\approx 15\%$) [8].

Recently, a diamond thermistor based on homoepitaxial CVD diamond films has been demonstrated [39]. The sensing properties as shown in Fig. 2.2(b) have been described to be comparable to synthetic diamond. However, its characteristics have been studied within a limited temperature range (25-500°C).

With this supportive background [40], it is expected that CVD diamond films which are typically polycrystalline and cannot be used for most high performance active electronic devices, will prove to be an excellent temperature sensing material, superior to that of any other material in terms of temperature range, speed, stability and sensitivity. Its chemical inertness except to oxidizing agents at high temperatures ($>650^\circ\text{C}$) [41] and radiation immunity can permit highly stable operation under extremely hostile environment. The relatively high resistivity as compared to other semiconductors at useful doping levels ($10^{15}-10^{18}\text{cm}^{-3}$) can lead to a simple two wire resistance measurement which is impracticable for RTDs. Such a temperature sensor will possibly be able to replace Ge resistance thermometer in cryogenic aerospace systems [21] and platinum RTD in shock wave tunnels [36] with less constraint on the



(a)



(b)

Figure 2.2 Static temperature response curves of thermistors made of semiconducting (a) natural and synthetic crystalline diamonds [38] (b) CVD diamond films with various doping levels [39].

sensor design to reduce dynamic response time [35].

2.3 THEORETICAL ANALYSIS OF THERMISTORS

The electronic transport phenomenon in polycrystalline semiconductors including polycrystalline diamond is not well understood at this time. However, if sufficient allowance for effects unique to polycrystalline material is given, then most of the qualitative analysis for crystalline material can, in general, be applied to polycrystalline materials as a first approximation. The most important aspect is the understanding of the temperature dependence of the resistivity ρ . While the general shape of the resistance versus temperature curve for semiconductors can be predicted, quantitative theoretical calculations are not accurate enough for them to be adopted directly for temperature sensing, especially in case of polycrystalline material. Nevertheless, they provide the fundamental basis for the design and improvement of sensor properties such as sensitivity and range.

In an intrinsic semiconductor, as the temperature approaches absolute zero (-273°C), all the electrons are bound in the valence band i.e., energy $E < E_v$. With rising temperature, electrons are thermally excited in increasing number in to the conduction band i.e., $E > E_c$, leaving behind electron vacancies or holes. Since the current carrier concentration increases with temperature leading to reduction in resistivity, intrinsic semiconductors always have a negative temperature coefficient (NTC) of resistivity.

If the difference between the Fermi level, E_F and conduction band or valence band edge is large compared with kT , the expressions for electron and hole densities in a semiconductor are given respectively by [42]

$$n = N_C \exp\left[\frac{E_F - E_C}{kT}\right] \quad (2.3.1)$$

$$p = N_V \exp\left[-\frac{E_F - E_V}{kT}\right] \quad (2.3.2)$$

$$\text{where } N_C = 2 \left[\frac{2\pi m_e kT}{h^2} \right]^{\frac{3}{2}} \quad \text{and} \quad N_V = 2 \left[\frac{2\pi m_h kT}{h^2} \right]^{\frac{3}{2}}$$

and m_h and m_e are the effective masses of the holes and electrons respectively and h is Planck's constant.

The controlled addition of impurities to a semiconductor can make a large change in its resistivity, both in its absolute value and in its rate of change with temperature. However, the following charge neutrality condition is always maintained.

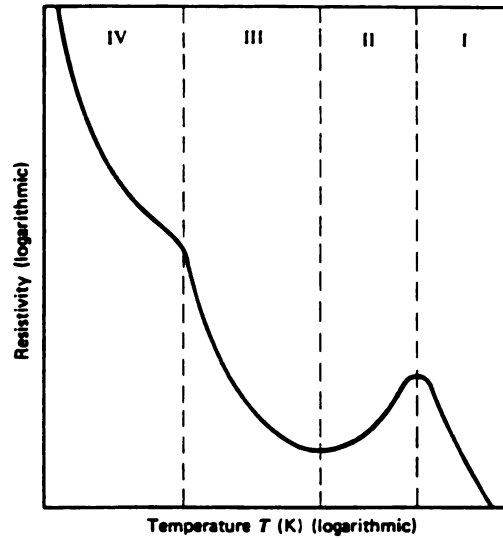
$$n + N_A^- = p + N_D^+ \quad (2.3.3)$$

where n , p , N_A^- , and N_D^+ are electron, hole, ionized acceptor, and ionized donor densities respectively. The resistivity of any semiconducting material, whether doped or not, is given by [42]

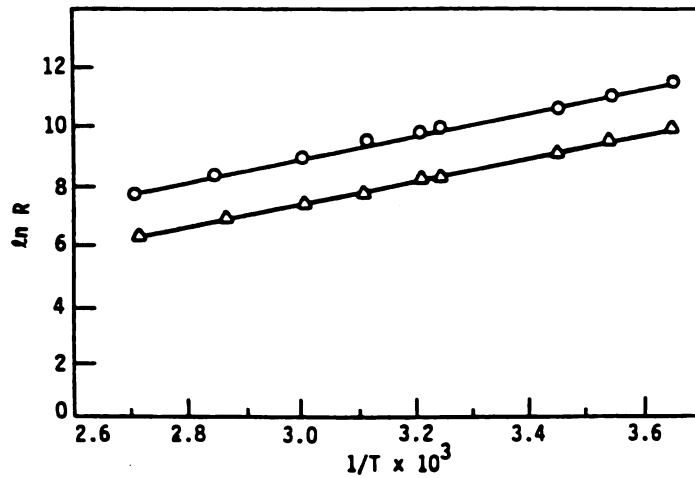
$$\rho = \left[q (n(T) \mu_n(T) + p(T) \mu_p(T)) \right]^{-1} \quad (2.3.4)$$

where μ_n and μ_p are electron and hole mobilities respectively. The T in parenthesis indicates that the mobilities and carrier concentration are strong function of temperature. In effect, this temperature dependence is the basis of resistivity change with temperature for semiconductor temperature sensors. The mobility due to impurity scattering μ_i dominates at low temperature. The mobility due to lattice scattering follows a power law of the type $\mu_L \propto T^{-S}$ and dominates at higher temperatures where $S = 0.5$ to 2.8 depending on the semiconducting material [43].

The variation of resistivity with temperature of a doped semiconductor is shown qualitatively in Fig. 2.3(a) [44]. Four regimes of temperature can clearly be identified, one conduction process being dominant in each. In the high temperature range (I), the semiconductor behave as intrinsic material and the conduction is dominated by the thermally excited carriers i.e., n_i , because $n_i \gg N_A, N_D$. In this case $n = p = n_i$, Eq. (2.3.1) and (2.3.2) give



(a)



(b)

Figure 2.3 (a) Electrical resistivity of a semiconductor similar to Ge as a function of temperature on logarithmic scales [44] (b) \log_e resistance of two commercial thermistors plotted against reciprocal of temperature in region II of curve given in (a).

$$n_i = (np)^{1/2} = 2 \left[\frac{2\pi kT}{h^2} \right]^{3/2} (m_e m_h)^{1/4} \exp \left[-\frac{E_g}{2kT} \right] \quad (2.3.5)$$

When substituting into Eq. 2.3.4, the pre-exponential factor becomes independent of temperature if $S=1.5$ or a weak function of temperature if $S \neq 1.5$ and, hence, the exponential function will dominate the temperature response of resistivity. Then, it can be written as

$$\rho \propto \exp \left[\frac{E_g}{2kT} \right] \quad (2.3.6)$$

In the extrinsic region (II), all the impurities are still fully ionized but n_i is much less than the impurity concentration. Then the resistivity, dominated by the temperature dependence of the mobility, corresponds to that of the majority carriers. The resistivity is again determined by Eq. 2.3.4 with n and p replaced with N_D and N_A respectively.

In range III, the ionization of the majority impurity atoms ceases to be complete. The density of occupied acceptor states in a P-type semiconductor is given by

$$N_A^- = \frac{N_A}{1 + 2 \exp [(E_A - E_F)/kT]} \quad (2.3.7)$$

However, almost all the donor states will be ionized, hence, $N_D^- \approx N_D$. Substituting this expression into the charge neutrality equation (2.3.3) and assuming $n \ll N_A^-$ for a p-type semiconductor yields

$$p = \frac{N_A}{1 + 2 \exp [(E_A - E_F)/kT]} - N_D \quad (2.3.8)$$

Solving this equation in terms of p (using the expression from Eq. (2.3.2)), one gets

$$\frac{p(p+N_D)}{(N_A-N_D-p)} = \frac{1}{2} N_V \exp \left[-\frac{E_a}{kT} \right] \quad (2.3.9)$$

where $E_a = E_A - E_V$, is the acceptor activation energy. This equation can be simplified by applying assumptions based on the compensation of impurities. For a highly

compensated P-type semiconductor, it can be assumed that $N_A > N_D \gg p$ in this temperature zone (freeze-out region) so the above equation simplifies to

$$p = \left[\frac{N_A - N_D}{2N_D} \right] N_V \exp \left[-\frac{E_a}{kT} \right] \quad (2.3.10)$$

and if no compensation is present, the assumption $N_D \ll p < N_A$ will apply. Then Eq. 2.3.9 will give

$$p = \frac{1}{2} \left[N_V N_A \right]^{\frac{1}{2}} \exp \left[-\frac{E_a}{2kT} \right] \quad (2.3.11)$$

Similar expressions can be derived for electrons in n-type semiconductors. The resistivity for p-type semiconductor can then be found using Eq. (2.3.4) where the hole density p will be substituted from Eq. (2.3.10) or (2.3.11).

$$\rho = \left[q\mu_p(T)p \right]^{-1} \approx \text{constant} \cdot \exp(\epsilon_1/kT) \quad (2.3.12)$$

Hence, the slope of $\ln \rho$ curve on $1/T$ scale should be almost linearly proportional to ϵ_1 which is equal to either E_a or $E_a/2$ depending upon the situation whether the semiconductor is compensated or not. This temperature dependence is shown in Fig. 2.3(b) [9].

In region IV, the thermal energy is too low to excite electrons into the conduction band and they are restricted to the impurity atoms. The conduction is believed to take place by charge carriers jumping directly from one impurity atom to the next known as hopping conduction. The activation energy ϵ_3 required for hopping conduction is, in general, much smaller than normal activation energy E_a of the dopant. The resistivity can approximately be written as [156],

$$\rho = \rho_0 e^{\epsilon_3/kT} \quad (2.3.13)$$

where ρ_0 depend upon the material and density of donors and acceptor atoms.

Of particular interest in temperature sensing is the region III, and to some extent region IV, which occur in the temperature range (30-200 K) where resistance thermometry is mostly employed. It is because of the linearity of the $\ln \rho$ curves on reciprocal of temperature scale (see Fig. 2.3(b) [9] in region III). This linearity is typical, contributed by Eq. (2.3.12), but other empirical equations can also be made to fit the experimental curves. One equation uses a temperature-dependent pre-exponential factor [9], and fits the experimental data more closely than Eq. (2.3.12). It is given by

$$\rho = C_2 T^{-c} e^{\beta/T} \quad (2.3.14)$$

where C_2 and c are constants and obtained by curve fitting to the experimental data. The constant C_2 is small and may be positive or negative. Neglecting the temperature dependence of the pre-exponential factor, the resistivity from Eq. (2.3.14) at temperature T within region III, can be represented by

$$\rho = \rho_0 e^{\beta (1/T - 1/T_0)} \quad (2.3.15)$$

where the resistivity ρ_0 is measured at the absolute temperature T_0 .

Another way to represent the temperature response is to expand the exponent in Eq. (2.3.15) to obtain

$$\rho = \rho_0 \exp \left[A_0 + \frac{A_1}{T} + \frac{A_2}{T^2} + \frac{A_3}{T^3} + \dots \right] \quad (2.3.16)$$

This relationship lends itself to better computer curve fitting so that the resistance to temperature relationship can be very accurately represented.

The temperature coefficient of resistance α is defined as

$$\alpha = \frac{1}{R} \frac{dR}{dT} \quad (2.3.17)$$

This is, in effect, the measure of sensitivity of the temperature sensor. For semiconductor temperature sensors α is very sensitive to temperature. From Eq. (2.3.15) and (2.3.17), we get

$$\alpha = \frac{1}{R} \frac{dR}{dT} = \frac{-\beta T^{-2} R_0 e^{\beta(1/T-1/T_0)}}{R_0 e^{\beta(1/T-1/T_0)}} = -\beta T^{-2} \quad (2.3.18)$$

Following this brief theoretical analysis, the second major part of this review will deal with the synthesis and characterization of diamond thin films and their application as a sensor for thermal signals.

2.4 PROPERTIES OF DIAMOND

Diamond is one of the most technologically and scientifically valuable crystalline solids found in nature, as it has a combination of properties effectively unrivaled by any other known material. Among its unique physical properties are extreme hardness (10^4 kg/mm^3), high chemical inertness, optical transparency (225 nm to far-infrared), radiation immunity, and high thermal conductivity (typically 20 W/cm-K). Additional properties are extremely low friction coefficient (0.05), low thermal expansion coefficient ($1.1 \times 10^{-6} \text{ K}^{-1}$), high tensile and compressive strength (0.5×10^6 and 14×10^6 psi respectively) and wide energy band gap (5.45 eV) [45]. It is a typical covalent solid in which carbon atoms are joined in tetrahedral arrangement forming a diamond-cubic lattice. Diamond crystals are most commonly found in octahedral and dodecahedral shapes with faces parallel to the {111} and {110} planes respectively. A simple cubic with faces parallel to {100} faces also exists but is less common [46].

Diamonds are classified according to their optical and electrical properties into four types [47,48]:

Type Ia: These diamonds are optically transparent. They contain up to 0.1% nitrogen in small aggregates or platelets which induces infrared absorption and limits thermal conductivity to 9 W/cm-K (at room temperature). Electrical resistivity is $> 10^{16} \Omega\text{-cm}$.

Type Ib: These diamonds contain up to 0.2% paramagnetic nitrogen incorporated in the lattice. They are typical high-pressure synthesized diamonds. Optical, thermal, and electrical properties are similar to type Ia diamonds.

Type IIa: This very rare type is practically free of nitrogen and transparent to ultraviolet above 225 nm. Thermal conductivity at room temperature ranges up to 26 W/cm-K. Electrical resistivity is in general similar to type Ia diamonds.

Type IIb: Extremely rare in nature and virtually nitrogen free, these diamonds contain boron in small quantities. This produces a bluish color. They are p-type semiconductors with electrical resistivity of only 10 to 1000 Ω -cm.

Diamond is extremely inert chemically and is not affected by any acid or any other chemicals, except those which act as oxidizing agents at high temperature. These provide the only effective way to attack diamond at temperatures below ~ 1300 K and at normal pressure [47]. Substances such as sodium nitride are known to attack diamond in molten state as low as ~ 700 K [47]. In oxygen itself, diamond starts to be oxidized at about ~ 900 K [47].

The only other possible form of chemical attack is by two groups of metals. The members of the first group are avid carbide formers, and include W, Ta, Ti and Zr. At high temperatures (>550 °C) these will react chemically with diamond to form their respective carbides. The second group includes Fe, Co, Mn, Ni, and Cr, and also the platinum group of metals. In molten state these metals are true solvents for carbon [47].

2.5 CHEMICAL VAPOR DEPOSITION OF DIAMOND

The motivation and interest for the diamond synthesis started since the discovery by Tennant in 1797 [46] that it is simply a crystalline form of carbon. Early attempts, mostly based on unscientific approach, proved unsuccessful. Later on, with the

progress in understanding of chemical thermodynamics, the pressure-temperature range of diamond stability was acquired. The real breakthrough came in 1955 at General Electric where a high-temperature high-pressure (HPHT) process for diamond synthesis was discovered [49]. In this process, diamond is synthesized in its thermodynamically stable phase using a molten transition metal solvent-catalyst. After the formation synthetic diamond remains kinetically stable as it is brought to ordinary atmospheric conditions of pressure and temperature. This is due to the large activation energy required for the conversion of diamond into graphite which is the thermodynamically stable form of carbon at normal atmospheric conditions.

An entirely different approach has been directed towards growth of diamond from the gas phase using hydro-carbon species at low pressure and moderate temperature, that is, in the thermodynamically metastable region of diamond [46,50]. Although these efforts were successful in growing diamond earlier than the HPHT method, they did not attract much attention due to the low growth rates ($<0.1\mu\text{m/h}$) achieved and the simultaneous deposition of significant amount of graphite. Nevertheless, the critical role of atomic hydrogen in achieving metastable diamond growth as a preferential etchant for removing graphite against diamond was established. An important breakthrough by Soviet scientists in early 1970's indicated the conditions under which gas activation techniques can greatly increase the growth rate of diamond and suppress the graphite deposition [51]. The key feature of this work was the three approaches, namely catalytic, electric discharge, and heated filament, which produced higher concentration of atomic hydrogen than that normally present in the thermal dissociation of hydro-carbon gases. Since then, several techniques have been developed for rapid chemical vapor deposition (CVD) of diamond films.

Of numerous methods presently used for CVD deposition of diamond using gas activation, hot filament [52,53], d.c. plasma [54,55], r.f. plasma [56,57], microwave discharge [58-61], thermal d.c. plasma [62] and combustion flames [63] are a few to

mention. Interestingly, all these techniques share several common features:

- (i) High-energy densities are produced in the gas phase, sufficient to result in the production of radical species, notably atomic hydrogen.
- (ii) The nature of the hydrocarbon precursor used is relatively unimportant.
- (iii) Very similar substrate temperatures are used (600°-1000°C).
- (iv) Deposits may vary from nanocrystalline to single crystal diamond with no or little non-diamond C, depending upon proportions of C, H, O in the supply of gases, but without reference to the type of gas phase activation used.

These common features strongly suggest that there is a common mechanism for the growth process, and thus the choice of method is dependent upon considerations of efficiency, convenience, cost and applicability to the problem at hand [64].

Semiconducting diamond, an attractive material for electronic devices, has been grown homoepitaxially, and polycrystalline diamond films have been grown on many substrates [46,53]. Heteroepitaxial growth of diamond films, a necessity for most electronic device applications, has not yet been accomplished except on cubic BN [65]. Recently, a novel technique named as "artificial epitaxy" has been reported [66]. In that approach, diamond seed crystals were aligned by placing them in inverted pyramid shaped craters micromachined on a silicon substrate surface. An oriented diamond growth of limited size is also reported [67].

2.6 HOT-FILAMENT CVD

Since the hot-filament CVD method is employed for the synthesis of thin diamond films in this research, an overview of the deposition system and influence of associated growth parameters will be briefly discussed here.

2.6.1 The Deposition System

Thermally activated or hot-filament CVD (HFCVD) is one of the most common techniques for diamond film growth. A conventional HFCVD system is composed of a vacuum chamber equipped with a filament made of W, Re or Ta, a substrate holder, a reactant gas inlet and an arrangement for the measurement of temperatures of filament and substrate [52]. Beyond these primary requirements, many additional features have been added by many researchers to improve growth rate, film size and reproducibility, to allow for in situ probes for gas thermodynamics and surface reactions, and to have automatic fail safe operation. The filament at 2000-2400°C is used to dissociate gas mixtures containing 0.5-5% of carbon carrying gas in hydrogen usually at sub-atmospheric pressures (10-700 torr). The dissociated products at these temperatures consists mainly of hydrocarbon radicals, for example, CH₂, C₂H, CH, C₂H₂, CH₃, and atomic hydrogen. These radicals lead to preferential growth of diamond against graphite on the surface of an appropriately prepared substrate placed typically 1 cm from the filament. The substrate to filament distance is critical to meet the opposing requirements to minimize thermalization of the substrate and radical recombination.

The main advantage of HFCVD method is its relative simplicity, inexpensiveness and ease to scale up to large substrate areas and shapes. However, various components in the system can add impurities into the films due to increased vapor pressure in the presence of filament at very high temperature [64]. The role of these impurities in the electrical properties of the films may be very critical. The brittleness and the

deformation of the filament due to carbodization at high temperature is another problem. However, these problems can be taken care of by using various alternative materials and techniques.

2.6.2 Effect of Gas Composition

As mentioned earlier, the nature of the hydrocarbon precursor used for diamond deposition is relatively unimportant [64]. The main requirement is the dilution of few percent (0.5-5.0) hydrocarbon gas in hydrogen. Diamond has been shown to deposit, with varying growth rate, from a variety of organic compounds including acetone (CH_3COCH_3), ethanol ($\text{C}_2\text{H}_5\text{OH}$), methanol (CH_3OH) and diethyle ether ($\text{C}_2\text{H}_5\text{OC}_2\text{H}_5$) [68]. The variation in growth rate is possibly due to varying efficiency of each compound in supplying C_2H_2 and other radicals thought to be mainly responsible for diamond growth [69]. Harris et al. has also investigated the relative importance of various species for diamond nucleation and growth [70].

2.6.3 Effect of C-H-O Ratio

To date, for most of the diamond CVD experiments, highly diluted mixture of a carbon carrier with hydrogen, with and without oxygen are common. The carbon carrying species are usually less than 1%. A relative reduction in carbon component in the gas mixture leads to an improvement in the quality but a reduction in the growth rate of the deposited diamond [52]. It also has a pronounced influence on the morphology of the deposited film [46] (see Fig. 2.4(a)) [71]. The best quality diamond films are grown in a pre-dominantly hydrogen atmosphere. In any case, atomic hydrogen should be in a super-equilibrium state for a successful diamond growth. Hydrogen atoms play a crucial role in film growth since they have been shown to etch preferentially non-diamond carbon, provide stabilization for sp^3 bonding (diamond structure) and promote the generation of the main pre-cursors (C_2H_2 and CH_3) for the diamond

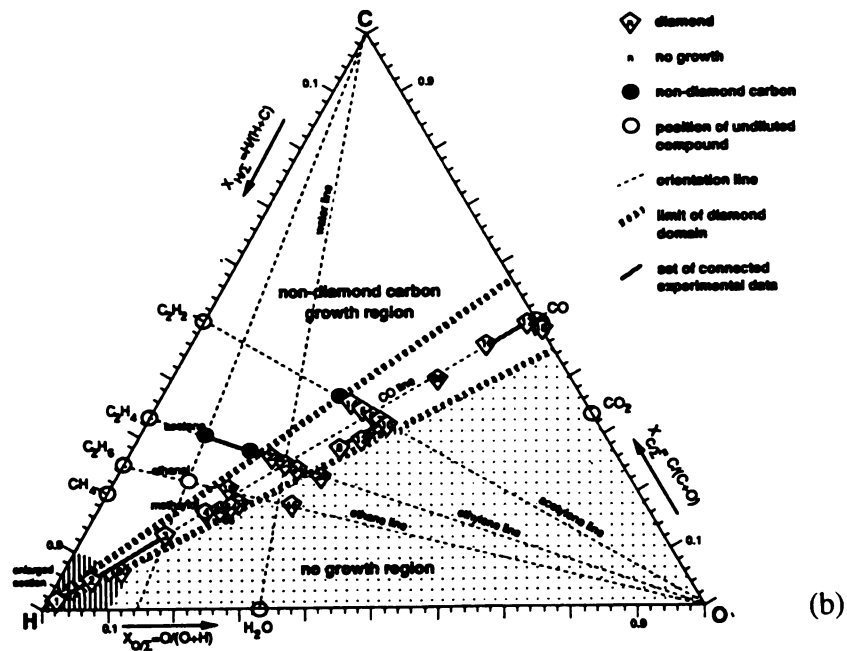
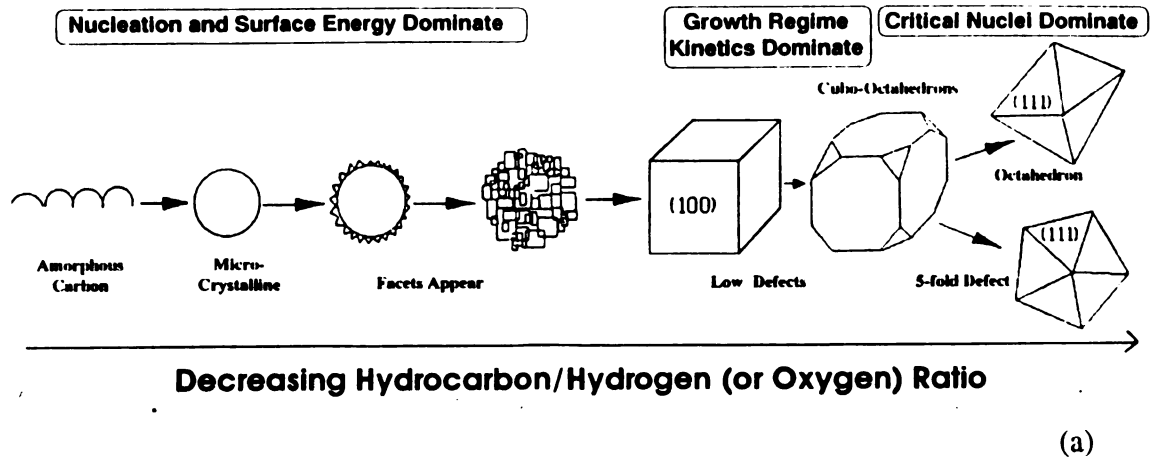


Figure 2.4 (a) Influence of C-H-O ratio on the morphology of CVD deposited diamond films [71] (b) Atomic C-H-O diamond deposition phase diagram with the diamond growth domain [72].

growth. Recently, an elegant carbon-hydrogen-oxygen (C-H-O) phase diagram as shown in Fig. 2.4(b) for diamond deposition has been introduced [72]. Given the magnitude of three components, the presence and quality of deposited diamond can be evaluated. The region of phase diagram feasible for diamond growth has been defined on the basis of experimental data collected from the literature and theoretical analysis.

2.6.4 Effect of Oxygen

Various studies [73-75] have shown that addition of oxygen in HFCVD growth environment leads to higher quality films at increased growth rate. This has been attributed to the following effects caused by oxygen:

- (i) Formation of more reactive surface.
- (ii) Formation of additional radicals necessary for diamond growth.
- (iii) Destruction of gas phase pyrocarbon forming species and increase in atomic carbon density.
- (iv) Increase in atomic hydrogen density which tends to selectively etch the non-diamond carbon from the surface.
- (v) Oxygen may itself act as selective etchant of non-diamond carbon.

2.6.5 Effect of Substrate Temperature

The substrate temperature for diamond CVD, in almost all the techniques, has been in the range of 800-1000°C. However, a small variation in the temperature may greatly influence the growth rate and grain size [52]. On substrates hotter than 1300°C, only graphitic carbon, if any, is deposited [52]. From C-H-O containing mixtures, diamond may deposit as low as 400°C, but at very low rates [61]. The effect of substrate temperature may well be visualized from Fig. 2.4(b) such that with increasing temperature, the width of region of diamond growth reduces and at $T > 1300^\circ\text{C}$, it shrinks

down to almost zero [72]. Hence, the freedom of C-H-O composition fades away with rising temperature.

2.7 ANALYSIS TOOLS

A number of analysis tools are used to monitor and characterize various stages of CVD process of diamond. Most of them are, however, used either to study in situ gas reaction and substrate surface chemistry or physical composition of the films. In this research, diamond films were characterized after deposition. For this application Raman spectroscopy, scanning electron microscope (SEM), secondary ion mass spectroscopy (SIMS) and surface profilers are the most appropriate tools and were used extensively. A brief description of each in context with its specific use in diamond film characterization is given here.

2.7.1 Raman Spectroscopy

Raman spectroscopy is based on the phenomenon of inelastic scattering of radiation by a medium. When monochromatic radiation of wavenumber ν_0 is incident on a material, the transmitted radiation contains, in addition to ν_0 , a pair of new wavenumbers of the type $\nu'_{\pm} = \nu_0 \pm \nu_M$. They are caused by inelastic scattering due to creation or annihilation of phonons and known as Raman scattering. In molecular systems, the wavenumber ν_M are found to lie principally in the range associated with transitions between rotational, vibrational and electronic levels. In case of diamond, they are dominated by the intramolecular vibrational transitions corresponding to optical phonons.

In the spectrum of scattered radiation, the new wavenumbers are termed as Raman lines or bands and collectively are said to constitute a Raman spectrum. Raman bands at wavenumbers $\nu_0 - \nu_M$ are referred to as Stokes bands and those at wavenumber $\nu_0 + \nu_M$ as anti-stokes bands. The strong Raman line at ν_0 , i.e., without

change of frequency, arises from the scattering centers, like molecules, which are much smaller than the wavelength of the incident radiation. It is known as Rayleigh scattering. The intensity of anti-stokes lines is usually much smaller than that of Stokes-lines. Therefore, Raman spectra presented here is based on signals from Stokes-lines.

Raman spectroscopy offers the advantage of sensitivity not only to crystalline material, but also to the various possible non-crystalline phases. A diamond film shows the characteristic Raman peak at relative wavenumber of 1332 cm^{-1} [76]. Well-ordered graphite, similarly, has only one Raman peak at $\sim 1600\text{ cm}^{-1}$ [77]. However, the presence of disorder or small crystallite size gives rise to a peak at 1355 cm^{-1} [77,78]. Hence, most graphitic carbon phases produce two Raman peaks, sometimes referred to as the "D" and "G" peaks. The breadth, position, and relative intensity of these two peaks can vary significantly by the presence and relative density of sp^3 to sp^2 hybridization. The peak at around 1550 cm^{-1} has been commonly attributed to the presence of graphite i.e., sp^2 hybridization. This is not an accurate assignment, since it has been argued to arise from diamond-like carbon (DLC), which may not be graphitic in nature [64]. In addition, films with nanocrystallites show a broad peak centered at $\sim 1133\text{ cm}^{-1}$ [79]. Despite some objections, the quality of diamond deposit is generally judged from the relative intensity of the peaks at 1332 and 1550 cm^{-1} [64]. Robbins et al. has published a comprehensive analysis of various attributes to the shape of Raman Spectra [80].

2.7.2 Scanning Electron Microscope (SEM)

Another very useful tool for studying the morphology and visual analysis of diamond films is scanning electron microscope (SEM). Since the CVD diamond films generally have micron or sub-micron size grains, optical microscopes which has an upper limit of magnification of about $2000\times$ and, at that magnification, a small depth

of field, cannot resolve them effectively. SEM, on the other side, has a capability to resolve objects in dimensions down to 100°A . The increased resolution arises from the much smaller wavelength λ_e of electrons used in the illuminating beam, given approximately by [81]

$$\lambda_e(^{\circ}\text{A}) = \sqrt{\frac{150}{V}} \quad (2.7.1)$$

where V is the electron acceleration voltage that is usually in terms of tens of kilovolts. SEM is helpful in analyzing the diamond films for voids, cracks, adhesion with the substrate, thickness measurement, selectivity of patterns, and uniformity of surface, and crystal orientations, etc.

In the present work SEM was mostly used for inspection of surface morphology and to determine the thickness of diamond films. It was also used to analyze patterns, nucleation density and growth selectivity. The need for a conducting specimens somewhat limited its utility for undoped films on electrically insulating substrates. Moreover, a prolonged exposure to high power electron beam caused some charge accumulation and blackening of the diamond surface.

2.7.3 Secondary Ion Mass Spectroscopy (SIMS)

Secondary ion mass spectroscopy, as the name implies, is a form of mass spectroscopy used to analyze secondary ions emitted from a surface after being sputtered by an ion beam. By moving the sputtering beam of ions across the surface in a raster fashion and setting the spectrometer to detect a particular mass value, topographic scans of a given element's concentration can be made. Using a static beam and sputtering a hole into the surface, a depth profile normal to the plane of surface can be generated. It was this mode in which SIMS was used to analyzed the boron doping profile in semiconducting diamond films in this work.

An oxygen ion beam was used to sputter diamond films and underlying SiO₂/Si substrate. Oxygen sputtering has been shown to cause highly anisotropic etching of diamond films and make holes along the grain boundaries down to the substrate in few minutes [82]. This effect can cause a signal to be picked up from the substrate right from the early phase of the scan while most of the diamond film is still intact and, hence, generate an erroneous data. A further difficulty arises when the wall of the holes, which are not exactly perpendicular, have some contribution to the signal. Therefore a great deal of caution is necessary to evaluate and interpret the SIMS data.

2.7.4 Surface Profiler

SEM is by large the most effective tool for visual surface analysis and thickness measurement using a edge of a conducting film. However, quantification of these parameters is not easy. Now, electromechanical systems are commercially available that can scan across a surface and readout vertical variations with a resolution better than 5°A! [83]. In addition to sheer convenience, a major advantage over SEM is that the step measurement is independent of optical properties of the film and substrate. One such system, Sloan DekTak II surface profiler, was used in this work to measure the diamond film thickness and surface uniformity.

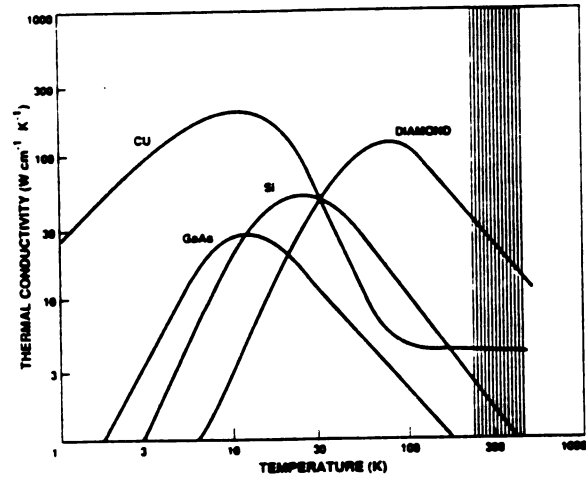
In principle, the instrument uses a linear variable differential transformer (LVDT) to convert vertical motion of the core to electrical signals. The transformer core is attached to a diamond stylus that contacts the sample surface. The instrument shows the scan data interactively on a CRT display which can be printed. A number of computational and statistical functions are provided to manipulate the data to ascertain specific informations. These functions were frequently employed to accurately determine the thickness and surface roughness of diamond and other films.

2.8 ELECTRONIC PROPERTIES

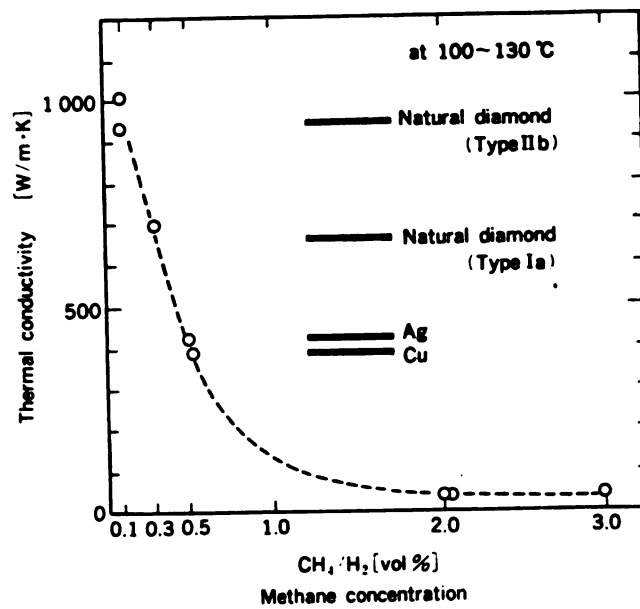
Diamond has been known as an excellent electrically insulating material. The discovery of semiconduction in natural diamond [84] revealed its excellent electronic properties [47,85] in addition to its already known unrivaled physical properties. It is a covalent solid with diamond cubic lattice structure and energy band gap of 5.45 eV. When doped, it exhibits semiconducting properties that are superior to those of commonly used semiconductors. Table 2.2 gives a summary of principle properties of diamond along with representative data for SiC, GaAs and Si [86]. It is obvious from these data that, from an electronic perspective, diamond should be a good candidate for high temperature (due to large band gap) high speed (due to carrier mobility) and high power (due to high thermal conductivity and breakdown voltage) electronic devices.

For fast dynamic response time of temperature sensors, the thermal conductivity of the base material is an important factor. Diamond, as shown in Fig. 2.5(a) [87], has clearly an edge over other competing materials in this respect. However, the thermal conductivity of diamond films is relatively less (3-17 W/cm-K) than that of natural diamond depending on their quality. A diamond film grown with relatively higher concentration of carbon carrying gas generally has poorer thermal conductivity and the quality (see Fig. 2.5(b) [88]). At AT&T Bell Labs. it has been found that the thermal conductivity of polycrystalline diamond films is directly proportional to the quality, thickness and the grain size [89]. An interesting finding was that the thermal conductivity of poor quality diamond films improves on heating (possibly due to reduced role of grain boundaries against phonon scattering) in contrast to high quality films and crystalline diamonds.

Electrical transport measurements on B, Al, and Be doped synthetic diamond have been reported in [90]. These specimens were found to be p-type semiconductors with impurity activation energies of 0.17-0.18, 0.32, and 0.2-0.36, eV respectively. Similar measurements by Wilson [91] in the temperature range of 88 K to 293 K on B



(a)



(b)

Figure 2.5 Comparison of thermal conductivity of (a) natural diamond with several other solids as a function of temperature [116] (b) CVD diamond films using different methane concentrations with natural diamonds, Ag and Cu [88].

doped specimens yielded nearly 30 discrete activation energies ranging between 2.9 and 87 meV. These data were interpreted as evidence of impurity conduction or hopping transport which is commonly observed in heavily doped and highly compensated semiconductors at low temperature [92-94]. In both natural and synthetic semiconducting diamonds acceptors are typically compensated by deep nitrogen donors with activation energy of about 4 eV above the valence band [94,95]. The acceptor activation energy for boron in natural semiconductor diamonds has been recognized at 0.37eV [47].

The electronic transport phenomenon in CVD diamond films is quite complex. So far, there have been few efforts to evaluate the electrical properties of these diamond films [96-100]. This reported work has actually been limited to ascertain resistivity, dopant concentration, Hall concentration and mobility, and dopant activation energy in a limited temperature range. However, due to a large scatter in the reported data, no comprehensive model could be developed so far. Furthermore, a few reports about other kinds of measurements such as capacitance versus voltage (CV) measurements on Schottky structure using diamond as a semiconductor [101], high field effect in diamond thin films [102] and effect of annealing [103] and frequency [104] at various temperatures on the resistivity of undoped diamond films have also been published. At present, since most of the literature deals with the undoped films [99-103], the conduction mechanism in doped diamond films is still not clear. Gildenblat has recently published a comprehensive review of understanding of the subject to date [105]. At present, there exists a need to measure all parameters and their interdependence necessary to develop a comprehensive model of conduction mechanisms over a wide range of doping and temperature in diamond films before any real high performance high-temperature high-power electronic devices may be developed. In this regard, previous work on natural and synthetic diamonds [95,106,107] and similar semiconductors [156,157] can extend very useful support.

2.9 FILM AND BULK PROPERTIES

Since the main interest in diamond is spurred by its potential application in semiconducting devices, the primary effort in CVD diamond deposition is focussed on achieving device quality films. Although the excellent physical and electronic properties of diamond promise devices of extra-ordinary characteristics, semiconducting CVD diamond films, so far, do not possess the electronic properties to the same degree of excellence as single crystal bulk diamond [43]. For example, thermal conductivity, electrical resistivity, hardness, carrier charge carrier mobility of polycrystalline diamond films are relatively inferior than listed in Table 2.2. Some critical electronic properties such as carrier mobility are usually orders of magnitude less than single crystal bulk natural diamond. The major difference in these properties is contributed by the high density of defects in single crystal and grain boundaries in the polycrystalline films.

Thin films generally have high density of defects due to growth process [108], lattice mismatch [109], differences in thermal expansion coefficients between adjacent films or substrate and film [110], and stress [111]. For a variety of reasons, film growth is generally done on materials other than itself, and the resulting semiconductor thin films are usually polycrystalline. The conduction mechanism in polycrystalline films is dominated by surface scattering and defect dominated properties [112,113]. The defects in polycrystalline materials are mainly the grain boundaries. The foregoing description is equally applicable to polycrystalline diamond films grown on non-diamond substrates. The electrical properties of thin diamond films tend to vary grossly from single crystal bulk diamond [43]. At present, no universal explanation of transport characteristics exist for thin diamond films.

The surface of a thin film affects the electrical transport properties of a material by limiting the transversal motion normal to surface plane. When the thickness of the film becomes less than or comparable to the charge carrier mean free path, the

Table 2.2 Comparison of semiconductor properties of diamond with SiC, Si, and GaAs [86].

Properties	Diamond	β -SiC	GaAs	Silicon
Lattice Constant ($^{\circ}\text{A}$)	3.567	4.358	5.65	5.43
Thermal expansion ($\times 10^{-6} \text{ }^{\circ}\text{C}$)	1.1	4.7	5.9	2.6
Density ($\text{g}\cdot\text{cm}^{-3}$)	3.515	3.216		2.328
Melting Point ($^{\circ}\text{C}$)	4000	2540	1238	1420
Bandgap (eV)	5.45	3.0	1.43	1.1
Saturated electron velocity ($\times 10^7 \text{ cm}\cdot\text{s}^{-1}$)	2.7	2.7	1.0	1.0
Carrier mobility ($\text{cm}^2 \text{ V}^{-1} \text{ s}^{-1}$)				
Electrons	2200	400	8500	1500
Holes	1600	50	400	600
Breakdown ($\times 10^5 \text{ V cm}^{-1}$)	100	40	60	3
Dielectric constant	5.5	9.7	12.5	11.8
Resistivity ($\Omega \text{ cm}$)	10^{13}	150	10^8	10^3
Thermal conductivity ($\text{W cm}^{-1} \text{ K}^{-1}$)	20	5	0.46	1.5
Refractive index	2.42	2.65	3.4	3.5
Hardness (kg mm^{-3})	10^4	3500	600	1000
Johnson figure of merit ($\times 10^{23} \text{ W } \Omega \text{ s}^{-2}$)	73856	10240	62.5	9.0
Keyes figure of merit ($\times 100 \text{ W cm}^{-1} \text{ s}^{-1} \text{ }^{\circ}\text{C}$)	444	90.3	6.3	13.8

scattering of charge carriers from the surface has measurable effects on the transport properties and can dominate the electrical characteristics of the film. The extent of influence of surface scattering depends upon the nature of scattering mechanisms involved, i.e., either totally elastic (specular reflection) or totally inelastic (diffuse reflection), or combination of both [114].

Measurements of resistivity and Hall coefficient are necessary for determining both the mobility and carrier concentration which are generally dependent on surface scattering and thickness of thin films. The film Hall coefficient is usually less than that of bulk material [115]. Hence, errors in measurements can arise from specimen contours; electrode size, geometry, position, and symmetry; and spatial and thickness homogeneity [116].

Two models have been widely used to interpret the electrical properties of elemental polycrystalline thin film semiconductors.

(1) *The Segregation Model*, in which the impurity atoms segregate to the grain boundaries and become electrically inactive [117,118]. The films show enhanced resistivity that they actually have.

(2) *Grain Boundary Trapping Model*, It is commonly characterized by the presence of a potential barrier ϕ_b created by capturing of free carriers [119,120] by the active trapping sites at the grain boundaries. These barriers present obstacles to the transport of carriers between grains, and the conduction is dominated primarily by the thermionic emission. This model was originally developed for polysilicon [119] and was refined later by others [121-123].

The application of these models to polycrystalline diamond films may be useful in interpreting the relevant experimental data and development of its own model for conduction mechanism.

2.10 DEVICE FABRICATION TECHNOLOGIES

For electronic device fabrication, in addition to evaluation of electronic properties of the diamond films, many technological problems are required to be resolved. The main issues are controlled doping of the films, film patterning, and formation of physically stable and ohmic contacts. The diamond films grown without intentional doping are usually good insulators. Semiconductivity may be induced in synthetic diamonds in a variety of ways. However, doping during growth of synthetic single crystal diamonds and CVD diamond films has so far produced only p-type conductivity. The most common method is the introduction of specific impurities such as Be, Al or B for p-type doping to suitable growth mixtures of carbon and solvents [90]. It is also a common method in case of CVD diamond films in which Boron is commonly added into the growth mixture in solid (pure boron powder [58], B_2O_3 [124,98]) or gaseous phase (B_2H_6 [125], Boric acid vapor [126]). Introduction of active impurities by means of ion implantation has also received considerable attention [127-130]. Boron doping through diffusion using a rapid thermal processor (RTP) was demonstrated in a metal-semiconductor field effect transistor (MESFET) with ultra-shallow channel ($\sim 500\text{\AA}$) [131]. The few reports on P doping to induce n-type conductivity [91,127,132] are not very encouraging. The defect sites created by ion implantation of dopants such as C^+ [130], P^+ [127], were found to be responsible for the observed n-type conductivity.

Film patterning is another important issue in the absence of any conventional chemical etchant of diamond. Several reports to pattern diamond films have been published [133,138-141]. Although several distinct techniques have been used but they can be grouped into two broad categories: selective deposition by enhancement [134,135,138] or burying [133,136,140,141] of the diamond nucleation sites and selective etching through oxidation [137,141]. However, most of these techniques have several disadvantages and are not compatible with standard planar IC processes.

Hence, they cannot be adopted directly and a considerable amount of refinement or modification required in each case for actual device fabrication.

Anticipating the high temperature operation of diamond devices, ohmic contacts, which are physically stable on the diamond as well as the substrate surface on which the diamond film are deposited, are an essential requirement. Electrical characterization of contacts of a number of metals with homoepitaxial diamond films has been investigated [142]. Moazed et al. [143] have demonstrated the formation of ohmic contacts using W or Mo that react with diamond at high temperature ($\sim 900^\circ\text{C}$). Indium was found to form ohmic contact without high temperature anneal [144]. Heavily boron doped diamonds ($>10^{19}\text{ cm}^{-3}$) also form ohmic contacts with most evaporated metals without post deposition processing [144]. A novel method of making dual side contacts to a diamond thin film has been reported [145]. Another report dealing with conversion of rectifying contacts to ohmic by damaging the metal diamond interface by ion implantation [146] seems to agree with the argument that every metal contact on the rough semiconducting surface will behave pseudo-ohmic [147]. Homoepitaxial films need special considerations since the same metal contact which is ohmic on polycrystalline diamond surface may turn into a rectifying one [148]. Surface treatment before metalization may have significant effect on the behavior of contact [149]. For interconnects running between diamond devices and to bonding pads in an IC on non-diamond substrate (which is silicon in most cases) pose new challenge. In this regard, the numerous metallization studies involving refractory metals [150,151] for conventional monolithic Si ICs may prove very useful.

Using the technology developed to date, a number of rudimentary devices using natural and synthetic diamonds have been developed. They include a thermistor [37-39], bipolar junction transistor (BJT) [152], Metal-Oxide-Semiconductor field Effect Transistor (MOSFET) [58,153], point contact transistor [154], Schottky diode [154,155], resistors [124] and light emitting diodes [130,155]. However, most of these

devices were barely working models of respective device principles but never demonstrated the clear advantage of diamond properties over the existing devices from conventional semiconductors. This aspect, therefore, emphasizes the need to develop and refine the device fabrication technology preferably in line with the modern state-of-the-art IC technologies.

SEMICONDUCTING DIAMOND FILM SYNTHESIS AND CHARACTERIZATION

3.0 INTRODUCTION

This chapter deals with the synthesis and physical characterization of boron doped semiconducting diamond films produced as part of this dissertation research. After a brief description of the HFCVD system for diamond deposition, two methods used to enhance the low intrinsic nucleation density of diamond on non-diamond substrates namely ultrasonic treatment and diamond-photoresist seeding are discussed. Since the diamond deposition depends upon a number of experimental parameters, section 3.3 covers the influence of various parameters on the diamond growth and their optimization work for the good quality diamond films. Next, the implementation of in situ boron doping and its effect on the quality of diamond films using solid dopants is discussed. Lastly, a critical effect for device fabrication i.e., etching of SiO_2 during diamond growth is analyzed.

3.1 THE DEPOSITION SYSTEM

The diamond films for this research were deposited in a hot-filament CVD system. The system was originally designed and built at Ford Scientific Research Laboratory. Several modifications and improvements were incorporated during the course of

this research to perform certain specific experiments or to improve the reproducibility, growth rate and quality of the films, and ease of system operation. Some salient features of the system are described here to enhance the explanation of the experimental parameters explained later in the present and following chapters.

This HFCVD system is basically an improved version of the system used for initial diamond depositions using this technique by Matsumoto et al. [52]. The improvements are mainly in terms of control and stability of growth parameters, boron doping and flexibility of operation. A simplified schematic diagram of the system is shown in Fig. 3.1. The main vacuum chamber is a 6" hollow cube made of stainless steel provided with openings for flanges on its each face. CH_4 or C_2H_2 , H_2 and CO were used as reactant gases. The flow rate of all three gases is precisely adjustable independently by mass flow controllers. In addition, nitrogen is used to purge and backfill the chamber. A glass view port provides an in situ visual access to the substrate and various components inside the chamber. The pressure of the system is monitored by a baratron pressure sensor which supplies suitable signals through a controller to a downstream valve which maintains the chamber pressure to be within 0.1% of the preset value (up to 100 torr).

The filament is a horizontal array of seven 2" long parallel Ta wires (0.005" diameter, 99.9% pure) spaced at 8 mm. The filament wires are prevented from sagging down on heating by using spring force loaded Mo clips. Ta, in stead of conventional materials such as W or Re, was selected because it was found to be less brittle and more resistant to shocks and vibrations after heating and thus prolonging its operational life time. It has also been found to cause no or vary small metal impurities in the deposited diamond films. The temperature of the filament is monitored by a two wavelength pyrometer and controlled automatically to within $\pm 2^\circ\text{C}$ by a controller using an SCR based power supply. The filament typically draws 25-30 A current at 25-35 VAC at nominal temperature of 2400°C .

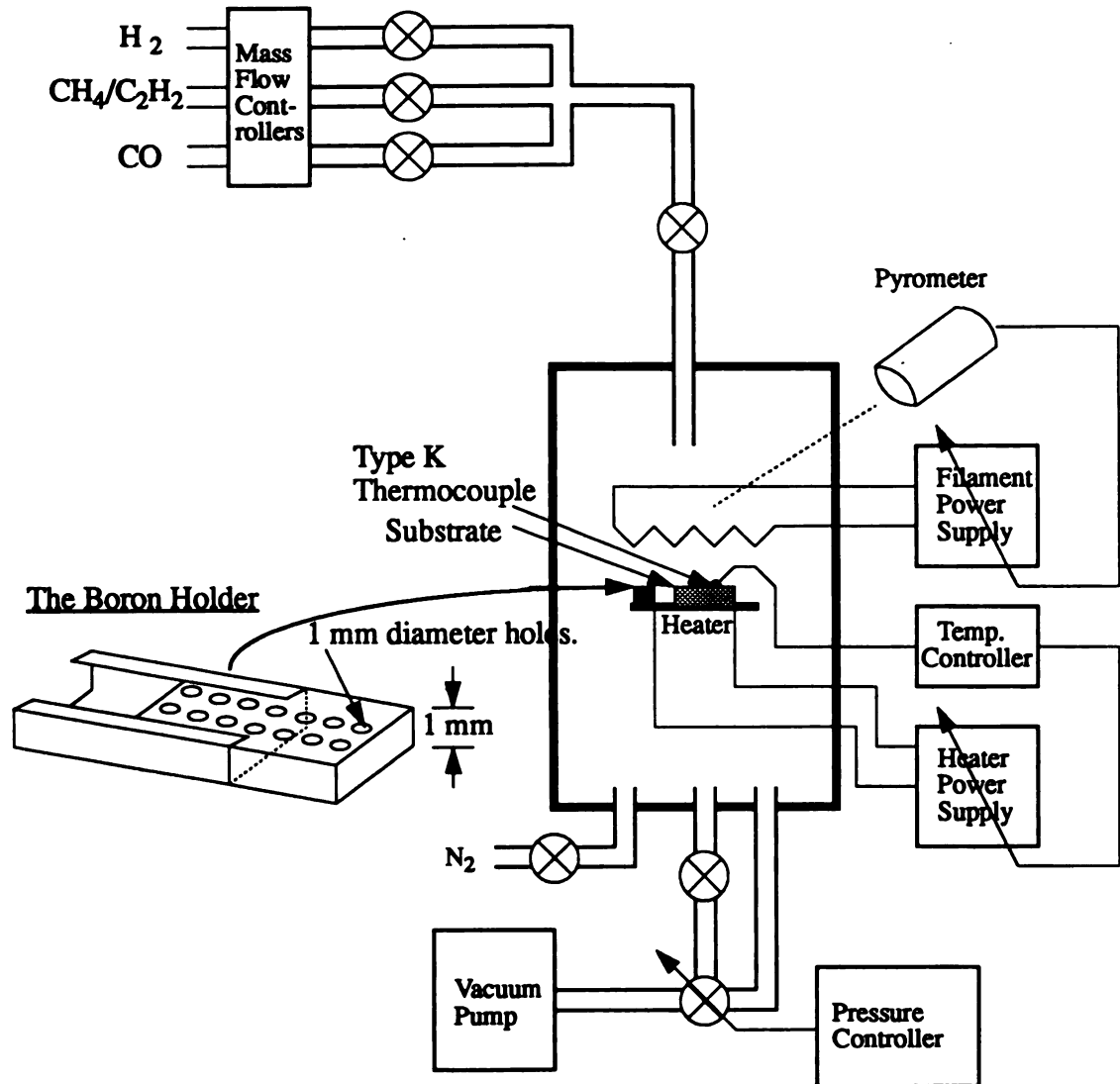


Figure 3.1 A simplified schematic diagram of diamond HFCVD system.

The substrates are placed on a 1¾" diameter Boralectric heating plate (made of BN with graphite heating element embedded inside) below the filament. The heater is supported by a frame with a provision of controlled vertical motion up to 0.75". The controlled vertical movement is important in view of dual requirement of very short and precise (3/16") spacing between filament and substrate during deposition and accessibility of the top surface of heater for handling of the substrates and related components. The temperature of the substrate, an extremely important parameter for CVD diamond growth, is monitored by a type K thermocouple at its top surface. The substrate temperature is controlled to within 1°C of the set temperature by controlling the heater current in a feed back control system through a microprocessor based digital temperature controller. The top surface temperature monitoring is unique in the sense that in almost all cases reported in the literature, the temperature of the back surface is monitored which obviously causes an indefinite error in temperature measurement. The heater typically draws 5-8 A current at about 50-70 Vac to maintain a temperature of 890°C in the presence of filament at 2400°C. It is important to point out here that all the components in the proximity of substrate are made of high temperature compatible refractory metals/ceramics which cause minimal impurities in the deposited diamond films.

The overall system performance is highly reproducible. Though the deposition process is manually started and terminated, yet once started, it can virtually operate in self supervisory mode indefinitely which is important for long duration deposition.

3.2 THE NUCLEATION METHODS

The intrinsic nucleation density for diamond growth on most non-diamond substrate materials is generally very low i.e., 10^4 cm^{-2} . To synthesize a diamond film without voids in a reasonable time duration, there is a need to enhance the existing nucleation density. In this research, the methods of ultrasonic treatment (UT) and

diamond-photoresist (DPR) seeding were used. A brief description of these methods is given here.

3.2.1 Ultrasonic Treatment (UT) Method

It is a widely used method to promote nucleation density for diamond growth on non-diamond substrates [133-135,138]. During this work, a suspension of diamond powder with 0.1 μm size particles in a solution of organic solvents is prepared in a beaker. With substrate placed inside, the beaker is suspended in an ultrasonic bath and agitated for 30 minutes. Following the treatment, the substrate is rinsed with acetone and methanol. The surface of the substrate following the treatment does not look any different than the one without treatment visually under optical microscope (1200X magnification).

3.2.2 Diamond-Photoresist Seeding (DPR) Method

This method to enhance nucleation density for diamond growth is based on the idea of spreading diamond seed crystals, suspended in photoresist, on the substrate surface. During CVD diamond deposition, the photo-resist evaporates in initial stages and the diamond particles act as nucleation sites for the diamond growth. All the developmental work on this method to achieve uniform diamond films with optimally smooth surface was done during this research work.

3.2.3 Comparative Analysis

Both nucleation methods were quite successful in improving the nucleation density. Raman spectra of the diamond films deposited on the substrates nucleated by the two methods, as shown in Fig. 3.2, have strong peak at 1332cm^{-1} . This similarity is indicative of absence of any role of residues of photo-resist in the growth of diamond.

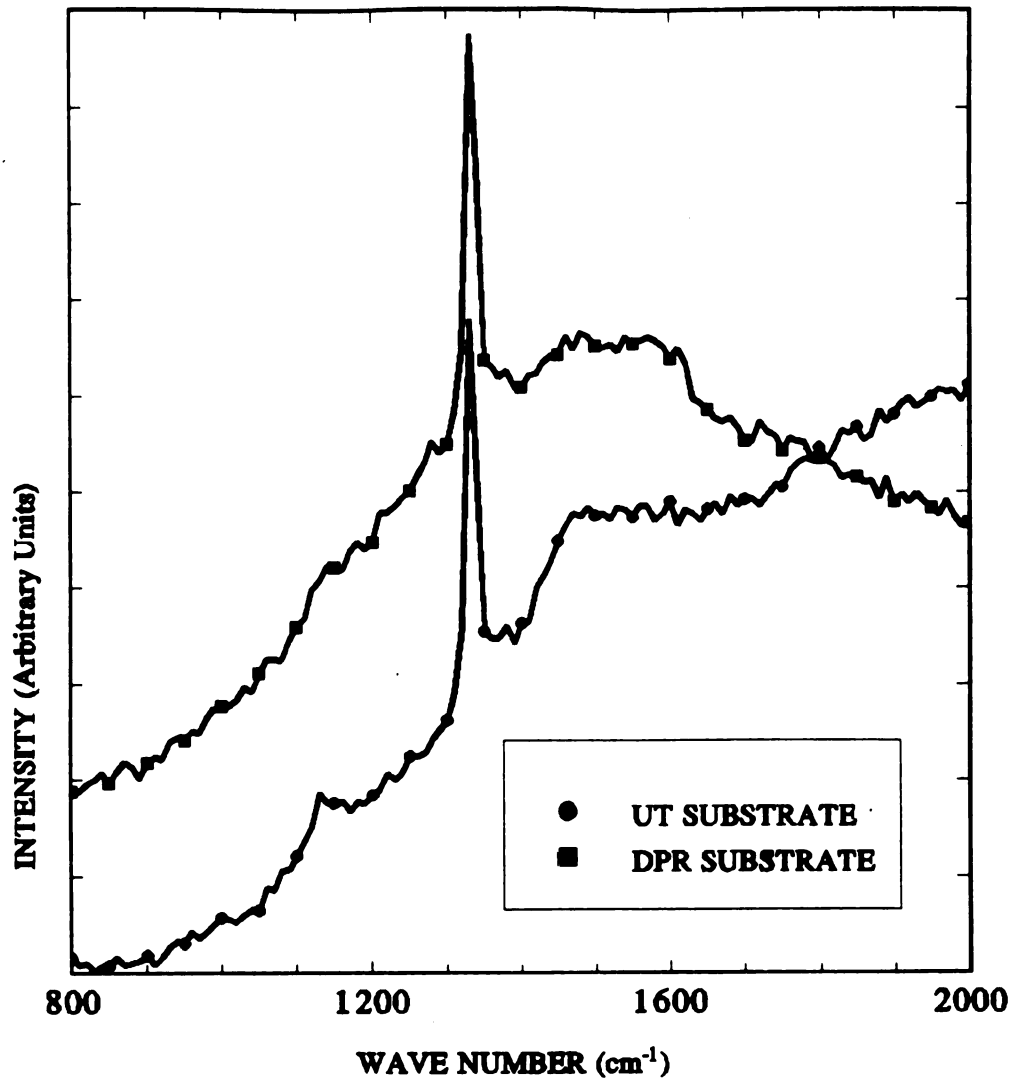


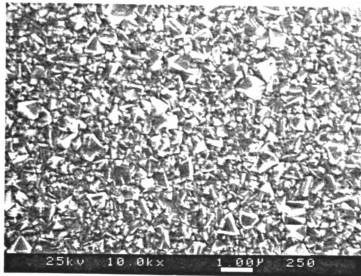
Figure 3.2 Raman spectra of diamond films on oxidized silicon substrates seeded by UT and DPR nucleation methods.

The nucleation density was determined by counting the number of diamond grains in an area of $3\text{cm} \times 3\text{cm}$ on SEM micrographs taken at various parts of a specimen. SEM micrographs of the diamond films deposited on the substrates pre-treated by the two methods are given in Fig. 3.3. Two main differences between the two films are visible. First, the nucleation density of UT specimens was relatively 5-8 times higher than that of DPR specimens which were found to have nucleation density of about 10^8 cm^{-2} . Second, a relatively large variation in the grain size is observed in case of UT specimens. DPR specimen has fairly uniform grain size ($\sim 1 \mu\text{m}$).

Considering the two methods from technological view point, DPR seeding method has following advantages over ultrasonic treatment method:

- (1) Since only the diamond seed particles form the active nucleation sites, the nucleation density and the grain size in the deposited diamond film is easily controllable through the size and density of diamond particles to be suspended in the photo-resist and the spin speed of substrate during photo-resist coating.
- (2) The substrate surface is not scratched or damaged by the seeds or photo-resist. This allows a clean interface between the diamond film and the substrate surface.
- (3) The method is compatible with the lithographic process used in IC technology.
- (4) Since the diamond seed particles do not need to scratch the substrate surface, this method is not dependent on the hardness of the substrate material and equally effective on any substrate.

A major advantage of UT is that it can produce relatively high nucleation density which is, however, not desired in the present case. Owing to these differences, most of the films deposited for electrical measurements were seeded with DPR method.



(a)



(b)

Figure 3.3 SEM micrographs of diamond films on oxidized silicon substrates seeded by (a) UT and (b) DPR nucleation methods.

3.3 DIAMOND DEPOSITION PROCESSING PARAMETERS

Since CVD growth of diamond is essentially in metastable phase, the selection of experimental parameters and their stability throughout the growth process is very important to achieve reproducible high quality diamond films. Specifically, they include reactant gas composition, absolute and relative flow rates of gases, system pressure, substrate to filament spacing, and substrate and filament temperatures. These parameters were varied or fixed as follows to optimize the quality and growth rate of diamond films:

- (a) Filament temperature: 2200 - 2400°C (2400°C)
- (b) Gas composition: H₂, along with one of the carbon sources from methanol, acetone, CH₄ and C₂H₂ in the presence or absence of CO. (H₂, C₂H₂ and CO)
- (c) Substrate temperature: 830 - 950°C (890°C)
- (d) Gas flow rates: CH₄ and C₂H₂: 0.5 - 1.0 sccm; CO: 0 or 12 sccm; H₂: 100 sccm (H₂:C₂H₂:CO 100:0.5:12.0 sccm)
- (e) Chamber Pressure: 50 - 100 torr. (50 torr)
- (f) Substrate to filament distance: 3/16"
- (g) Boron doping source: B₂O₃ or pure boron powder (0.1 - 2.6 mg).

The typical values of parameters used for diamond deposition used in this work are given in the parenthesis. Additional parameters are the choice of substrate material, size and shape and pre-treatment technique.

The aim of varying these parameters is to obtain or verify an optimum condition suitable for the high purity diamond films at fast growth rate with controlled amounts of uniformly distributed boron impurity. The deposited films were characterized by SEM, Raman spectroscopy and surface profiler. The purity of the deposited diamond films were ascertained in terms of absolute ratio of peaks corresponding to diamond (1332 cm⁻¹) and graphitic carbon (around 1550 cm⁻¹) commonly known as sp³/sp²

ratio. The height of each peak was determined by subtracting the background signal from the Raman spectrum using computer routine. The influence of major parameter on the purity and growth rate of the diamond films is described below.

3.3.1 Reactant Gas Composition

Methane and acetylene are commonly used as carbon sources for CVD diamond growth. The role of two gases in providing principle growth species such as CH_3 and C_2H_2 is still not understood and has been discussed in the literature [69,70]. In addition, good quality diamond films have been deposited using other organic solvents [68]. In this research, a number of films were deposited using Methane, acetylene, acetone and methanol, and their effect on the growth rate and the purity was ascertained.

Typical Raman spectrum of the films deposited using each of the four carbon sources is shown in Fig. 3.4. An inspection of these Raman spectra reveal no significant difference in terms of sp^3/sp^2 ratio between films deposited using methane and acetylene. However, the intensity of the Raman signal was generally weaker for the films growth with methane. The films grown with acetone and methanol showed poor diamond quality. Especially in case of methanol, diamond peak was totally absent in most samples. Therefore, acetone and methanol were dropped out of this study in favor of methane and acetylene.

While considering the flow rate of these carbon gases, both methane and acetylene produced good films at lower concentration (0.5 sccm in 100 sccm of hydrogen). However, a sharp deterioration in purity was observed with increase in flow rate in each case.

Oxygen is also frequently used in diamond CVD reaction and has been shown to improve its purity and growth rate [73-75]. However, adding even a small amounts of oxygen resulted in failure of filament. Therefore, an alternative way was adopted and

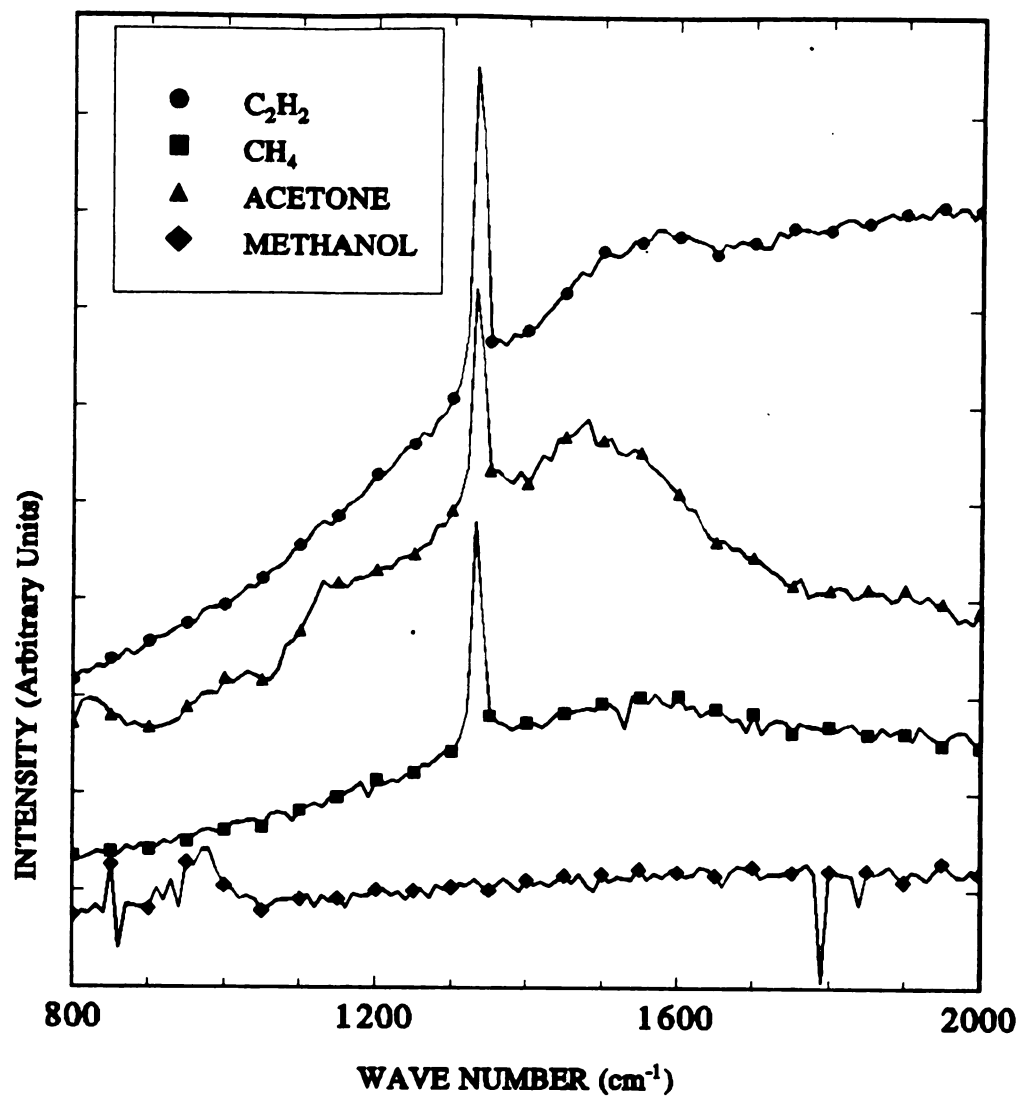


Figure 3.4 Raman spectra of diamond films deposited by using methane, acetylene, acetone and methanol as carbon source.

CO instead of pure oxygen was used. The effectiveness of CO in supplying oxygen or modifying the character of the film can be observed from the Raman spectra, as shown in Fig. 3.5, of films deposited with and without CO. A degradation in purity in the absence of CO is clearly visible from the presence of a large graphitic peak. However, an SEM inspection of the film without CO did not reveal any significant difference.

3.3.2 System Pressure

Generally diamond films are deposited at sub-atmospheric pressures. Though there are reports of diamond depositions over a wide pressure range i.e., 5-700 torr, a pressure <100 torr is commonly used [64]. This indicates that pressure is not a critical parameter. In an effort to increase the growth rate, diamond deposition at various selected pressures in the range of 50-100 torr was done. In SEM inspection, all the films showed well faceted grains with no distinguishable features from film to film. Raman spectra of the films showed more pronounced effect (see Fig. 3.6(a) for sp^3/sp^2 ratio). The purity seems to be largely unaffected by pressure except at 70 torr. A negligible effect with a downward trend with increasing pressure on the growth rate as shown in Fig. 3.6(b) was observed.

3.3.3 Substrate Temperature

Among many deposition parameters, the substrate temperature has a unique significance. Given all the parameters optimized for the good quality of diamond growth, only a small window of substrate temperature ($\pm 20^\circ\text{C}$) supports the optimized quality.

To investigate these effects, a number of diamond films were deposited at different temperatures. The influence of temperature variation on growth rate and the purity of the film as determined by surface profiler and Raman spectroscopy

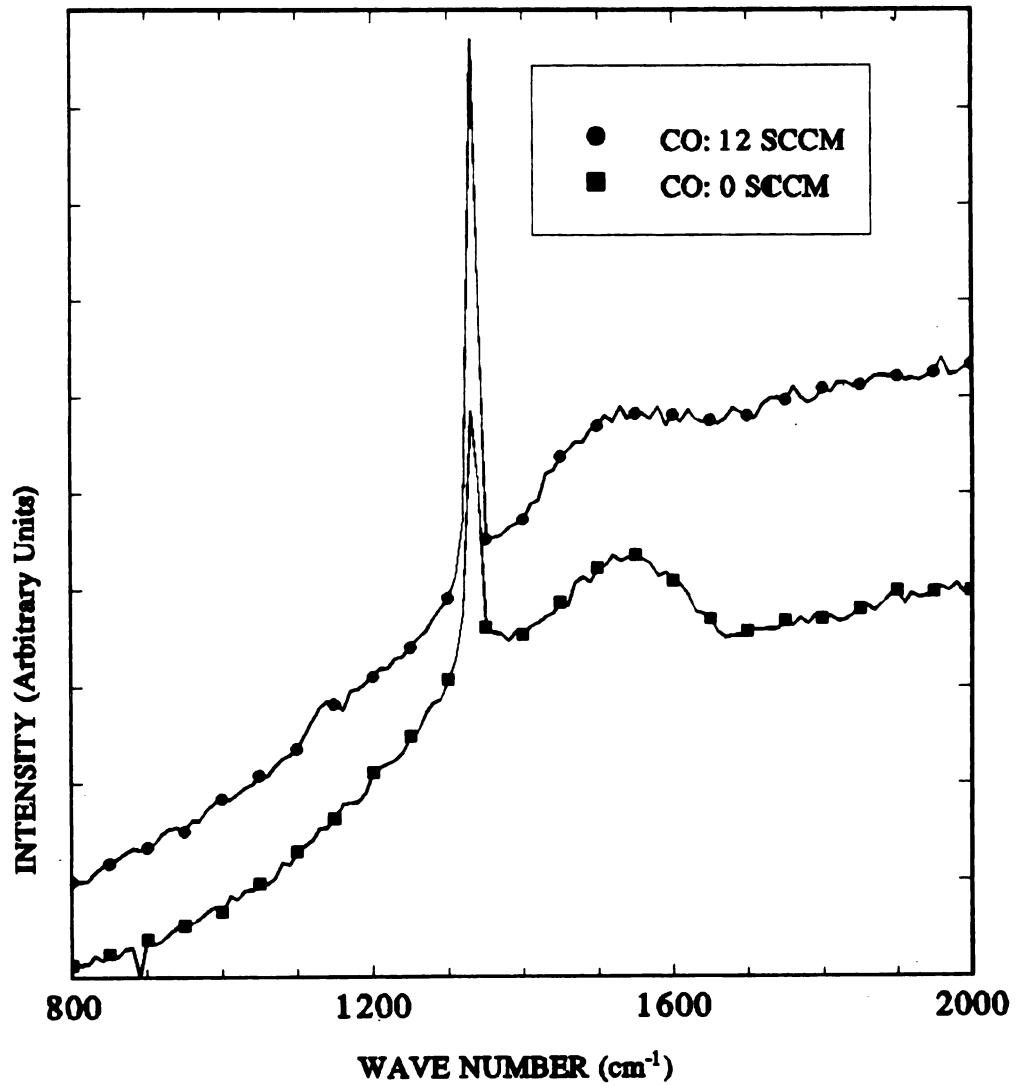


Figure 3.5 Raman spectra of the diamond films deposited with and without CO.

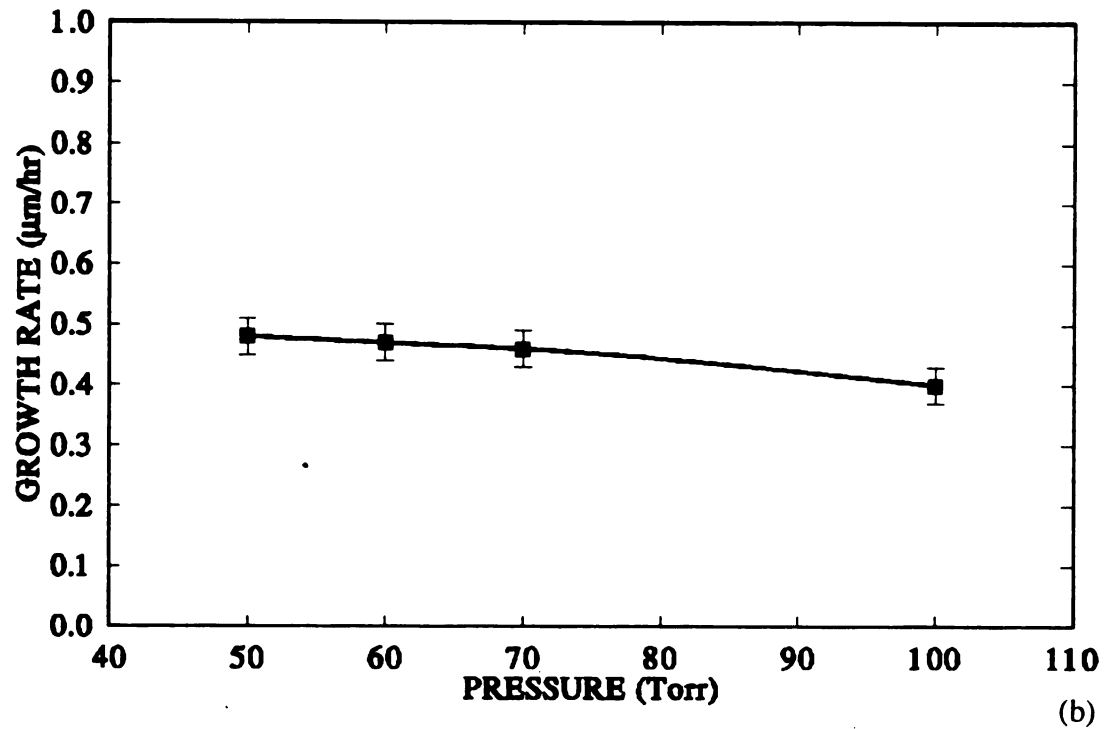
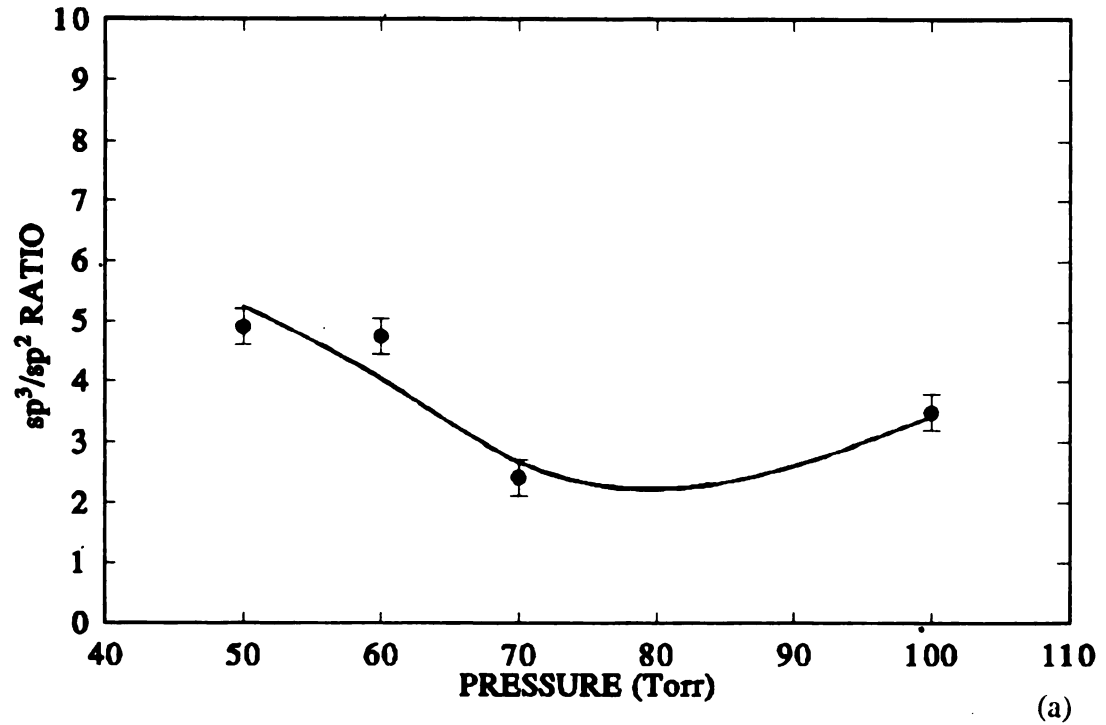
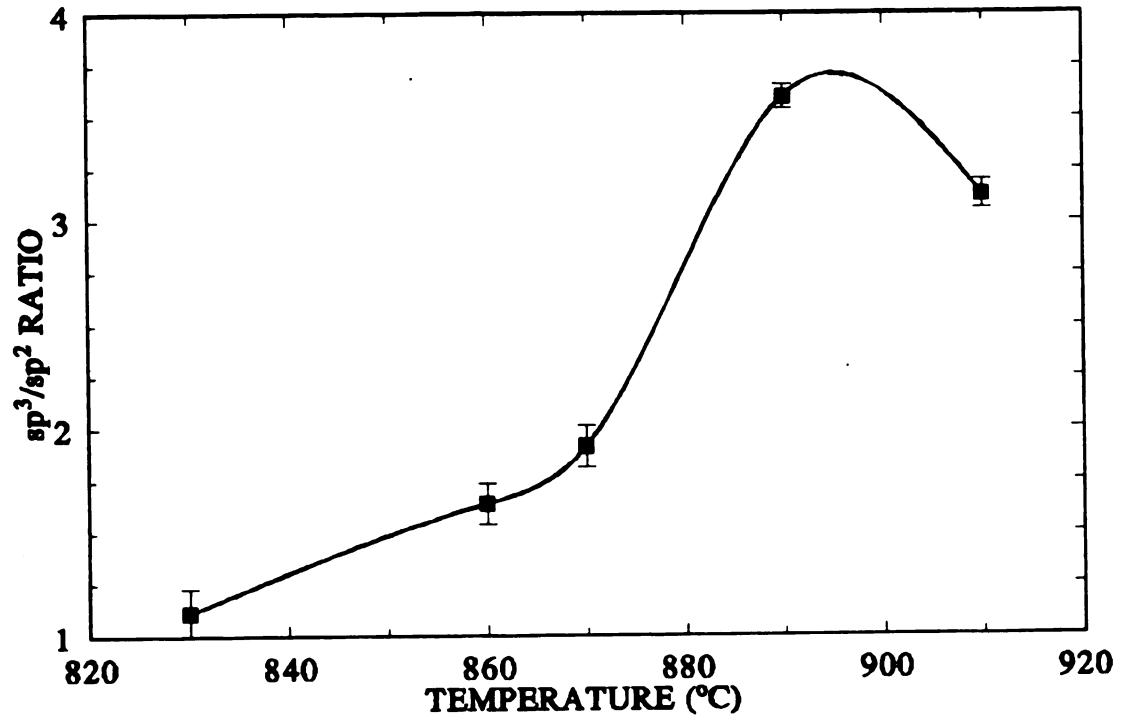
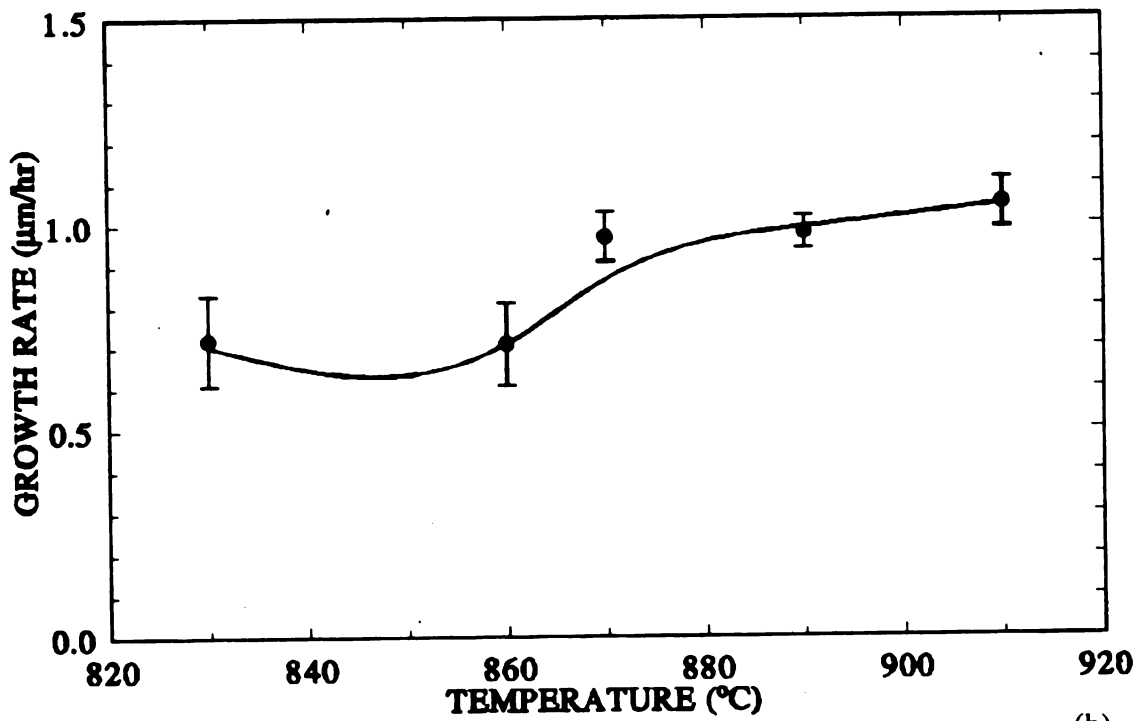


Figure 3.6 Effect of system pressure on the (a) quality (sp^3/sp^2) ratio and (b) growth rate of the diamond films.



(a)



(b)

Figure 3.7 Effect of substrate temperature on the (a) quality (sp^3/sp^2) ratio and (b) growth rate of the diamond films.

respectively is given in Fig. 3.7. A sharp degradation of purity while moving away from the 900°C is clearly visible from the curve in Fig. 3.7(a). However, it should be recognized that this temperature is optimal for a given set of other parameters. The growth rate, as shown in Fig. 3.7(b), despite large error in measurement, has a small upward trend with temperature.

3.3.4 System Operation

The operation of the deposition system primarily consists of sequence of actions to bring up the processing parameters namely gas flow rates, chamber pressure, filament and substrate temperatures to the desired level. However, it was found that the order and time rate of changing a parameter has great influence on the purity and nucleation density of the deposited diamond films. Therefore, a few critical steps in this respect are mentioned here.

- (1) After setting the substrate(s), boron powder holder (if any) and adjusting the filament to substrate surface spacing to 3/16", the chamber is evacuated to <10 mtorr.
- (2) Filament and heater temperatures are brought up slowly in hydrogen environment (>20 torr) in the respective order manually to their desired temperatures. It is important to avoid heavy inrush current or sudden temperature changes especially beyond the desired temperature which may lead to any damage to heater, filament or substrate.
- (3) Carbon sources are switched on only after the substrate temperature is reached beyond 800°C. Below this temperature mostly non-diamond carbon deposits are formed which lead to poor quality films.
- (4) For UT substrates, the substrate temperature is maintained at 850°C for first 15 minutes. A higher temperature at the beginning leads to poor nucleation density apparently by destroying potential nucleation sites. After this period, the

temperature is raised to desired temperature. In case of DPR substrates, this practice was unnecessary since nucleation sites are well defined seed crystals.

- (5) The presence of a very thin conducting carboneous layer on the surface of CVD diamond film surface has been suggested [158]. A simple method was used to remove this layer. In that, only carbon containing gases are shut down and all other parameters are left unchanged, including hydrogen, gas for 3 minutes before the termination of the deposition process. In this period hydrogen, being the preferential etchant, is assumed to etch away the carboneous layer. The effectiveness of this method was verified by conductivity measurement of the patterned films. The films cleaned by this method were treated in the $\text{CrO}_3 + \text{H}_2\text{SO}_4$ solution for 5 minutes. An insignificant change in the film conductivity was observed contrary to indicated in [158]. This fact indicates that films were clean prior to this treatment. If this cleaning procedure is not followed before terminating the deposition process, relatively higher conductivity in otherwise similar samples was observed which is indicative of the presence of this carboneous layer.

After the evaluation of all the experimental parameters individually, a set of values for these parameters is available which could produce high purity films with optimum growth rate. Some of the value individually or in combination are reactor dependent. Therefore, this formulation should be considered more specific to the present deposition system than a general one.

3.4 BORON DOPING

CVD diamond films deposited without intentional doping are usually good insulators. Semiconductivity may be induced by incorporating controlled amounts of suitable impurities. B, Al, and Li are known to act as p-type dopants in diamond [47]. In natural semiconducting diamonds (type IIb) boron has been found to be responsible for low resistivity. Therefore, a number of techniques involving gaseous

(B_2H_6 , $B(OCH_3)_3$) and solid (B_2O_3 , B powder) sources to incorporate boron into CVD diamond films have been devised. Since gaseous doping sources are highly poisonous, only solid sources were considered in this research.

Two solid sources i.e., B_2O_3 and pure B powder through separate techniques were investigated. First, the vapor from saturated solution of B_2O_3 in organic solvents (acetone or methanol) were introduced but this method did not produce good quality diamond films. In the second method high (5N8) purity amorphous boron powder was introduced directly into the chamber. The powder is placed on the substrate holder (heating plate) using a specially designed holder as shown in Fig. 3.1. The holder consists of Mo plate (1 mm thick) with a number of 1 mm diameter holes drilled in it. The plate is inserted in a clip which covers its one face and a selected number of holes are filled with boron powder. One holes takes on an average 0.2 mg of boron powder. The boron holder is placed very close to the substrate (within 1 cm) at a fixed place on the substrate holder for better reproducibility of temperature and, hence, of doping concentration. The temperature of the boron powder is assumed to be equal to the substrate temperature as measured by thermocouple and is not measured independently. The vapor pressure of boron at growth temperature appears to be sufficient to evolve boron vapor for controlled doping the diamond films.

The effectiveness of using solid boron as dopant source is evaluated through SIMS and Van der Pauw [159] measurements. SIMS depth profile of a $3\mu\text{m}$ thick diamond film is shown in Fig. 3.8. The boron concentration is fairly uniform throughout the thickness of the film. Since oxygen plasma was used to sputter diamond films during SIMS scan, the large oxygen signal is assumed to be mainly contributed by the plasma. The source of large signal corresponding to silicon is not clearly known. It is assumed to be contributed by the silicon substrate which was possibly exposed right from the early stages of the scan due to creation of holes by oxygen plasma along the diamond grain boundaries [82]. SIMS of diamond films also confirmed the absence of

any other impurity which can interfere with the electrical measurements or caused by the metallic components of the chamber itself.

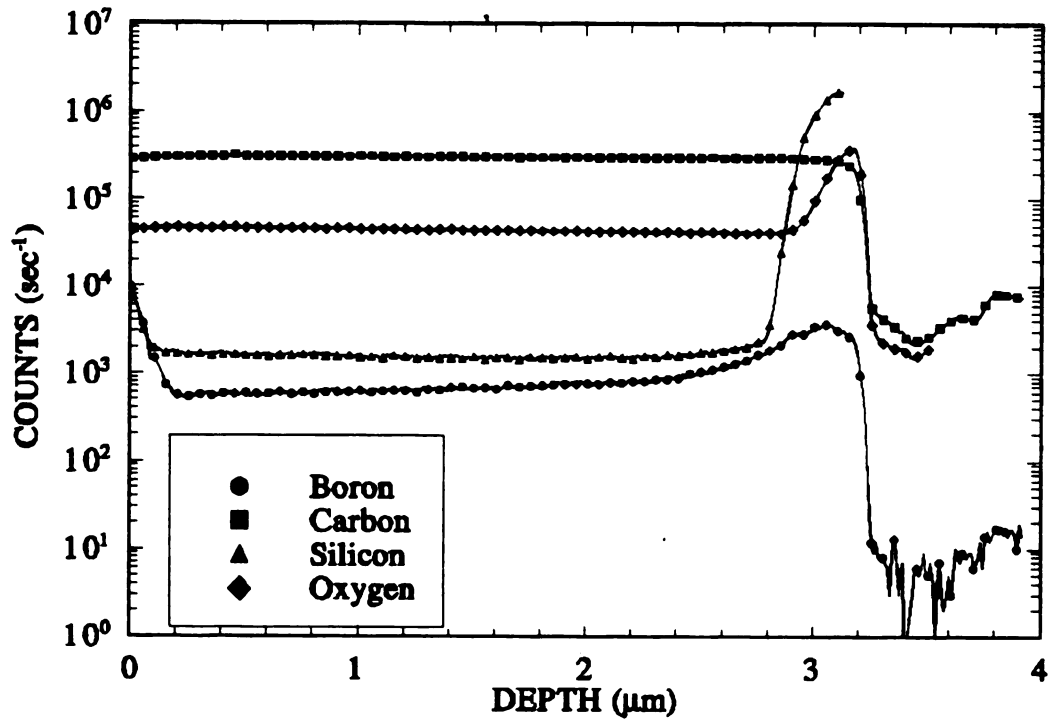


Figure 3.8 SIMS depth profile of a diamond film deposited on oxidized silicon

The Hall concentration measured by Van der Pauw method against quantity of boron powder used for doping the diamond films is shown in Fig. 3.9. The two separate curves in the figure correspond to diamond films deposited directly on oxidized silicon and the films deposited on undoped diamond films as buffer layer. The later samples were annealed at 600°C and 1000°C for 35 and 8 minutes respectively. The Hall concentration varies in the range of 10^{15} – 10^{19} corresponding to 0.1–2.6 mg of boron powder used to dope diamond films. Though quite non-linear, the change in

Hall concentration with boron powder quantity is monotonic in each curve. From the two curves one can see that the Hall concentration is comparable in the two types of samples except in one case. Although there is a some scatter in the data, the controlling of doping through quantity of boron powder appears to hold sufficiently.

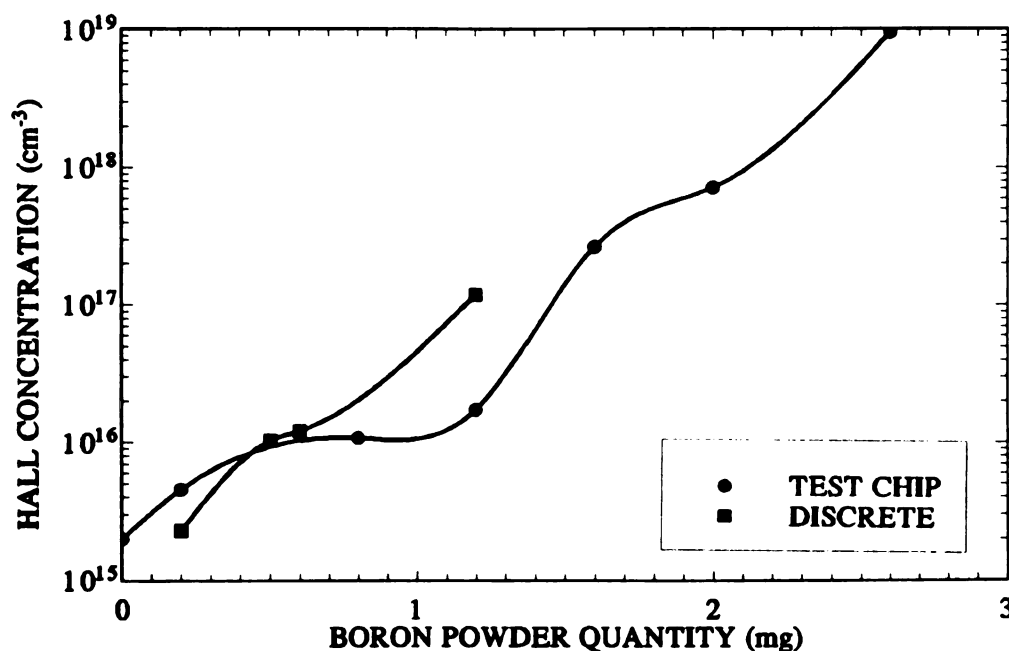


Figure 3.9 Measured Hall concentration at room temperature against the quantity of boron powder used for the doping of diamond films during deposition.

Raman spectra of doped diamond films is shown in Fig. 3.10 and 3.11. The two figures correspond to diamond films deposited directly on oxidized silicon and the films deposited on undoped diamond films as buffer layer respectively. All the films display typical Raman spectra of diamond with a strong peak at 1332 cm^{-1} . To estimate the effect of boron on the purity of diamond films directly on oxidized silicon

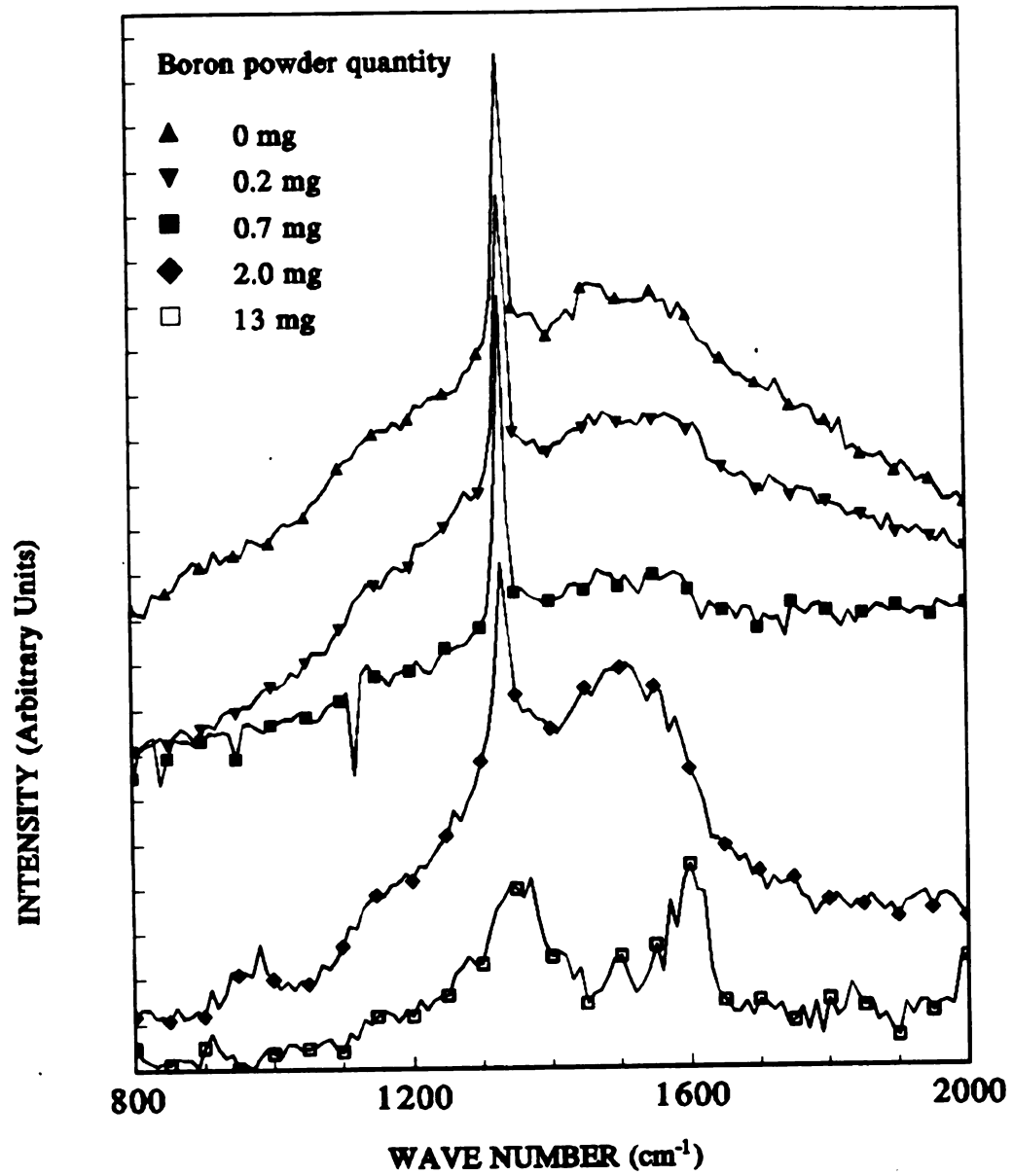


Figure 3.10 Raman spectra of the diamond films deposited on oxidized silicon substrate using various amounts of boron powder quantity.

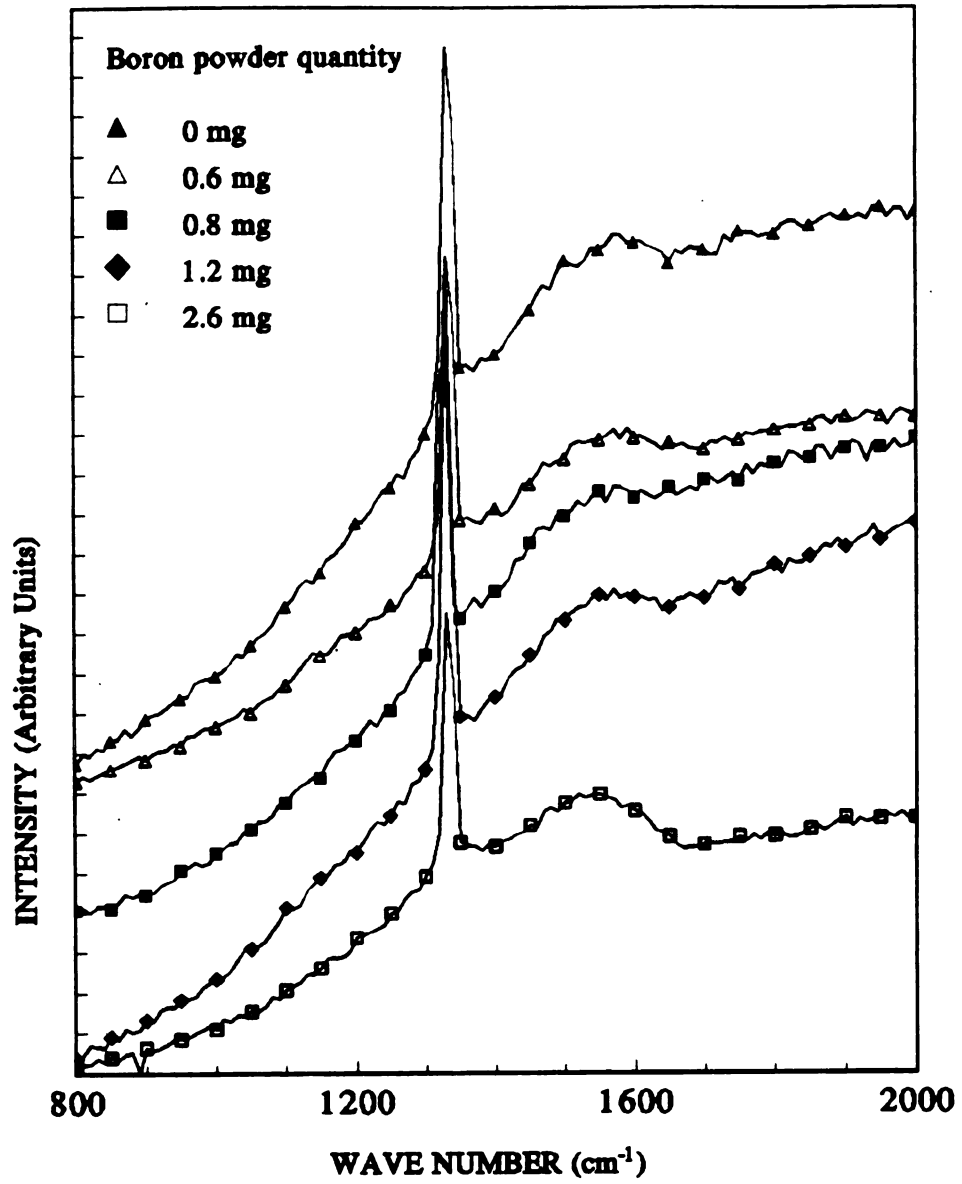


Figure 3.11 Raman spectra of the diamond films deposited on undoped diamond films deposited on oxidized silicon substrate using various amounts of boron powder quantity.

and on undoped diamond film buffer layer, measurements of diamond and graphitic peaks from the Raman spectrum were made. Plots of the sp^3/sp^2 ratio corresponding to two types of films, as given in Fig. 3.12, show an interesting trend. The increasing quantity of boron powder initially improves the purity of diamond, in agreement with others [96], but leads to degradation beyond a certain limit. This limit is reached earlier (at about 0.6 mg of boron powder) and the purity degrades very sharply for the diamond films deposited directly on oxidized silicon substrates. In case of doped films deposited on undoped diamond films, the degradation is much slower and starts at higher boron powder quantity (at about 1.2 mg).

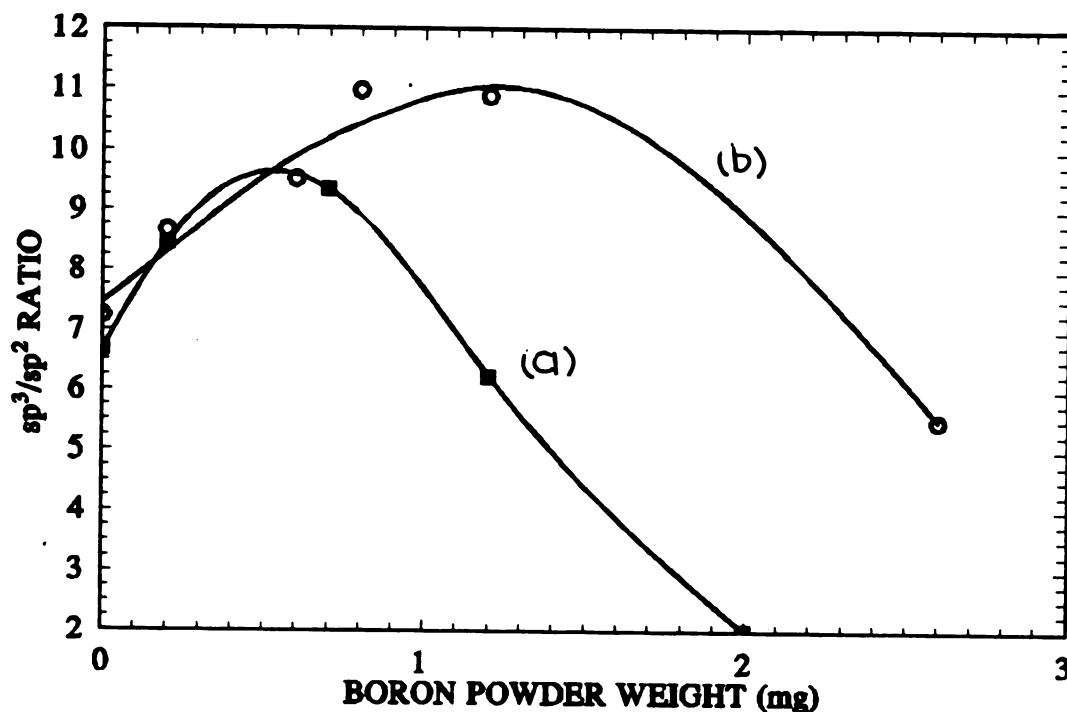


Fig. 3.12 Comparison of the effect of boron powder quantity on the purity of diamond films deposited on (a) oxidized silicon and (b) undoped diamond films.

The purity of doped diamond films on undoped buffer layer is better for comparable amounts of boron powder. Therefore, it is suggested that heavy boron doping is more deleterious in the early phase of diamond growth and does not degrade much the growth on an existing high purity diamond film. As a result of these observations, all the films for the electrical measurements were deposited on undoped buffer layer.

The Raman spectra of doped homoepitaxial films deposited on thin diamond wafers along with a co-deposited polycrystalline film are shown in Fig. 3.13. All the spectra show strong peak at 1332 cm^{-1} . Since the diamond substrates were transparent to illuminating laser light, any clutter around diamond peak is believed to be the signal coming from the specimen holder. Comparing these spectra, two major differences are evident. The intensity of Raman signal (counts/sec.) for homoepitaxial films is much larger than polycrystalline films. The full width at half maxima (FWHM) of diamond peak is much smaller for homoepitaxial films (4 cm^{-1}) than polycrystalline films (12 cm^{-1}). From a short range high resolution scan of the polycrystalline film as shown in Fig. 3.14, an interesting point was observed. The diamond peak was observed to shift by about 2 cm^{-1} . Such a shift is usually attributed to strong internal strain in the material [64]. An important observation to note is that a peak corresponding to Diamond-like Carbon (DLC) or disordered carbon at 1355 cm^{-1} is totally absent which is another evidence of the superior quality of these films.

The doped diamond films were also inspected by SEM for any changes in surface morphology. SEM images of typical undoped and doped films are given in Fig. 3.15. Although the Raman spectra of the two films are similar, a major difference in the grain shape was detected. A sharp edged channels along the edges of most of the grains in doped films can be clearly visible. These are caused by defects in the lattice known as twinning. Also the crystal size tends to increase is size marginally. Beside these observations, both films appear similar. The degradation of film purity while doped by using higher quantity of boron powder can be seen in SEM image, as shown

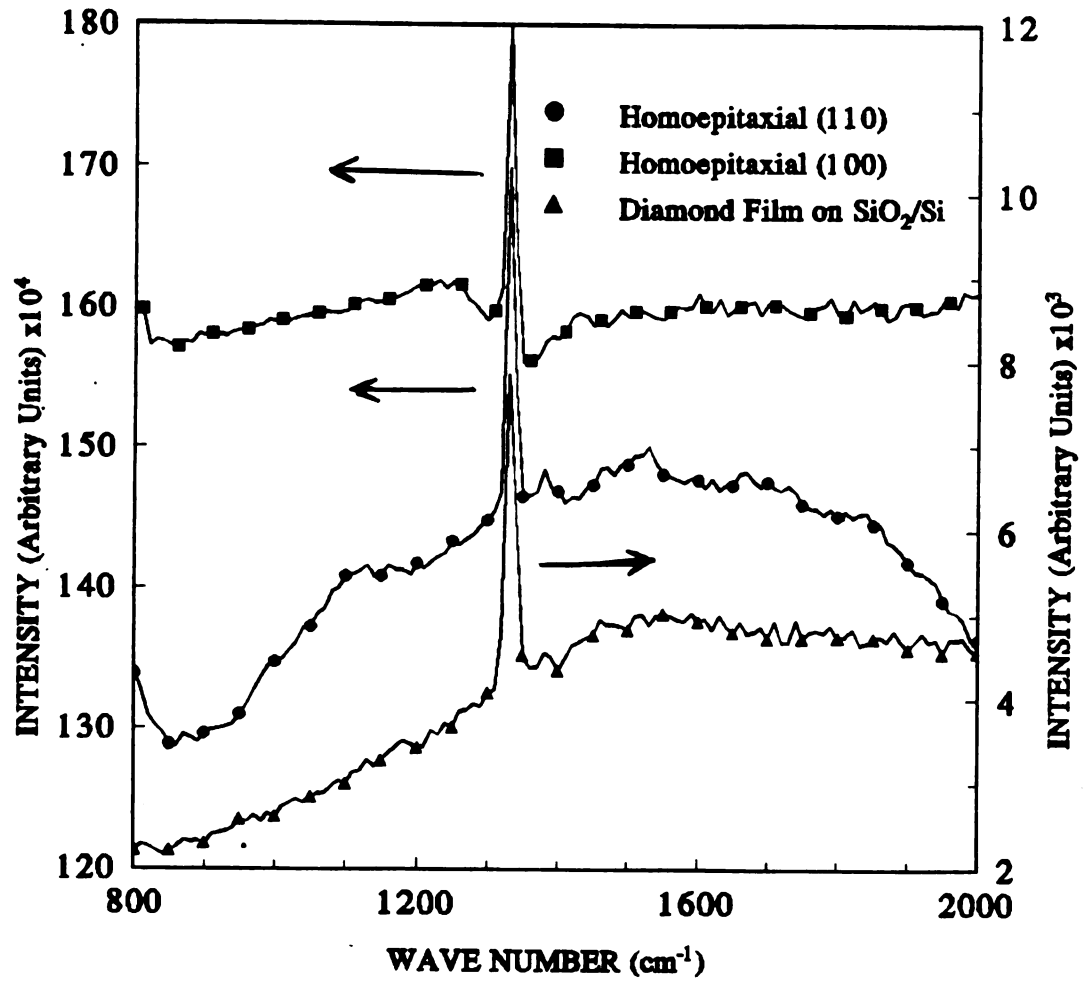


Figure 3.13 Raman spectra of the diamond films deposited on various surface orientation of single crystal diamond and oxidized silicon substrates.

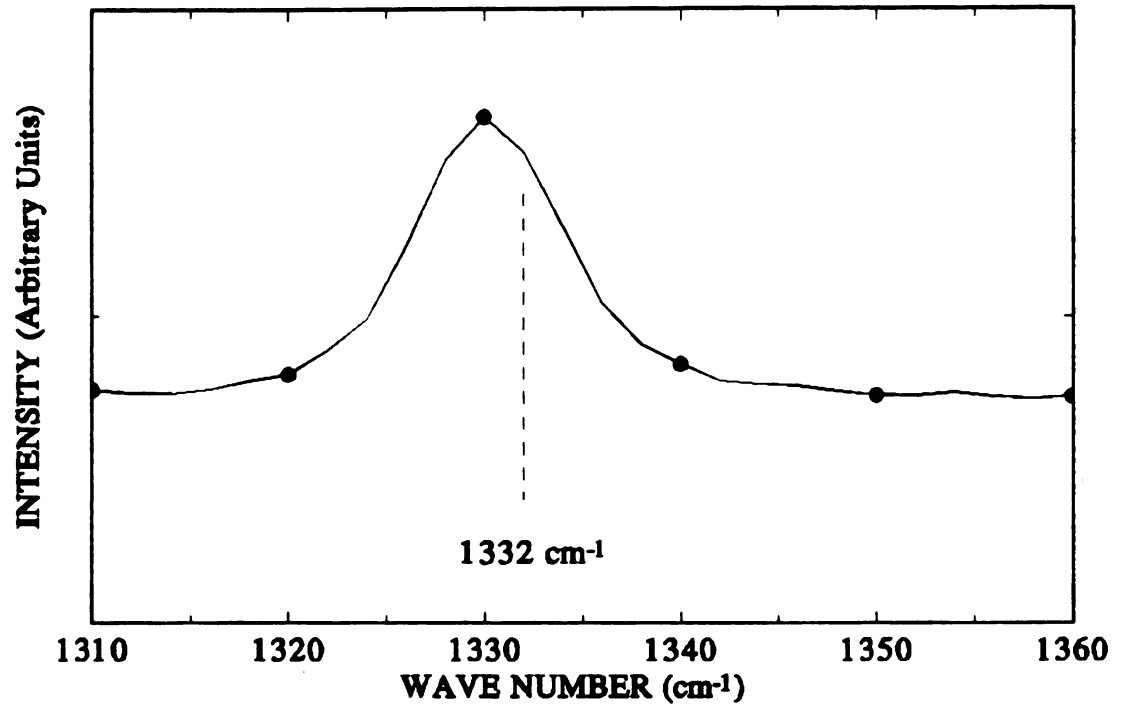
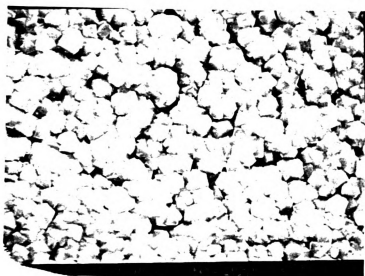
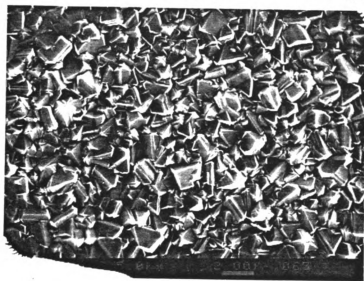


Figure 3.14 A short range high resolution Raman spectrum of a doped diamond film deposited on undoped diamond films.



(a)



(b)

Figure 3.15 SEM micrographs of (a) undoped and (b) doped diamond films.

in Fig. 3.16, of presumably heavily doped film deposited on SiO_2 . The diamond crystals in the film deposited has poorly faceted cauliflower type structure. This kind of crystal shape is usually attributed to poor quality diamond films.

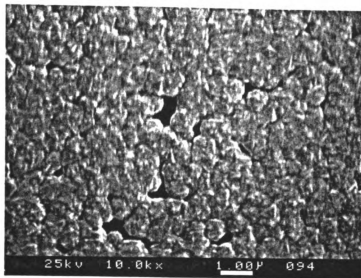


Figure 3.16 SEM micrographs of presumably heavily doped films on oxidized silicon.

3.6 SILICON DIOXIDE ETCHING

Most of the diamond films deposited for device applications were required to be insulated from the substrate materials. Since silicon was used as a substrate material and it is a semiconductor with low resistivity, an insulating overlay of SiO_2 was necessary. It was detected that the oxide was being etched during diamond deposition. Although there are indications in the literature about this effect [54] but no quantitative study has appeared so far. Since the presence of insulating layer is important for the

devices, SiO_2 etching was critically observed. A few observations in this respect are given below.

- (1) The etch rate of Si_3N_4 was found to be about three times that of SiO_2 .
- (2) A comparatively thicker layer of SiO_2 was observed to be etched slower. This effect is shown quantitatively in the Fig. 3.17. The oxide etch rate was determined by measuring oxide thickness before and after diamond deposition. The thickness of the SiO_2 before diamond deposition (at abscissa in Fig. 3.17) appears to have profound effect on the etch rate. SiO_2 layer on so called "dummy wafers" which had spent several months in the oxide furnace in nitrogen ambient, were found to be more resistant to etching than the SiO_2 layer which received no annealing in nitrogen ambient.

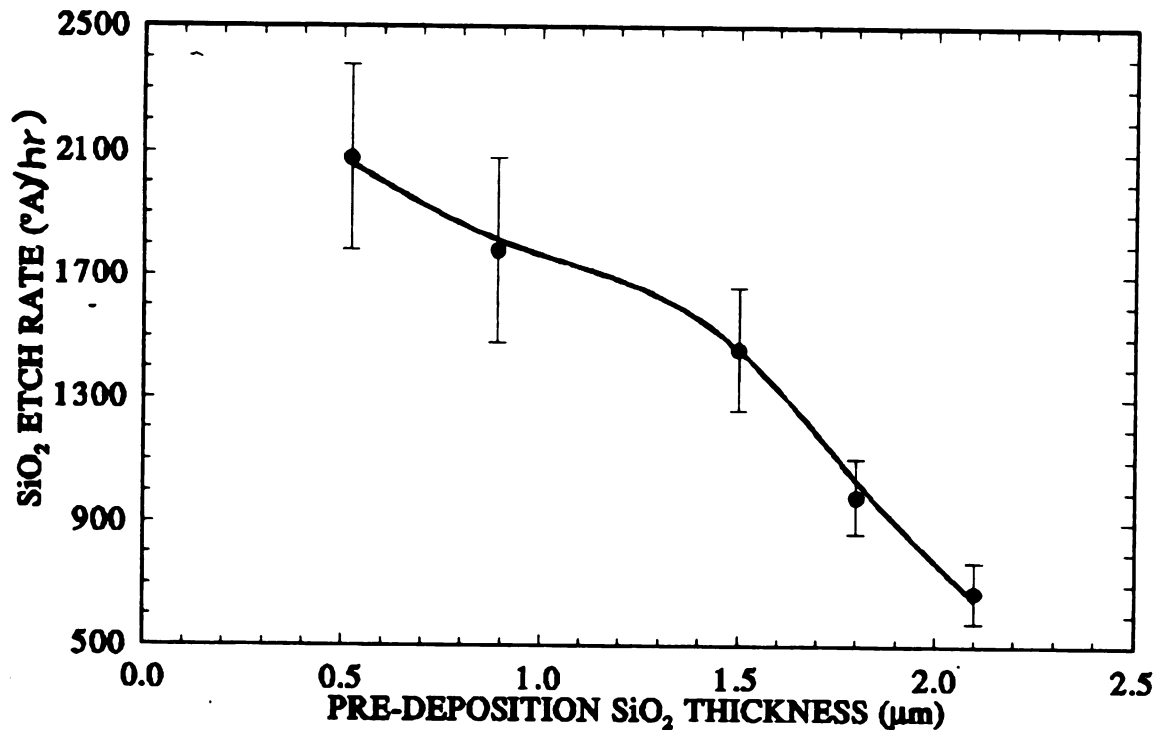


Figure 3.17 The effect of pre-deposition SiO_2 thickness on the etch rate of SiO_2 during diamond deposition.

- (3) Higher filament temperature leads to higher SiO_2 etch rate.
- (4) The etch rate was observed to increase during depositions accompanied with doping.
- (5) Higher flow rates of carbon containing gases lead to higher etch rates of SiO_2 .

In addition to these regular patterns of SiO_2 etching, some non-uniform etching at random was also detected which is believed to be the cause of hot spots created by the irregular combination of the above factors.

3.6 SUMMARY

In this chapter, the study to synthesize and characterize semiconducting diamond film for device fabrication has been presented. The new method of diamond pre-treatment (DPR seeding method) to enhance the low intrinsic nucleation density of diamond on non-diamond substrates was found to be advantageous over conventional UT method. Experimental parameters such as reactant gas composition, relative flow rate of gases, substrate and filament temperatures, pressure and system operation influence the diamond deposition process. Each parameter was optimized for high purity diamond growth at highest rate. Doping of diamond films to induce semiconductivity, essential for electronic devices, was implemented by unique method in HFCVD using solid boron powder as dopant. SiO_2 etching, an undesirable effect for device fabrication, was critically analyzed.

TEST MICROCHIP FABRICATION

4.0 INTRODUCTION

In this chapter, the design and fabrication of a test microchip and heat flux sensor array will be described. Appropriate techniques for patterning and metallization of diamond devices on oxidized silicon were developed before an actual chip fabrication could take place. Three major patterning techniques of diamond films through selective growth and selective etching were developed. An experimental study was conducted to find an appropriate metallization scheme which not only provided ohmic contact with diamond films but also remained physically stable at high temperatures. The heat flux sensors were fabricated on the cylindrical surfaces of a rods made of various materials. Due to non-planar surface, sensor fabrication was done through suitable modifications in planar technology.

4.1 TEST MICROCHIP DESIGN

The test microchip is a multipurpose tool to characterize the semiconducting diamond films and analyze the performance of active and passive electronic devices including MOSFETs and sensors for thermal signals. The size of the chip is 1cm×1cm

and contains four mask fabrication process. These masks are for diamond film patterning, metallization for contacts and interconnects, passivation layer/ gate insulator deposition and metallization for gate contact in the respective order. Fig 4.1 shows a composite overview whereas the individual mask layouts are shown in Fig. 4.2. The smallest feature size is about 160 μm . Although this feature size looks large when compared to modern planar CMOS technology of 0.8 μm , it was sufficient for the proof of concept rudimentary devices built for preliminary research using a new semiconductor material. Each chip was separated by cleaving or sawing (known as dicing) after the diamond deposition. The masks were designed using CAD software and fabricated on 2inch \times 2inch high resolution photographic glass plates (manufactured by Kodak) at Ford's photographic facility.

The design of the test microchip is based on optimizing the utility of devices for multiple applications. As shown in Fig. 4.1, it contains several devices including resistors of various size, geometry and orientation, two MOSFETs and a pattern for Hall measurements. Owing to immediate applications of resistive sensors for thermal signals, most of the devices are primarily resistors. There are three sets of identical resistors of two each i.e., R_1 , R_2 , and R_3 . One element of first two sets has been grouped and placed at the opposite sides of the chip to ascertain the spatial doping profile across the chip. the set R_3 consists of two single square resistors to directly measure the R_{\square} variations with strain, temperature, and doping profile in close proximity. The contact resistance was measured by utilizing the resistors R_1 , R_5 and R_6 . Note that all these resistors have the same contact size and width but vary in length. Thus measuring their resistance can be considered as an alternative to the sliding contact technique [81] for the measurement of contact resistance. The resistor R_7 and R_8 have been put in the design as extreme values to study the effect of geometrical aspect ratio on the observation of physical measurands. The large square pattern in the middle of the chip is meant for van der Pauw measurements.

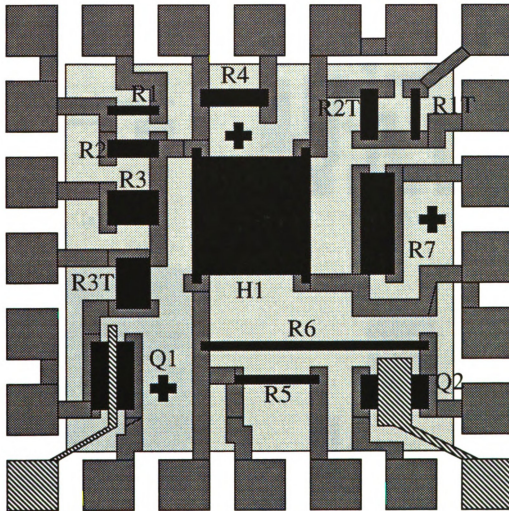
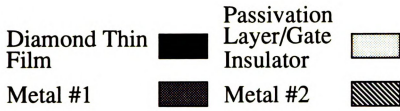


Figure 4.1 Composite mask layout of test micro-chip.

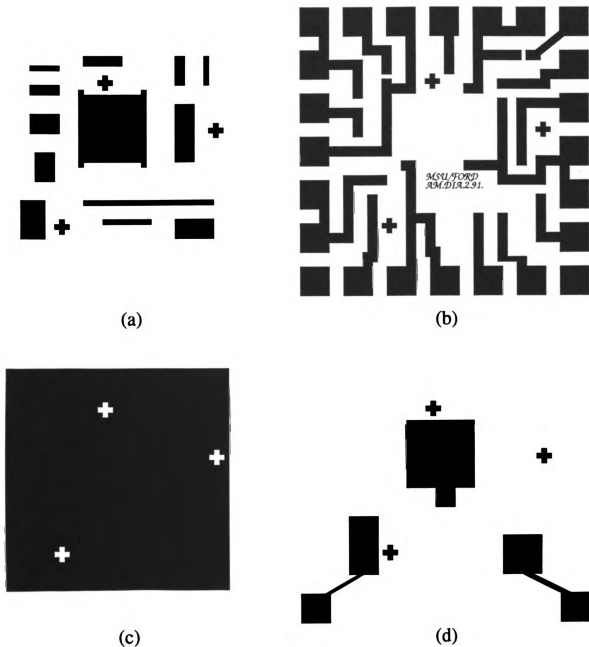


Figure 4.2 Test chip masks for (a) diamond, (b) Interconnect metallization, (c) passivation/ gate insulator and (d) gate metallization.

The width of most of the interconnection lines was 160 μm . There are no interconnections provided between devices on the chip itself. This was done to be able to test all the devices in isolation. The size of bonding pads was kept sufficiently large (1mm \times 1mm) so that they are visible for microprobe access without magnifying aids.

The third mask is to establish a passivation layer and a gate insulator. The insulator layer covers the entire area of the chip leaving out the bonding pads only. The purpose was to protect the devices during high temperature operation in an oxidizing or reactive ambient. The same insulation layer was also meant to act as gate insulator for MOS structures as well. The fourth and final mask, as shown in Fig. 4.2(d) is for metallization of gate contacts.

The following sections describe the development of appropriate techniques for patterning and metallization of diamond films on oxidized silicon for the fabrication of test chips.

4.2 DIAMOND FILM PATTERNING

The primary source of difficulty in direct patterning of diamond films on non-diamond substrates is the extreme resistance of diamond to chemical attack. An alternative approach to etching an existing film is to actually grow a patterned film through selective nucleation. Although many attempts employing varying methods of patterning of diamond films on non-diamond substrates through selective nucleation have been reported [133-136,138], these have not achieved sufficient selectivity. In most cases, a focused ion beam has been used to selectively enhance [136] or suppress [133,134] diamond nucleation sites which resulted in badly damaging the substrate surface. It is clearly undesirable for IC processing. Moreover, some of them were complex to implement [135]. None of these methods was developed to a point that it could be adopted directly. Therefore, there was a need to develop techniques for patterning the diamond films which should be simple in implementation, achieve good

selectivity and resolution, do not deteriorate the film quality and thickness uniformity and above all are compatible with the existing integrated circuit fabrication technology. Consequently, three major techniques which involved both selective nucleation and selective etching of diamond film were developed. These techniques not only preserve the high quality of the substrate surface but are also compatible with the existing integrated circuit fabrication technology.

The patterning techniques developed during this work can be subdivided into two major groups as shown in the tree structure in Fig. 4.3, that is, selective etching and selective deposition. The selective etching of diamond films on non-diamond substrates was implemented for the first time during this research. The specific details of each method are illustrated below.

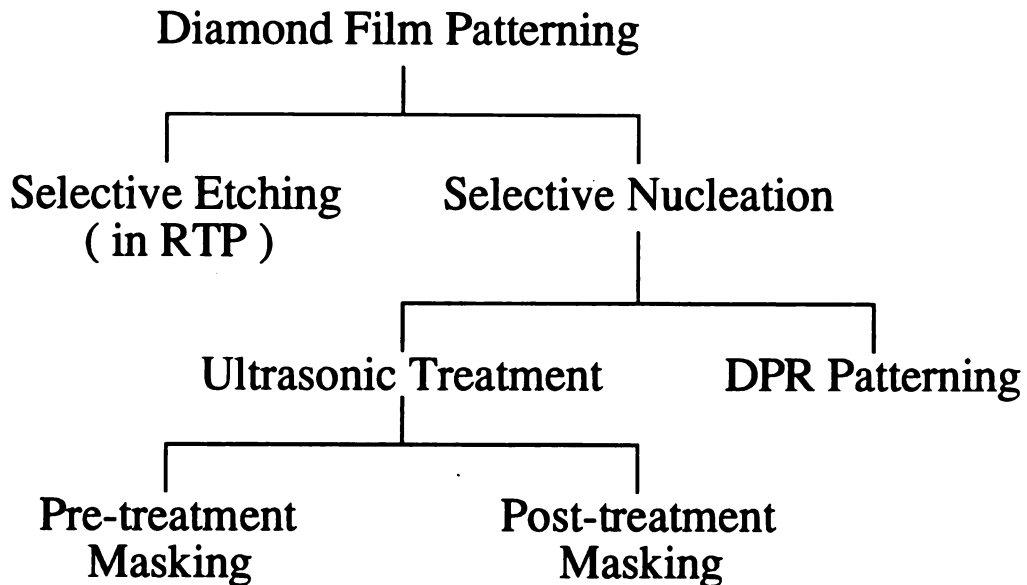


Figure 4.3 The hierarchal layout of diamond film patterning techniques.

4.2.1 Selective etching

All of the techniques of patterning CVD diamond films on non-diamond substrate reported so far are limited to the selective nucleation based on suppressing [135] or simply burying nucleation sites [134]. The only known method of patterning through selective etching is for homoepitaxial diamond films [137]. For polycrystalline diamond films on non-diamond substrates, a simple patterning technique based on selective etching of diamond films through oxidation was developed. However, the challenge was to control the etching at high temperature. A rapid thermal processor (RTP) was used for this purpose. High purity oxygen was passed over the diamond films during the etching process.

The onset of etching was found to be at approximately 650°C, with etch rates increasing at higher temperature. However, the etching, as observed through SEM, was highly non-uniform and this non-uniformity increased with etching time. SEM micrographs of the diamond films etched for various length of time have been shown in Fig. 4.4. One can observe that the etching starts with erosion of sharp edges and along the grain boundaries (Fig. 4.4(a)). Then holes start to emerge through the films mostly along grain boundaries (Fig. 4.4(b)). These holes reach the underlying substrate while most of the film is still intact (Fig. 4.4(c)). The cross sectional view of Fig. 4.4(c), as shown in Fig. 4.4(d), shows this effect more clearly. These holes keep widening with time, as shown in Fig. 4.4(e) and its cross sectional view in Fig. 4.4(f) where only skeleton of film is left, and ultimately the whole film disappears. The thickness of the films was measured through cross sectional views of SEM micrographs and surface profiler. Fig. 4.5 shows etched thickness against etching time of diamond films oxidized at 700°C under flowing oxygen. From the linear part of the curve, the etch rate was computed to be ~5 nm/sec. It is also easy to identify that the fast etch rate and the small thickness of the diamond films ($\approx 2\mu\text{m}$) dictates the use of an RTP. Conventional heat treatment time cannot be controlled with sufficient precision.

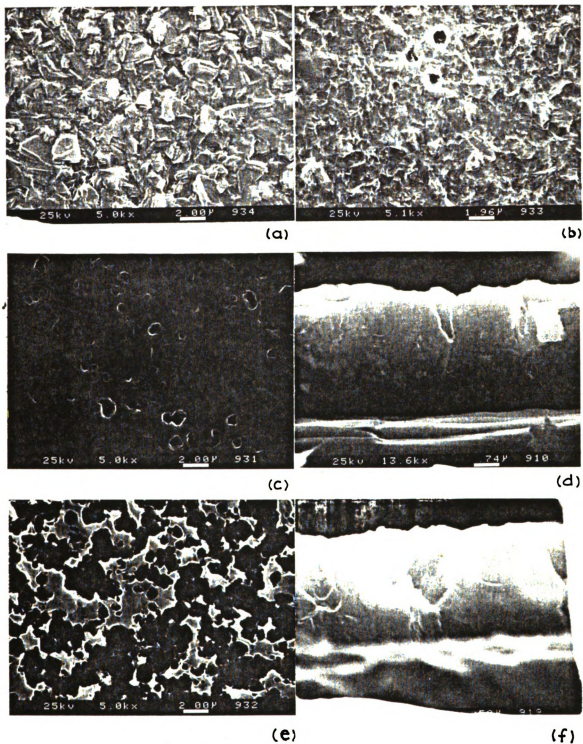


Figure 4.4 Undoped diamond films on silicon etched in RTP at 700°C for (a) 30 seconds, (b) 80 seconds, (c) 120 seconds and (e) 220 seconds. The cross-section view of films shown in (c) and (e) are shown in (d) and (f) respectively.

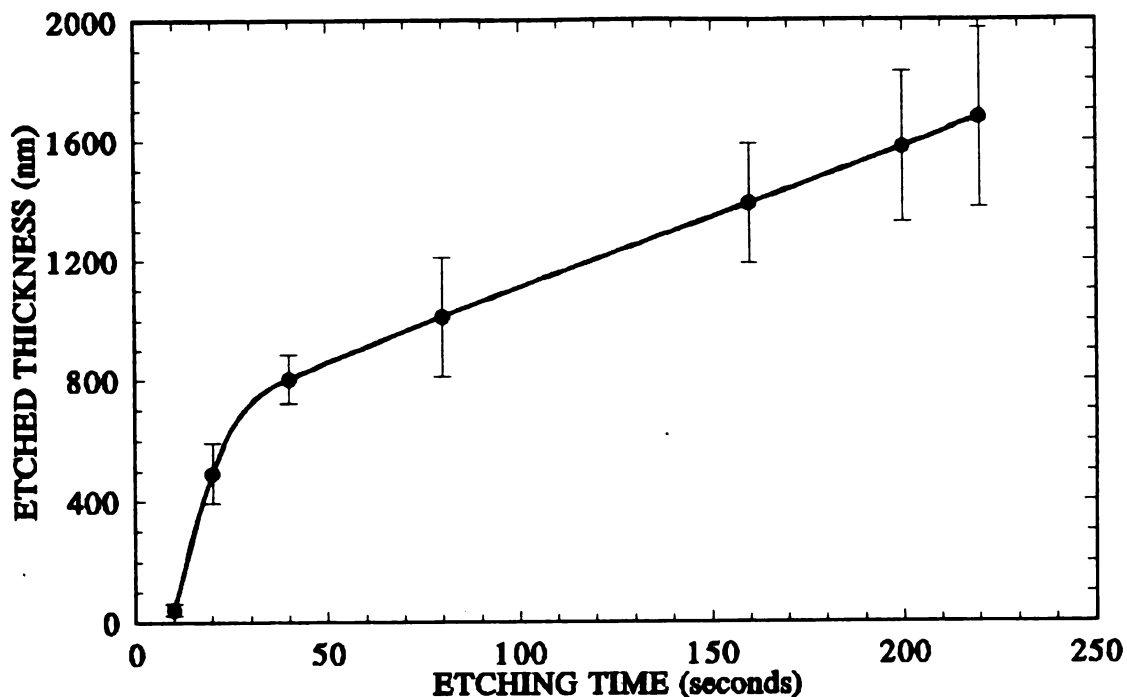


Figure 4.5 The plot of etched thickness against etching time of diamond film thickness in RTP at 700°C under an oxygen flow of 40 sccm. The increasing size of error bar is indicative of highly non-uniform etching.

A number of material including Ni, Pt, Ti, SiO₂ and Si₃N₄ were tried as masks. However, even those metals possessing a high melting point did not withstand the rapid thermal treatment and delaminated from the diamond film surface or formed their own oxides (e.g., Ni and Ti) which were hard to remove after the etching. Only Si₃N₄ deposited through low temperature plasma CVD was found suitable for this application. After establishing the etch rate, the diamond films, selectively masked with Si₃N₄, were etched at 700°C. The sequence of steps followed in this patterning technique is shown schematically in Fig. 4.6. The Si₃N₄ masking layer with a thickness of 0.88µm was deposited at 150°C by low pressure chemical vapor deposition method,

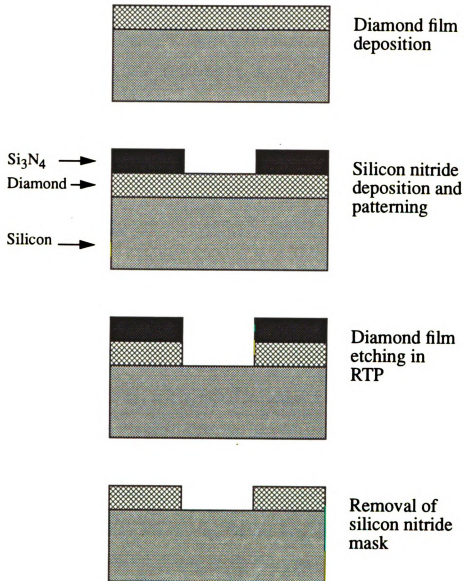


Figure 4.6 The schematic diagram of diamond film patterning technique through selective etching in RTP.

patterned by standard photo-lithography, and annealed at 500°C in nitrogen ambient for 30 minutes. To prevent the substrate and the masking layer from suffering thermal shock, the samples were heated to 450°C, still well below the onset of etching, before raising the temperature quickly to 700°C. The masking layer remained stable during oxygen etching and was later removed by dissolution in 50% HF. Fig. 4.7 shows micrographs of a selectively etched diamond film. As seen in the figure, the diamond film is completely removed from the etched locations without any damage to the film under the masking layer. An insignificant amount of underetching was observed.

4.2.2 Selective Deposition

The selective deposition was achieved through two main techniques namely ultrasonic treatment (UT) patterning and DPR patterning. The patterning through selective nucleation depends on generation of two areas on the substrate surface which have many order of magnitude difference in nucleation density. Since the conventional nucleation techniques lead to the generation of random nucleation sites and wide variation in grain size on non-diamond substrates, the effects of substrate material, surface condition and crystal orientation on the diamond nucleation was first explore through the following two experiments.

In the first experiment, silicon was used as a substrate material and its intrinsic nucleation density for diamond growth on several crystal orientation was acquired. For this purpose, grooves and craters of various geometrical shapes ranging from 1 to 10 μm^2 were created on the silicon (100) surface by micromachining through anisotropic etching using diluted solution of 30%KOH in water. This process exposed many additional well defined crystal orientations. These substrates were used for diamond film deposition both with and without pre-treatment by fine diamond powder in an ultrasonic cleaner. No substantial orientation dependent growth was observed on these samples.

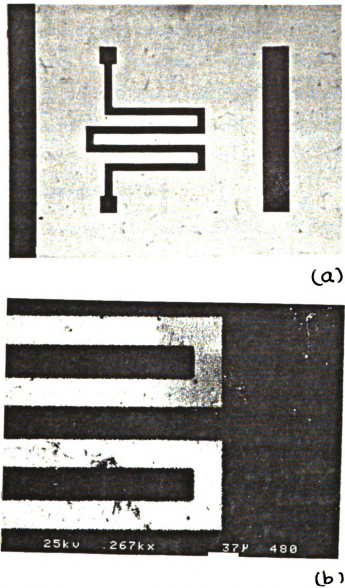


Figure 4.7 Diamond films patterned by selective etching at 700°C in RTP. The patterns in (b) is close up view of (a).

In the second experiment, diamond growth on the surface of various materials like polycrystalline silicon, Pt, Ni, and Si_3N_4 was investigated. No worthwhile nucleation on untreated substrates was observed. All substrates showed very low intrinsic nucleation density which substantially increased after UT treatment. Pt and Ni had relatively higher nucleation density than Si_3N_4 . All the thin films such as Pt, polycrystalline silicon and Si_3N_4 were unstable during diamond deposition.

4.2.2.1 Ultrasonic Treatment Patterning

In the ultrasonic treatment (UT) patterning method, the specimens were treated ultrasonically by fine diamond particles in order to provide a high density of nucleation sites for diamond growth. The associated patterning, as shown in fig. 4.8, was accomplished in two ways. In the first method, the surface was masked with a patterned layer of SiO_2 or Si_3N_4 that shielded the masked regions from ultrasonic bombardment by the diamond particles. This secondary layer was then removed before diamond growth. In post-treatment masking, the entire specimen was treated and then selectively masked just before depositing the diamond film. In the latter case, the masking layer suppressed the nucleation by burying the nucleation sites during the diamond growth.

In UT patterning, the treatment time depends on the desired nucleation density. However, in the pre-treatment masking technique, the treatment time along with the particle size in the diamond powder determines the required thickness of the masking layer. Electron beam evaporated Ni film (4000°A in thickness) failed as an effective mask. Despite being a relatively soft metal, an aluminum film (1.1 μm in thickness) deposited by thermal evaporation was partially successful such that the masked area exhibited a considerably lower nucleation density (see Fig. 4.9(a)). After several experiments with SiO_2 and Si_3N_4 , a minimum thickness of 0.6 μm of SiO_2 or 0.4 μm of Si_3N_4 were found to be effective masks for 30 minutes of ultrasonic bombardment with 0.1 μm diamond powder. Fig. 4.9(b) shows the diamond film patterned using 0.81

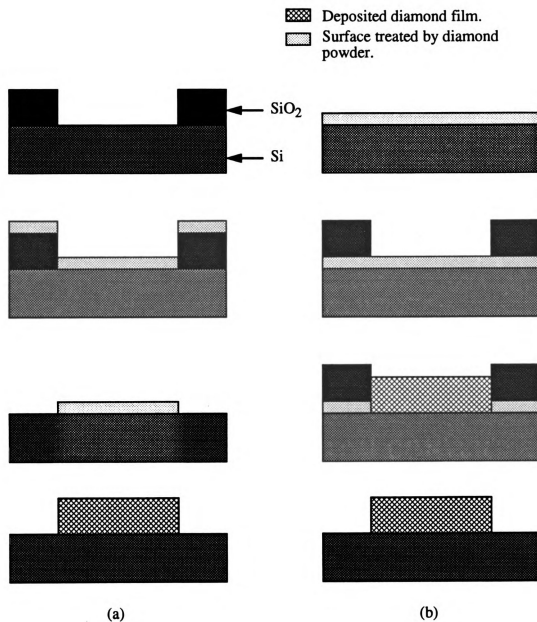
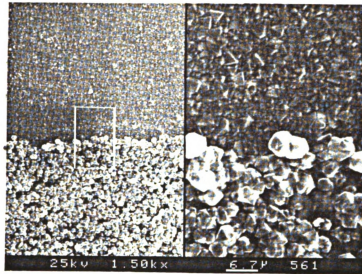
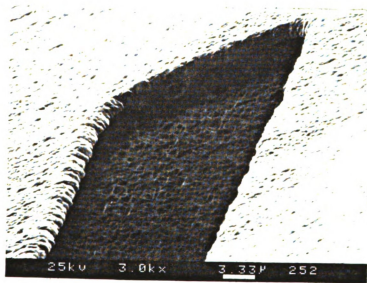


Figure 4.8 Schematic diagrams of selective diamond nucleation technique by UT using (a) Pre-treatment masking and (b) Post-treatment masking.



(a)



(b)

Figure 4.9 SEM micrographs of diamond films patterned by UT method using pre-treatment masking. The masks used were (a) Al film (1.1 μm) and (b) thermal SiO_2 (0.88 μm).

μm thick SiO_2 masking layer. The ultrasonic treatment leaves a large number of diamond particles sticking to the surface and some of them transfer to the masked area following the removal of masking layer. Most of them could be removed by ultrasonic cleaning in acetone.

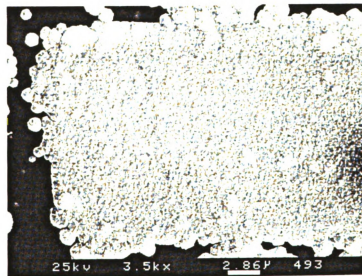
In case of post-treatment masking method, both an annealed Ni film ($1 \mu\text{m}$ in thickness) and a SiO_2 layer ($0.44 \mu\text{m}$ in thickness) were found suitable as masks. However, the handling associated with the deposition and patterning of the masking material on the specimen surface after UT degraded the uniformity and the density of nucleation. Fig. 4.10 shows two SEM micrographs of diamond films patterned through this technique. A degradation in uniformity of nucleation density is clearly visible in Fig. 4.10(a). Also the effectiveness of the masking layer was in question for long duration deposition. Due to these difficulties and the complexity of the process, it was rarely used for patterning of diamond films on non-diamond substrates. However, it seems to be the only viable method for selective homoepitaxial deposition of diamond films [58,139].

4.2.2.2 Diamond-Photoresist Patterning

Patterning by photo-resist mixed with fine diamond powder using standard photo-lithographic process is referred to as diamond photo-resist (DPR) patterning method. In this method, fine diamond particles act as seeds for the growth of diamond only in the patterned areas. However, in the initial experiments, the density of diamond nucleation and the thickness of diamond film was found to be grossly varying across the specimen surface. This effect was attributed to uneven spread of diamond seed crystals. Since the grain size and the density of the associated grain boundaries have a great influence on the properties of diamond films [164] it was necessary to control the nucleation density itself and its uniformity over the substrate surface. The film properties such as carrier mobility, thermal conductivity have been shown to degrade with



(a)



(b)

Figure 4.10 SEM micrographs of diamond films patterned by UT method using post-treatment masking. The masks used were (a) Ni film (4000 $^{\circ}$ A), (b) CVD SiO₂ (4400 $^{\circ}$ A).

decreasing grain size [164]. The homogeneity and surface smoothness is found to be better for small grain size films especially of small thickness. To meet the opposing demands, a grain size of $\sim 1 \mu\text{m}$ was considered to a good compromise.

When diamond powder was initially mixed in the photo-resist, it formed large clusters and when seeded by this DPR, these clusters led to highly inhomogeneous diamond film with a very uneven surface. To break these clusters, the diamond powder was initially dried at 60°C for 2 hours on a heating plate and then mixed in the photo-resist thinner (because of its low viscosity it forms more homogeneous suspension than photo-resist itself) and stirred magnetically for 15 minutes followed by 15 minutes ultrasonic agitation. This suspension was then mixed in the photo-resist and further stirred and ultrasonically agitated for 15 minutes each. This photo-resist was then coated on the Si substrate, inspected under SEM, deposited diamond on it, and re-inspected by SEM. The density of clusters was found to be negligible.

To optimized the deposited film thickness and surface uniformity and control the grain size, a number of samples, as listed in Table 4.1, using DPR seeding were prepared. These samples are grouped according to the quantity of photo-resist thinner and diamond powder mixed in 42 ml of the photo-resist. Following observations were recorded during SEM inspection of diamond films deposited on samples indicated in parenthesis.

- (1) Higher spin rate leads to lower nucleation density but higher uniformity (group A).
- (2) A photo-resist adhesion promoter such as (HMDS) improved the uniformity of nucleation density (group A). To improve PR adhesion, HMDS was applied by spin coating at 3500 rpm followed by baking at 80°C for 20 minutes prior to the application of DPR.
- (3) A higher initial spin speed leads to non-uniformity and clustering. The initial ramp up instead of sudden switching to ultimate spin speed appears to give

relatively more uniformity in nucleation distribution (group B)

- (4) Using a diamond photoresist which has rested for several hours leads to less clusters than a freshly agitated one (group C as compared to group B). The difference between the samples of group B and C is that the latter were spin

Table 4.1 Sample preparation for optimization of diamond film thickness and surface smoothness study. (Photoresist quantity = 42 ml)

Group	Diamond powder (mg)	Photo-resist thinner (ml)	No.	Spin speed (rpm) (10"/30"/5")
A	20.2	4	I	500/2000/500
			II	500/3000/500
			III	500/4000/500
B	41.7	6	IV	500/4000/500
			V	1000/4000/500
			VI	0/4000/500
			VII	0/3500/500
C	41.7	6	VIII	500/4000/500
			IX	0/4000/500
D	122.6	14	X	500/4000/500
			XI	500/4500/500
			XII	0/4000/500
			XIII	300/4500/500
E	142.6	16	XIV	0/4000/500

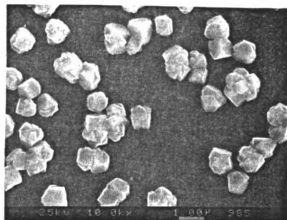
coated with DPR which was not stirred or agitated for about 24 hours.

- (5) The spin schedule of R/4000/500 rpm for 10"/30"/5" corresponding to sample XII is optimum in terms of uniformity of nucleation (group D). The initial spin speed R represents the ramp up.

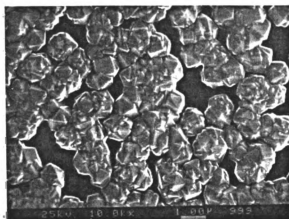
- (6) A larger quantity of diamond powder in a given solution of photo-resist and thinner gives a higher nucleation density (see Fig. 4.11) 142.6 mg of diamond powder and 16 ml of photo-resist thinner are sufficient to give optimum nucleation density i.e., $1 \mu\text{m}^{-2}$ (XIV).

From this study, an optimum quantities of diamond powder, photo-resist and photo-resist thinner in DPR suspension which leads to the diamond films with a nucleation density of $1 \mu\text{m}^{-2}$ and an optimally smooth surface. was achieved. The film surface roughness, as measured by a surface profiler, decreased sharply after this experiment. An SEM image of cross sectional view of a film grown after the above study has been shown in Fig. 4.12. An optimally smooth surface is clearly visible. However, as the film thickness grows, the surface roughness was also observed to grow proportionally. The plot shown in Fig. 4.13 shows this trend. A larger surface roughness of the thicker films results from the larger grains on the surface.

After an optimum spin schedule for DPR was achieved, the patterning of diamond films was achieved by patterning the DPR by standard lithography before diamond deposition. However, some scattered diamond seed particles were observed on the substrate which resulted in growth of diamond in undesired locations. To remove these residues, the substrates were developed by spraying the photo-developer and then slightly etching by a method depending upon the substrate surface. An SiO_2 surface was etched with buffered hydrofluoric acid (BHF) while DPR served as an automatic mask. This etching step removed most of the diamond particles left on the surface after spray development. Schematics of this patterning method are given in Fig. 4.14. SEM micrographs of diamond films patterned by this method are given in Fig. 4.15. The thin line parallel to the main pattern in Fig. 4.15(b) in its early phase of growth is shown in Fig. 4.16. One can clearly see that the line is basically a string of single grains. This gives a boost to the possibility of fabrication of devices with feature size near one micron.



(a)



(b)



(c)

Figure 4.11 SEM micrographs of diamond films deposited on substrates coated with DPR suspension of (a) 41.7 mg, (b) 122.6 mg and (c) 142.6 mg of diamond powder in 42 ml of photo-resist.

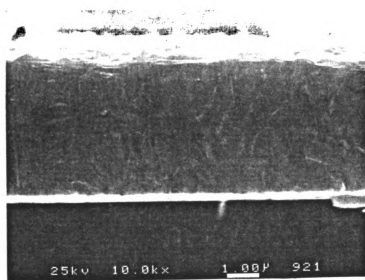


Figure 4.12 The cross-sectional view of a diamond film grown after thickness uniformity and surface smoothness optimization study.

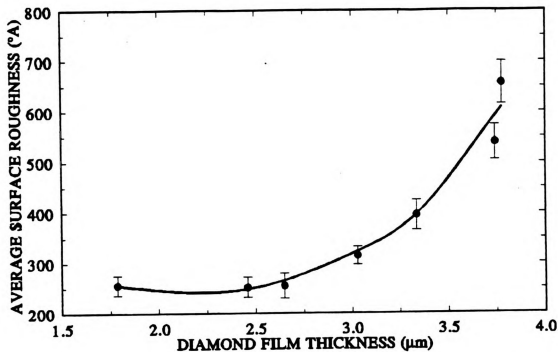


Figure 4.13 The effect of diamond film thickness on the surface roughness.

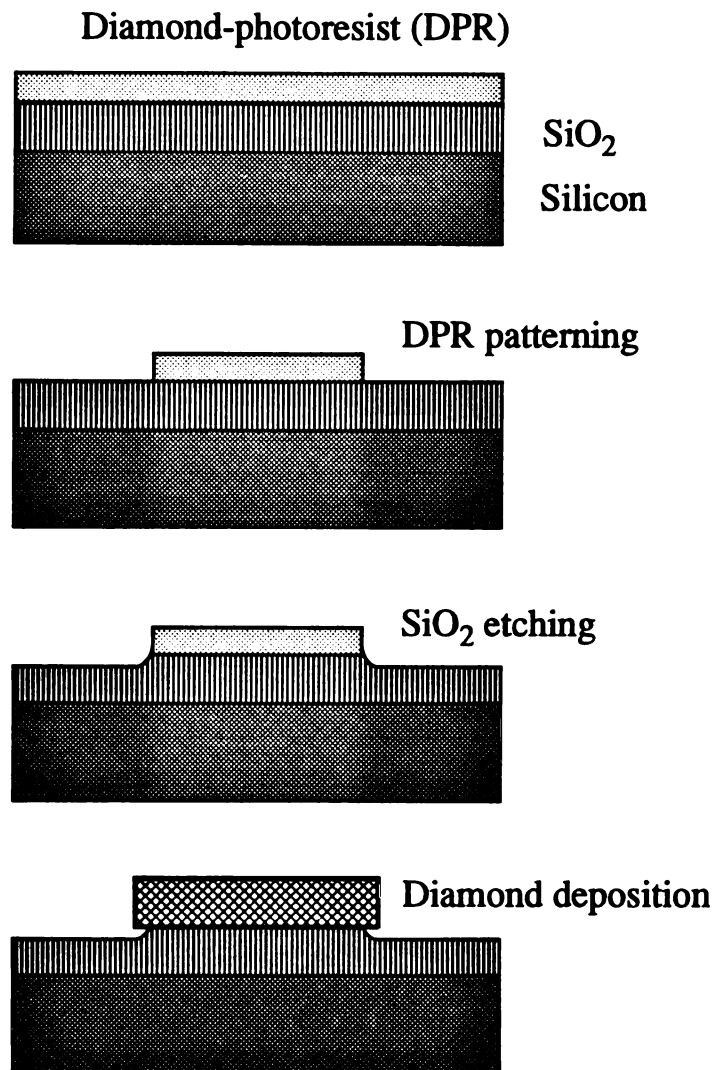


Fig. 4.14 Schematic diagram of DPR methods of patterning diamond films.

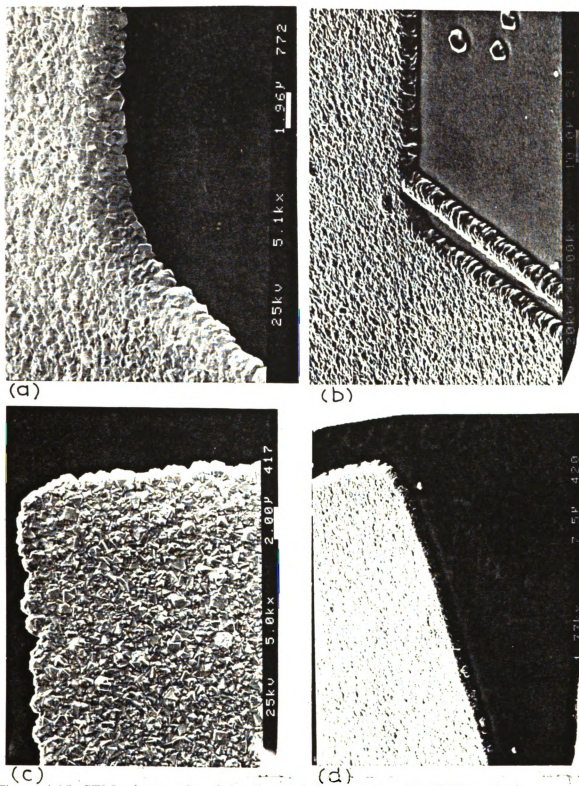


Figure 4.15 SEM micrographs of the diamond films patterned by DPR method.

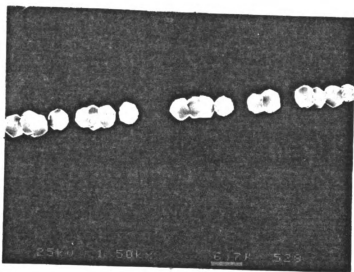


Figure 4.16 SEM micrograph of the diamond film line parallel to the main pattern shown in Figure. 4.15(b). The image was taken in the early part of growth.

Since the as grown diamond films have large internal stress, their delamination from the substrate surface especially after patterning was of great concern. Therefore, the films were subject to the well known scotch tape test. All the films showed good adherence with the silicon or SiO_2 substrate. Some of the films were scratched with a sharp knife edge. Fig. 4.17 shows SEM micrographs of a patterned film which was subjected to scratch test. As visible in the figure, the continuous film is strongly held with the substrate and only scattered diamond particles could be dislodged by scratching.

As shown by the micrographs, all the patterning techniques give good selectivity. The selectivity of DPR patterned films is practically limited by lithography and grain size in the deposited diamond films. In the case of RTP etched films, it is controlled by the stability of the deposited masking layer and underetching. Thus, the latter method gives excellent selectivity on relatively thin films. Looking at them from ease of implementation, DPR is the best of all. All the patterning methods presented here are adopted from IC fabrication technology, and so are compatible with it. The choice of a particular technique for an application depends primarily upon the substrate material. In general, the DPR method may be employed on nearly all substrates found in electronic device manufacturing. We note that the post-treatment masking method, without the ultrasonic treatment, may be used for selective deposition of diamond on a pre-existing diamond film or even single crystal diamond substrates. An appropriate combination of these techniques can realize three dimensional structures in diamond leading to many novel applications.

While all these techniques were evaluated for patterning diamond films on oxidized silicon for test chip fabrication, the DPR was a clear choice by virtue of its ease of implementation. Micrographs of test chips after diamond deposition at various magnification are presented in Fig. 4.18.

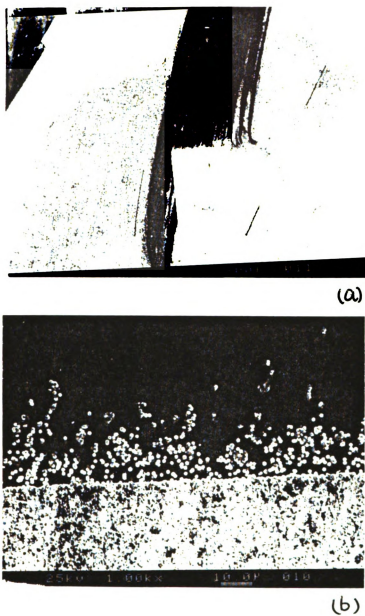


Figure 4.17 SEM micrographs of the diamond film scratched with knife edge. The picture shown in (b) is the higher resolution image of upper portion of pattern shown in (a).

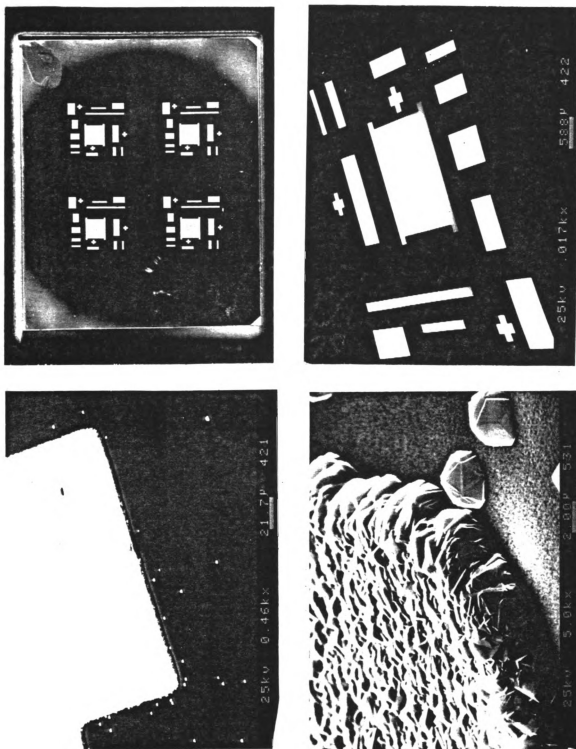


Figure 4.18 Micrographs of test micro-chip after diamond deposition using DPR patterning at various resolution.

4.3 METALIZATION

4.3.1 Problem Analysis

Metallization is an important process in the fabrication of an IC. During test chip fabrication, diamond films are deposited on SiO_2 . Hence, the contacts are required to behave ohmically with diamond film and adhere well on both the diamond and SiO_2 surfaces. The projected testing of these test chips at high temperatures in chemically and physically harsh environment makes the problem tough. Most of the previous metallization efforts [142,144,146,147] on CVD diamond films and single crystal diamonds remained focussed on to form good ohmic contacts only and very little was said about technological issues such as mechanical stability, adhesion on the diamond surface, pattern generation and high temperature behavior. Additional requirements of a good metallization scheme may include but not limited to low resistivity, small contact resistance, stability in oxidizing ambients, surface smoothness, ease of formation and etching/patterning, stability during processing at high temperatures i.e., minimal inter-metallic and metal to substrate chemical reactions, minimal junction penetration, and low electromigration, eutectic and surface diffusion.

In view of the requirement for high temperature operation under an oxidizing environment, high melting point and high oxidation temperature refractory metals appeared to be the natural choice. However, the choice from these metals for simultaneously good adhesion on diamond and SiO_2 surfaces was difficult. In this regard, the information available from conventional metallization schemes for relatively high temperature on silicon ICs [151,160,161] and metallization studies on CVD diamond films [142,143] were comparatively analyzed.

It is well known that most refractory metals react with SiO_2 [161]. This property was seen as an advantage here since these metals could form a layer with good physical stability. However, their high oxidation rates are undesirable. This aspect is

primarily determined by the heat of oxide formation. Using heat of oxide formation data, it was shown that group IV.A and V.A elements from the periodic table such as Ti, Ta, Zr, Nb and Hf, by virtue of their lower heat of formation as compared to SiO_2 , will reduce SiO_2 and form a metal oxide [151]. This process leads to a strong chemical bond with SiO_2 at relatively lower temperature. It has been shown from the Ti-O-Si phase diagram constructed from empirical data that Ti is not stable in contact with SiO_2 and reacts with it at temperature around 550°C to form TiO and Ti_3Si_3 which are in equilibrium with SiO_2 even at 950°C [160]. On the other hand, metals like Au, Pt, W and Mo that form an oxide with a heat of formation higher than SiO_2 do not reduce SiO_2 and, therefore, have poor adhesion on it. Therefore, refractory metals such as Ti and Ta, with their relatively higher melting point, are most suited for a base metal layer on SiO_2 in an envisioned multi-layer metallization structure. However, since the SiO_2 reduction process continues until the supply of either of the reactants lasts, this base layer should be thin enough to form only the required "glue" layer between metallization and SiO_2 and not deplete the SiO_2 layer completely. In addition, the environment during sintering process should, as far as possible, be oxygen free so as to prevent the oxidation of the metal layer by interaction with the ambient oxygen. Thus there is a need to protect the base layer by another protective passivation layer. An easy way to accomplish this is to lay the top metal layer before sintering instead of laying just a sacrificial layer.

Although most metals form pseudo-ohmic contact with small grain ($\leq 1\mu\text{m}$) polycrystalline diamond films, it may not be true in case of large grain polycrystalline diamond films [162] and single crystal diamond surface. From this perspective, among the metals being considered, Ti has been shown to make ohmic contact with both single crystal bulk diamond [152] and homoepitaxial diamond films [58,142]. Both Ti and Ta are known to react with diamond at temperature $< 800^\circ\text{C}$ to form their respective carbides [47]. Therefore, they can be considered appropriate for metallization.

The requirements of the top layer metal should include low resistivity, high melting point, oxidation resistant and high melting point of any alloys it forms with the base layer metal. There exist a number of choices such as Ni, Cu, Au, Pd, Mo, W, and Co. Out of all these metals, Pt stands the best chance due to its best overall combination of desired properties. These include high resistance to oxidation, high melting point, and fairly high melting point of alloys formed with Ti and Ta.

Pt has been reported to form three compounds with Ta namely Pt_4Ta , Pt_3Ta , and Pt_2Ta [163]. Although the melting points of these compounds are not precisely available, they are well above $1000^\circ C$. Pt_4Ta is found only above $1500^\circ C$. Pt forms three compounds with Ti: $TiPt_3$, $TiPt$, and Ti_3Pt , with melting points of 1950° , 1830° , and $1370^\circ C$ respectively [163]. Although, Ti_3Pt has a relatively low melting point, it is expected to remain mechanically stable at $1000^\circ C$.

4.3.2 Experimental Results

In general, for two layer metallization, the thicknesses of lower and upper layer is in the range of $300-600^\circ A$ and $2000-5000^\circ A$ respectively. As a starting point, a combination of $Pt(3000^\circ A)/Ti(500^\circ A)$ was selected for the test chips. Both metals were deposited using RF sputtering system. The pattern was generated by shadow mask. The mask was fabricated on thin Cu plate at the Ford photographic facility. The test chip after metallization is shown in Fig. 4.19. SEM micrographs of the as deposited metal film on the diamond film surface and around the edge of the diamond film are shown in Fig. 4.20. The diamond film morphology appears to be completely preserved. Also the metal film appears to be featureless and very smooth. Due to deposition of metal normal to the chip surface, the diamond film step coverage is not good.

These test chips were again tested at $1000^\circ C$ for the physical stability of metal film. They were heated for 15 minutes in vacuum (-10^{-3} torr). The observations of optical microscope and SEM inspection after heat treatment are as follows:

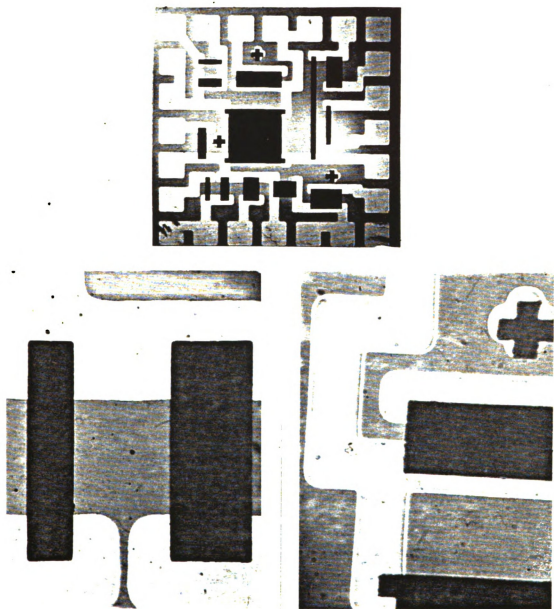


Figure 4.19 Test micro-chip metallization. The patterns on was generated by using shadow mask. The pictures in (b) and (c) are higher magnification images of (b). The diamond pattern in (c) on the left is 160 μm .

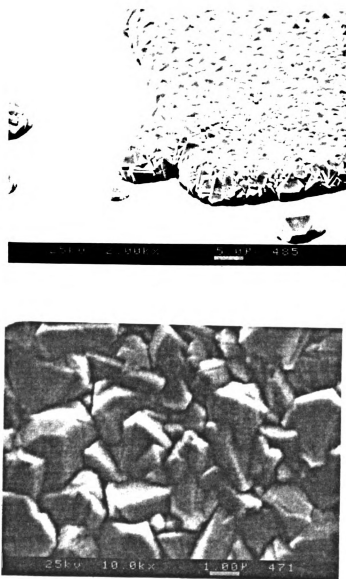


Figure 4.20 (a) Diamond film pattern on test chip with as deposited metal Pt (3000°A)/ Ti (500°A). (b) The top view of metallized diamond film surface in (a).

- (a) The metal film appeared to be either melted or at least softened up during heat treatment.
- (b) The metal may have reacted strongly with diamond and dissolved it partly (see Fig. 4.21(a) and (b)) to an extent that the diamond film almost lost its morphology altogether. Possibly Ti reacted with the diamond film to form titanium carbide.
- (c) The film formed small islands which were completely dissociated from each other in locations where the metal film thickness was relatively small i.e., in the boundary regions (see Fig. 4.21(c)). In the areas with a thick metal film, a similar behavior was observed but the islands were barely joining together (see Fig. 4.21(d) for high resolution view). Also the surface of the metal film broke open and left void spaces.
- (d) The metal appeared to pull away from the diamond film surface. This is truly visible along the diamond film edge and around scattered diamond crystals on the substrate surface (see Fig. 4.21(e) and (f)).

From these observations the following deductions were drawn.

- (a) Ti consumed diamond excessively during its reaction with diamond in forming its carbide and since this reaction continues (at temperature higher than 550°C) until the Ti layer is completely depleted, the thickness of the Ti layer used was more than desired. The same was true on the SiO₂ surface. There Ti reduces SiO₂ in the process of forming its own oxide. This is clearly not desired because the SiO₂ thickness must be saved to provide sufficient insulation from the underlying semiconducting silicon. Since Ti is used here only to act as a 'glue' layer, a thinner layer may be sufficient.
- (b) The initial thickness of the Pt layer was not sufficient. A relatively thick Pt film is more stable at high temperature as can be seen from Fig. 4.21(c) and (a) in case of SiO₂ substrate and a small patch of thick Pt film on top of diamond film

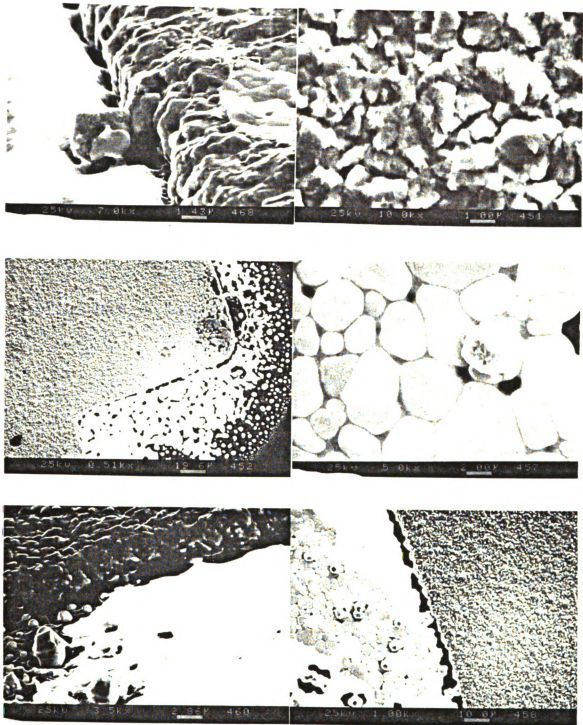


Figure 4.21 SEM micrographs of the metallization (Pt (3000 $^{\circ}$ A)/ Ti (500 $^{\circ}$ A) on test chip heat treated at 1000 $^{\circ}$ C.

respectively.

- (c) The annealing should be done under better vacuum (<1 mtorr range) so that there will be least amount of water possible to be absorbed by Ti to form its oxide. Also, a fast temperature rise to 1000°C leads to dissociation of ambient water molecules. Pt is known to absorb hydrogen at high temperature (>600°C) and become unstable.
- (d) Since all the required reactions namely formation of titanium carbide, oxide and silicide occur at relatively low temperature ($\leq 550^\circ\text{C}$), the annealing at 1000°C is unnecessary for metal films.

On the basis of above observations, the metallization scheme was changed as follows:

- (1) Decrease of Ti layer thickness from 500°A to 100-150°A.
- (2) Increase of Pt layer thickness from 3000°A to 1.2 μm .
- (3) Reduce annealing temperature from 1000°C to 600°C.

The test chips, after metal deposition, were annealed at 600°C for 45 minutes. The pressure was estimated to be in the range of 10^{-7} torr. An SEM inspection of this metal combination showed no sign of degradation. The annealing time was adjudged by in situ monitoring of the resistance of the metal film. The metal film resistance decreased during annealing and stabilized at one point. An example of the change of resistance with time is shown in Fig. 4.22. The resistance closely followed the relation

$$R(t) = [R(0) - R(45)] e^{-t/\tau} + R(45) \quad (4.1)$$

where $R(t)$ is resistance after annealing of time t measured in minutes. The time constant τ of 7 minutes was determined through curve fitting. Thus, an annealing of 35 minutes (five time constants) was considered to be sufficient for all later samples. It is recognized that part of the resistance change might be contributed by the diamond resistor itself but a stabilization of the total resistance is a clear indication of stabilization of the resistances of both the diamond film and the metal lines.

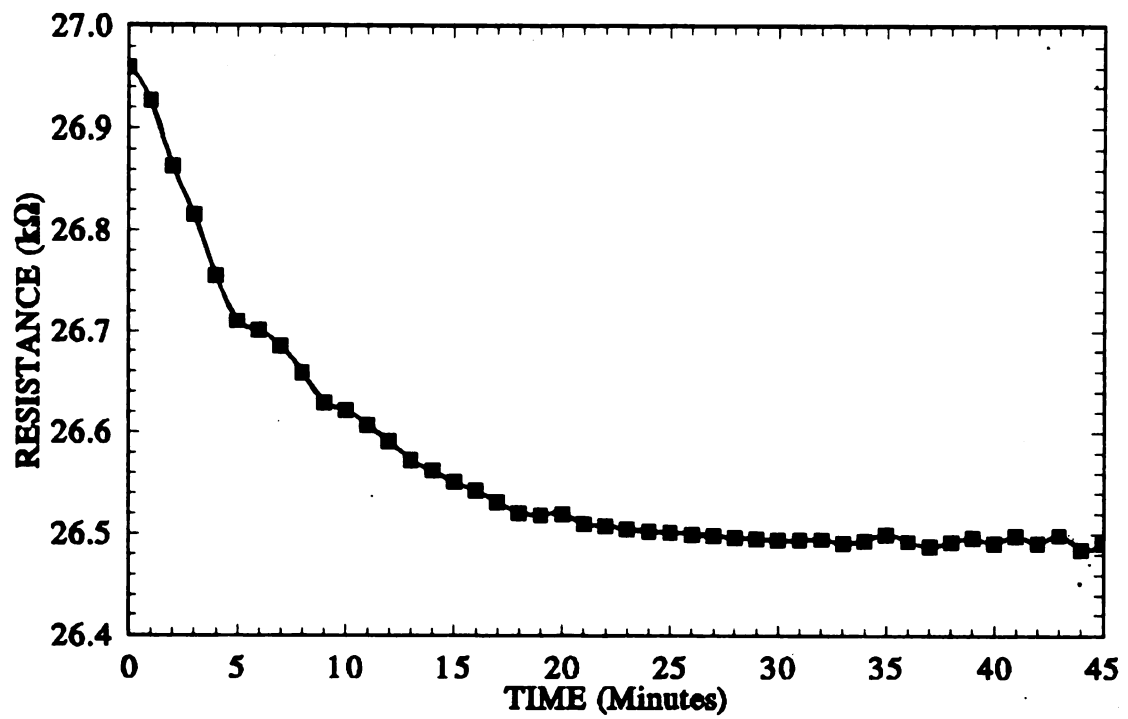


Figure 4.22 Resistance of a metallized diamond resistor with time during annealing at 600°C.

After annealing at 600°C, no appreciable change in metal film appearance was observed through SEM. After this the test chips were heated to 1000°C for 6 minutes under vacuum and again inspected through SEM. SEM micrographs of this metallization experiment are shown in Fig. 4.23. The metal appeared to be partially melted or undergone a solid phase crystallization. The metal on diamond film surface showed complete continuity. The metal was physically stable and erosion of the diamond film was minimal. The morphology of the grains appears to be preserved. Also, no island formation or breakage in the metal film was observed. The tendency of the metal film to pull away from the diamond film also appears to be reduced significantly.

The physical adhesion of the film was tested by the scotch tape test. Also it was scratched by a knife edge. The metal film showed excellent adhesion on both the SiO₂ and diamond film surface. The contact resistance was also measured before and after annealing. It decreased by a factor of 3.85 on the average. The formation of titanium carbide and diffusion of Pt into the diamond film are possibly responsible for this behavior. Overall this scheme appears to be successful for metallization of diamond films on oxidized silicon substrate.

Although suitable for the present purpose, the thick platinum layer was not appropriate for the lithographically masked wet etching process. The photo-resist mask was unable to withstand the etching process long enough for the pattern to form and either dissolved or delaminated. To make the metallization scheme universal, the platinum film thickness was reduced to 8000°A. This thickness could be etched with wet chemical etching solution with photo-resist masking. At the same time any change in its operational behavior was not detected. SEM micrographs on the test chip after this metallization and heat treatment at 1000°C for 8 minutes are shown in Fig. 4.24. The erosion of diamond is still minimal. The cross sectional step coverage is still lacking by the same amount. However, it provided the necessary contact and no degradation in electrical measurements or through visual inspection was observed. To verify the

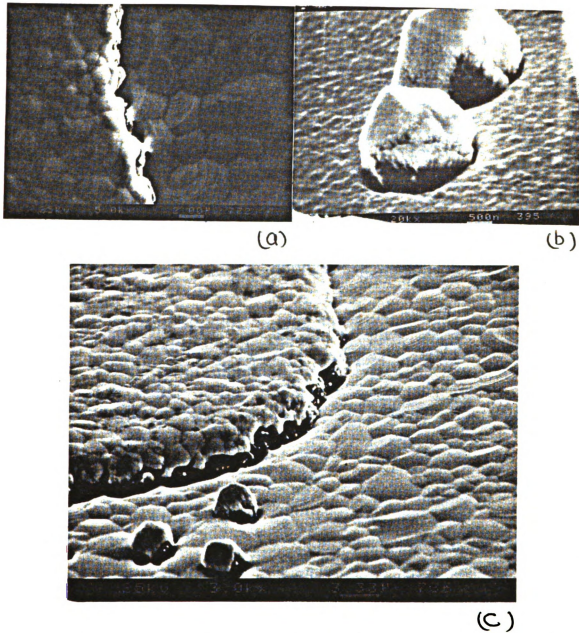
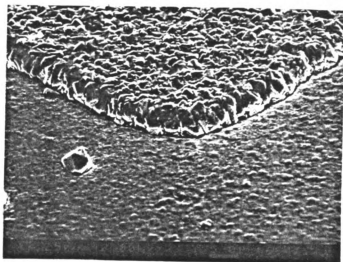
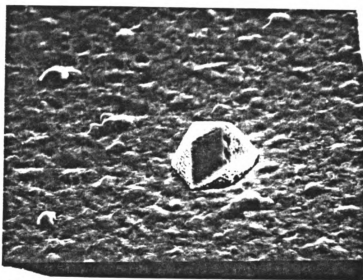


Figure 4.23 SEM micrographs of metallization Pt ($1.2 \mu\text{m}$ / Ti (100\AA) on test microchip after annealing at 1000°C . (a) The top view with diamond pattern in left half, (b) stray diamond crystals and (c) a 60° view around a metal contact on diamond.



(a)



(b)

Figure 4.24 SEM micrographs of metallization Pt (8000°A/ Ti (100°A) on test microchip after annealing at 1000°C. (a) a 60° view around a metal contact on diamond and (b) stray diamond crystal.

compatibility with IC technology, the gold wire bonding was made on the metal bonding pads before and after heat treatment. The gold wire adhesion was good and bonding formed a proper connection. A micrograph in Fig. 4.25 shows a wire bonded connection after heat treatment at 1000°C.

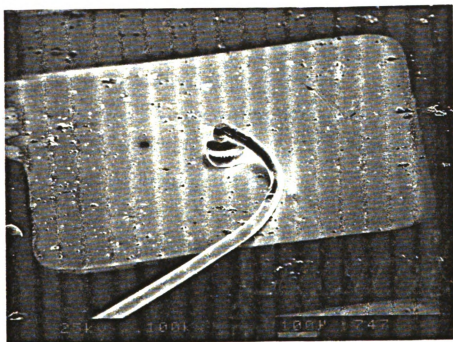


Figure 4.25 Gold wire bonding on the test chip bonding pad composed of Pt (8000°A/ Ti (100°A).

4.4 FABRICATION OF HEAT FLUX SENSORS

In order to measure abnormalities in the flow of heat associated with the shock wave in the wind tunnel, special temperature sensors at very high spatial resolution (few μm) operating with ultrafast dynamic response time (few μs) may be required. For this purpose, the sensors should be attached to the surface of a highly thermal insulating body which is small enough and of such shape as not to interfere with the aerodynamics. The sensors should be able to withstand physically harsh environment in the wind tunnel. Due to these stringent technological and operational demands, most conventional temperature sensors are rendered unsuitable. The remarkable combination of physical and electronic properties of chemical vapor deposited (CVD) diamond films especially high thermal conductivity, chemical inertness, radiation immunity, and wide energy band gap propose their possible application as high speed temperature sensors operating at elevated temperatures under such an environment. The present developments in the deposition, doping, patterning, metallization and passivation provide the basic fabrication technology for a micro-miniaturized temperature sensor array.

For this application, a cylindrical shaped substrate about 7.6 cm long with a 1 cm diameter was considered appropriate. However, placing the sensors on the curved surface of a cylindrical substrate made of high thermal and electrical resistivity material presents a major technological problem. A three dimensional lithographic technique was required to implement the DPR diamond and metal pattern generation. As a first attempt to solve this problem, the conventional two dimensional lithographic techniques were suitably modified to implement a close approximation to this three dimensional problem.

Of the many problems encountered, the uniform thickness of photo-resist (and DPR) and transfer of the pattern on the curved surface of the rod substrate were most critical. Solving the problem of holding of rod at high spin speed and controlling the

fluid dynamics of the liquid photo-resist for a uniform coating over a small angle (about 35°) required extensive experimentation. To transfer the pattern onto the curved surface of the substrate, flexible masks were prepared. The masks for diamond film and metal patterning are shown in Fig. 4.26. The feature size is $150\ \mu\text{m}$. Even though fairly large, the sensor size is sufficiently small for initial feasibility study. The alignment was done manually using a low magnification (15X) microscope.

A requirement of heat flux sensors is that they should be placed on good thermal insulators. Hence, diamond deposition on several materials including quartz, alumina, vycor glass and thermally oxidized silicon was attempted. Diamond films showed acceptable adhesion only on the thermally oxidized silicon rod and this was therefore selected as the substrate material for present application. SEM micrographs of a 12 diamond film sensor array on silicon rod are shown in Fig. 4.27. A high density of scattered diamond crystals, as visible in the figure, resulted from the failure of their removal due to non-polished surface of the rod substrate. The seed crystals were held in the channels present on the substrate surface during the lithographic process. Nevertheless, the density of such particles is not sufficient to form a continuous path between adjacent sensors and will not interfere with electrical measurements.

4.5 SUMMARY

The fabrication process of test micro-chip and heat flux sensors has been described. Appropriate patterning techniques for diamond films and high temperature compatible metallization scheme were developed. Of the three patterning techniques, DPR method was considered to be the most suitable for test chip fabrication from the perspective of selectivity, resolution and the ease of implementation. The metallization of test chip was done with thick Pt metal film ($0.8\text{-}1.0\ \mu\text{m}$) on top of a thin Ti layer ($100\text{-}150^\circ\text{A}$). This metallization scheme is not only high temperature compatible but also compatible with conventional chemical etching and wire bonding processes.

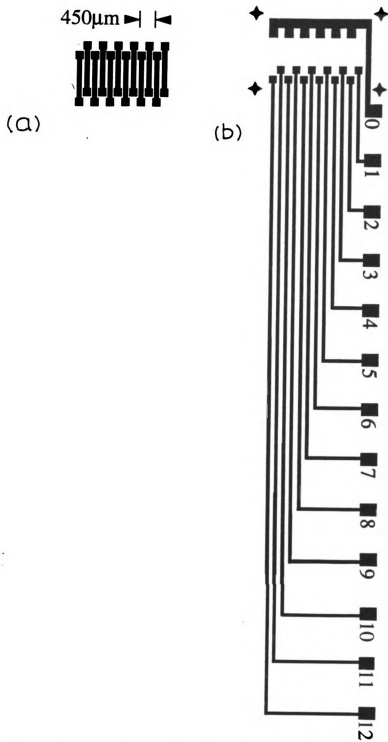
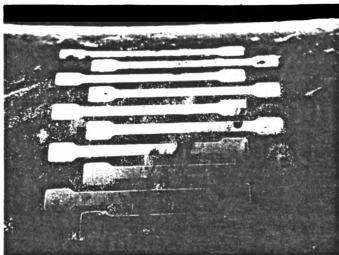
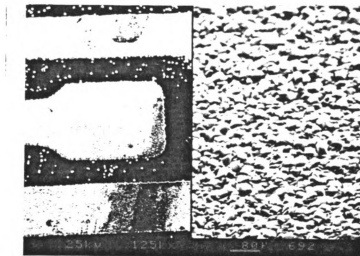


Figure 4.26 Mask set for diamond film heat flux sensors. (a) diamond and (b) metallization mask.



(a)



(b)

Figure 4.27 SEM micrographs of diamond film heat flux sensors on silicon rod. (b) is a high magnification images of (a).

ELECTRICAL CHARACTERIZATION

5.0 INTRODUCTION

For well known and widely used semiconductors, the fundamental material properties are generally well characterized. However, for a new semiconductor such as diamond, the properties such as carrier and impurity concentration, resistivity and carrier mobility are required to be measured and relations among various parameters developed before using it in any device. At present, these properties are either not measured or there is a large scatter in the reported values. It is possibly due to experimental difficulties involved in making these measurements as well as polycrystalline nature of CVD diamond films, the electrical properties of whom are sometimes dependent on deposition conditions. Therefore, fundamental electrical properties such as resistivity, carrier mobility, carrier and impurity concentration were quantitatively measured or evaluated and is the subject of this chapter. Since this research is primarily aimed at developing temperature sensors, these measurements were made over a wide temperature range. For this purpose, a special high temperature characterization system was designed and built. In addition, many technological issues such as control of doping and its uniformity and high temperature effects on the diamond films have also been addressed.

5.1 PRELIMINARY ANNEALING STUDY

To estimate the effect of high temperature treatment, test chips were heated at high temperatures and temperature response of resistivity was monitored. The temperature response was acquired by measuring the resistance of a selected resistor in situ using the experimental arrangement shown in Fig. 5.1. Fig. 5.2 shows the temperature response of the resistor after annealing at the indicated temperatures at a pressure of 10^{-7} torr. All the curves correspond to a single sample. The data for this figure was collected through an annealing experiment as follows:

- (i) The test chip was heated to 300°C. While at 300°C, the resistivity was monitored for any change with time. No change in resistivity occurred and sample was cooled down to room temperature. Now the temperature response of resistivity was measured up to 300°C. The measurements were repeated both with increasing and decreasing temperature. This data generated the curve corresponding to the annealing temperature of 300°C.
- (ii) The chip was heated to the 500°C. While at 500°C, the resistivity was monitored which was found to decrease gradually and stabilize slowly to a constant value in ~12 minutes. The sample was kept at the annealing temperature until the resistance stabilized. Then the sample was cooled down to room temperature. Now the temperature response of resistivity was measured up to 500°C. The measurements were repeated both with increasing and decreasing temperature. This data generated the curve corresponding to the annealing temperature of 500°C.
- (iii) The same procedure was adopted for 600 and 1000°C. While at these temperatures, the resistivity was found to change gradually but stabilized after 10 and 8 minutes, respectively.

The observations for the foregoing annealing experiments are as follows:

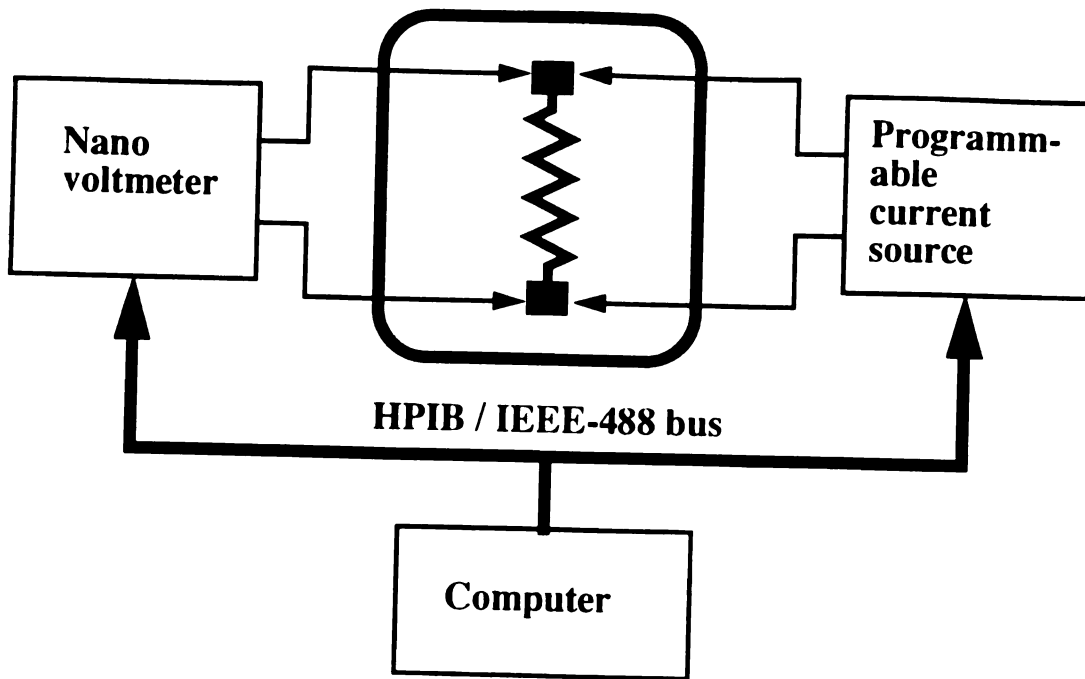


Fig. 5.1 Schematic diagram of experimental set up for I-V measurements. The same arrangement was used for two wire resistance measurements.

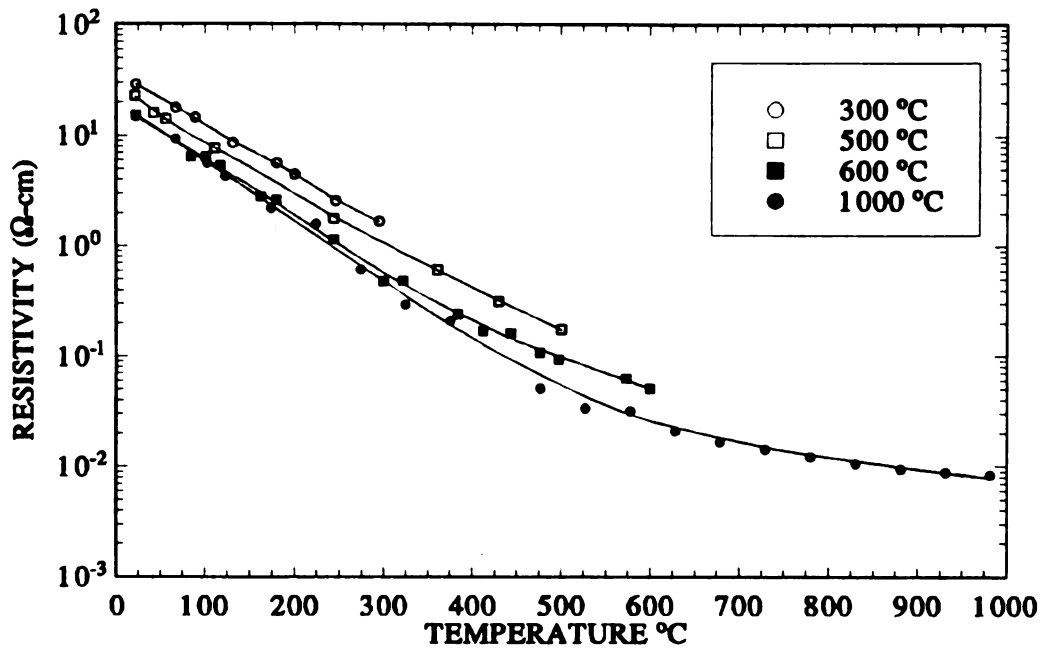


Figure 5.2 The temperature response of resistivity of diamond films sensor annealed at different temperatures. The annealing temperature is also indicated.

- (1) There is no effect of annealing up to 300°C on the resistivity. Fig. 5.3 shows the temperature response of resistance for two cycles up to 300°C. Both curves are reproducible.
- (2) Once sample is heated to a temperature $T > 300^\circ\text{C}$ for the first time, the resistivity decreases gradually and stabilizes slowly. Once cooled down to room temperature, the room temperature resistivity is found to be lower than the value prior to heating.
- (3) Once a sample undergoes annealing at a specific temperature, the temperature response of resistivity up to that annealing temperature is found to be reproducible. No further change in resistivity was observed if the sample is kept below that temperature. Fig. 5.4 shows this reproducibility of temperature response in the temperature range of 300-1273 K and 77-370 K after annealing for 35 minutes at 600°C and 8 minutes at 1000°C.

Based on these observations, following deductions were drawn.

- (1) No annealing is required for temperature sensors if the maximum operational temperature is not to exceed 300°C.
- (2) For a temperature sensor to operate beyond 300°C, an annealing at its maximum operational temperature is required. The time duration of annealing will be determined by the time required for the resistivity of the sensor to stabilize at the annealing temperature.
- (3) The room temperature resistivity of doped diamond films decreases after heating at temperature $>300^\circ\text{C}$. This effect is clearly visible in Fig. 5.2.

The decrease of room temperature resistivity due to annealing at temperature $T > 300^\circ\text{C}$, as shown in Fig. 5.2 is contrary to what has been found for undoped films [99,159]. For undoped diamond films the room temperature resistivity was found to increase

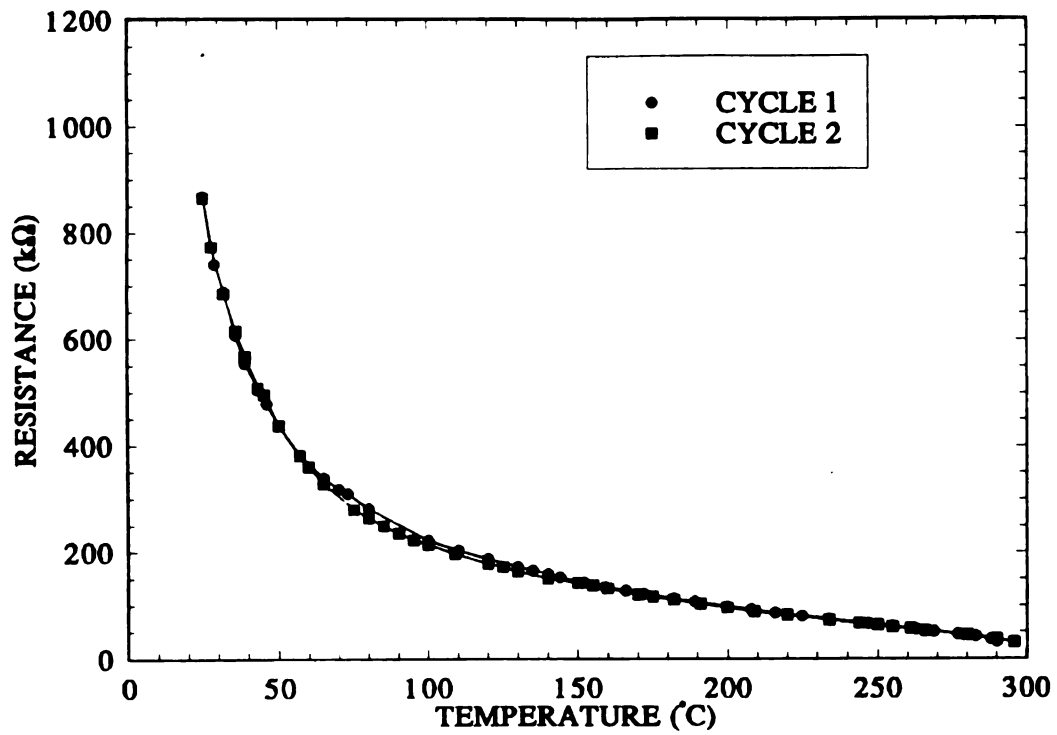


Figure 5.3 The reproducibility of temperature response of resistivity of unannealed diamond temperature sensor over a temperature range of 300-573 K.

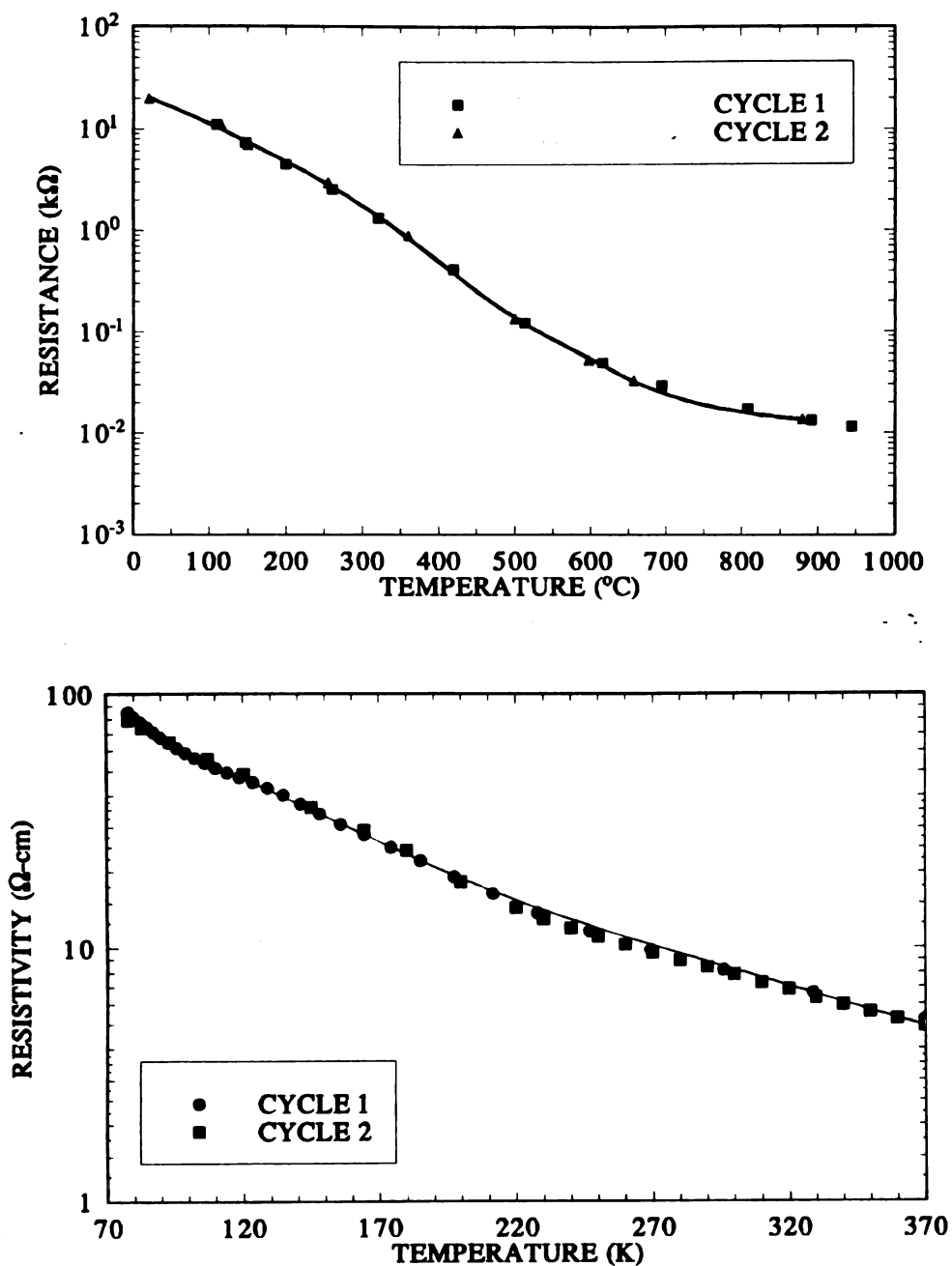


Figure 5.4 The reproducibility of temperature response of resistivity after annealing in temperature range (a) 300-1273 K and (b) 77-300 K.

with annealing beyond 300°C. Any report regarding change of room temperature resistivity of doped diamond films, whether increase or decrease, was not found in the literature.

The interest of present research is using diamond film temperature sensors up to 1000°C. For this purpose, the test chips were annealed at 1000°C and their resistivity was monitored in situ. The change of resistance of selected resistors with time, while at 1000°C, of two test chips with measured Hall hole concentration of $1.02 \times 10^{16} \text{ cm}^{-3}$ and $2.65 \times 10^{17} \text{ cm}^{-3}$ has been plotted in Fig. 5.5. From the figure, it is clear that the change in resistance became negligible after 8 minutes. Also, the time taken by the resistivity to stabilize appears to be independent of Hall concentration. Hence, it was decided to anneal all the sensors at 1000°C for 8 minutes before recording their temperature response.

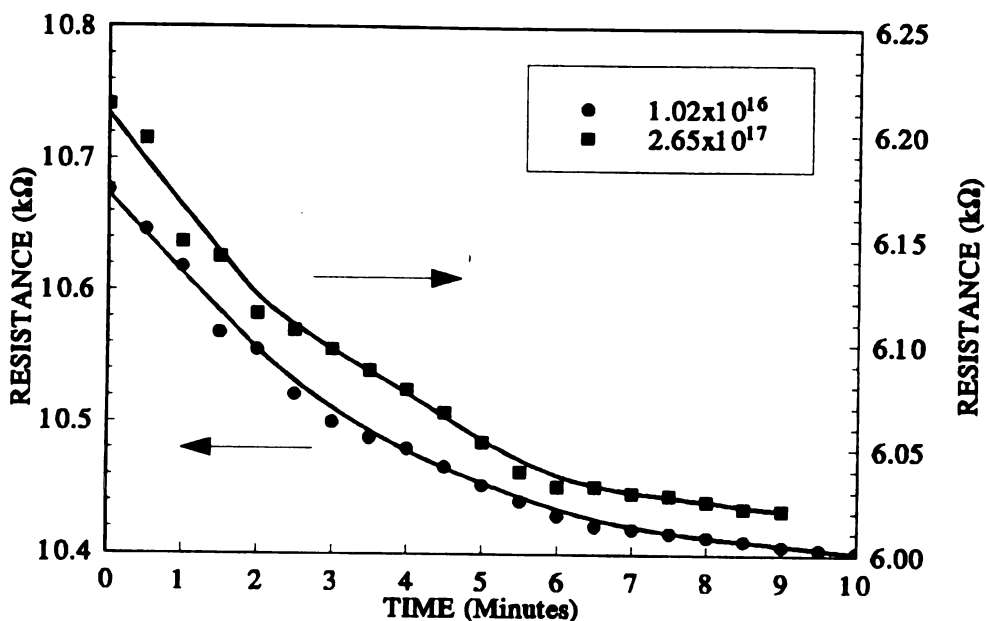


Figure 5.5 The time response of resistivity of two diamond film resistors during annealing at 1000°C. The measured Hall concentration for each sample is also indicated.

5.2 ELECTRICAL MEASUREMENTS

5.2.1 Overview

Most of the electrical measurements were aimed at characterization of diamond films for applications in temperature sensors. Primarily, they consisted of resistivity, current-voltage (I-V) and Hall measurements at various temperatures and in different ambients. The purpose was to acquire fundamental properties of p-type diamond films such as resistivity, carrier concentration and carrier mobility as a function of temperature. Two groups of samples are used in electrical measurements. Group one consists of test chips which were annealed at 600°C and 1000°C for 35 and 8 minutes, respectively. Moreover, boron doped diamond film for test chips were deposited on oxidized silicon with a buffer layer of undoped diamond film. Group two samples were not annealed and consisted of rectangular resistors or square pattern. The doped diamond films for these samples were deposited directly on oxidized silicon. They will be referred to as 'discrete' samples in the following discussion. The measurements on these samples have been summarized in Table 5.1. All the measurements in the temperature range of 77-575 K were made in commercially manufactured systems. A dedicated system was designed and built, during this research, to perform annealing and measure resistivity of diamond sensors in the range of 300-1273 K. A schematic diagram of the system is shown in Fig. 5.6.

5.2.2 Current-Voltage Measurements

Current-voltage (I-V) measurements were made to observe the behavior of electrical contacts. A programmable voltage source and an electrometer were placed in series with the resistor for these measurements. The measurements were made over the temperature range of 77-1300 K. Fig. 5.7 shows the I-V measurements at selected temperatures in the temperature range of 77-300 K at a pressure of 10^{-3} torr made on

Table 5.1 The organization of electrical measurements for the characterization of p-type diamond films.

Temperature range (measurement)		Measurement type	Sample type	Metallization	Ambient
I	77-350 K	I-V, ρ , μ_H , P	Test chips	Pt / Ti	Vacuum 10^{-3} torr
			Square Hall pattern	Al	
II	300-575 K	I-V, ρ	Rectangular resistors	Al	Static air
III	300-1300 K	I-V, ρ	Test chips	Pt / Ti	Vacuum 10^{-3} torr
	300- 1300 K	I-V, ρ	Test chips	Pt / Ti	Vacuum 10^{-7} torr
			Homoepitaxial diamond film	No metal	

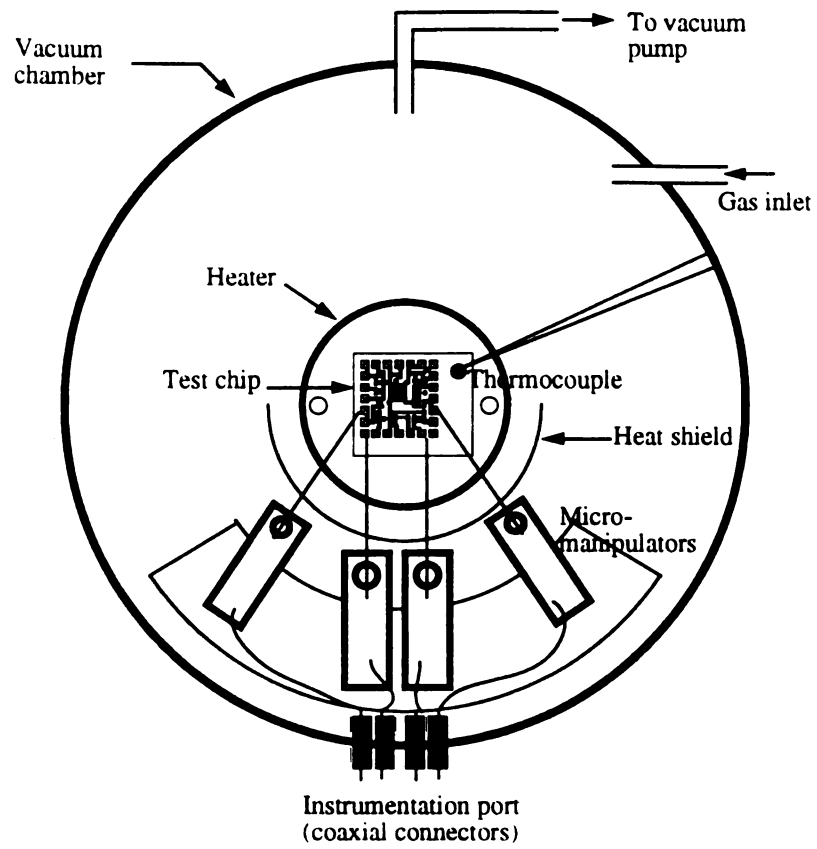


Fig. 5.6 Schematic diagram of the high temperature characterization system.

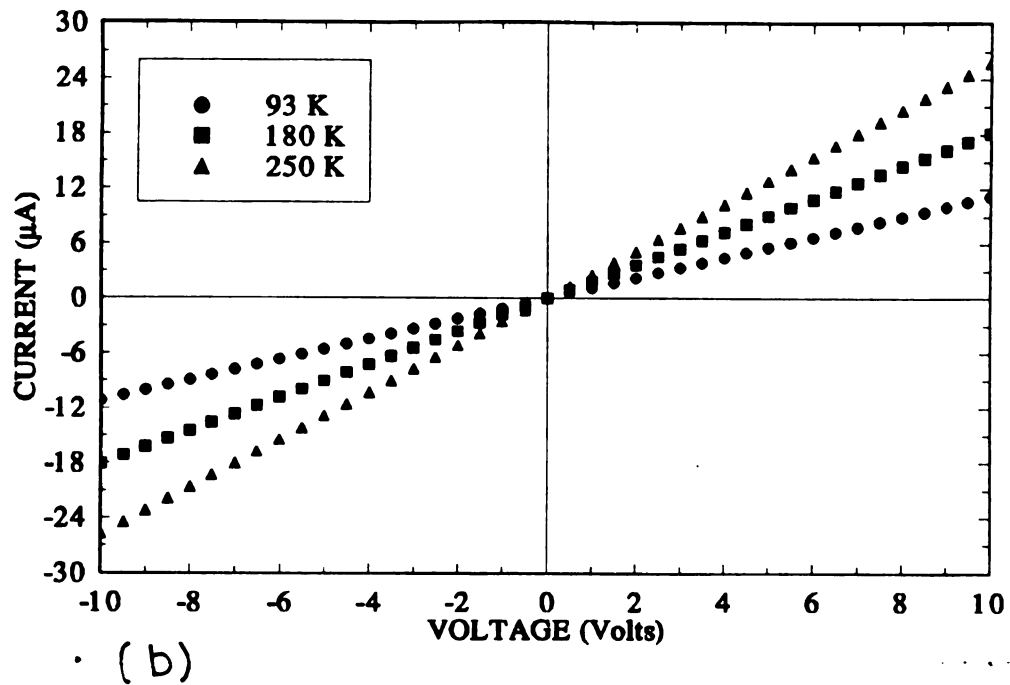
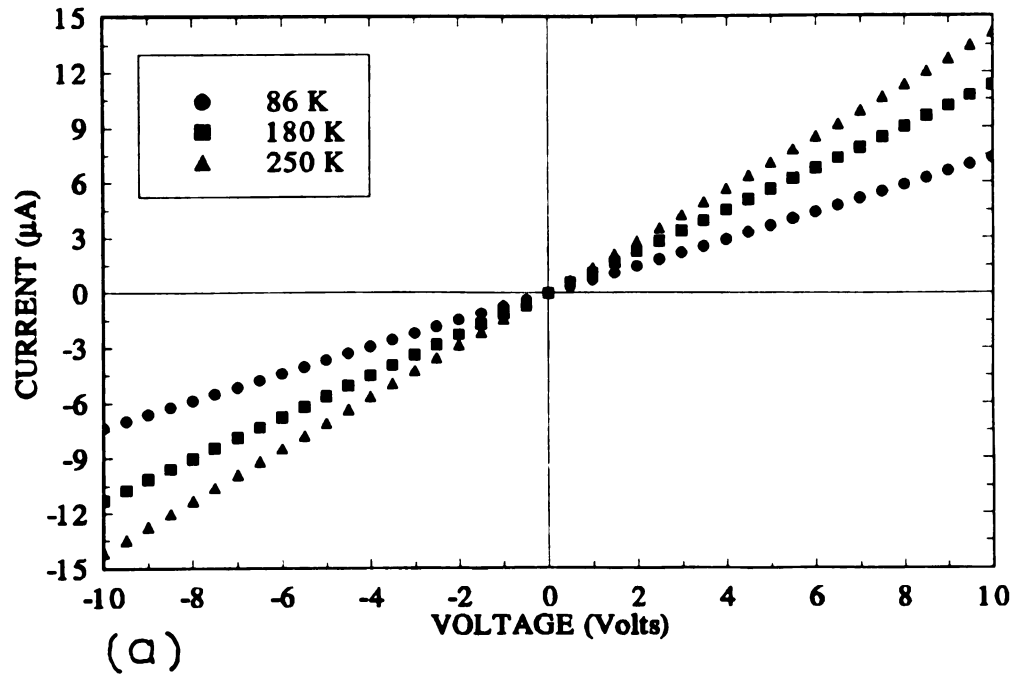


Figure 5.7 I-V characteristics of a test chip at selected temperatures in the temperature range 77-300 K (a) before and (b) after annealing at 1000°C.

same test chip before and after annealing at 1000°C for 8 minutes. All the curves appear fairly linear. The only difference between the curves at same temperature is the change in slope that is due to change in resistivity during annealing process. Any deviation from the linearity at higher voltage (and current) is due to heating effect which will be discussed in next chapter.

A similar behavior was observed in case of I-V measurements at selected temperatures in other temperature ranges as shown in Fig. 5.8. The measurements shown in Fig. 5.8(a) and (b) were made at selected temperatures on discrete and test chip samples in the range of 300-573 K (in static air) and 300-1273 K (at a pressure of 10^{-7} torr), respectively. Though metallized with different metals, i.e., Al and Pt/Ti respectively, both type of samples showed fairly linear behavior over the respective temperature ranges.

5.2.3 Conduction Type Measurement

The type of conduction was determined by two methods. First, by observing the sign of the thermal EMF i.e., the Seebeck effect, using the hot probe method [81]. Second, by observing the sign of the Hall voltage. P-type conductivity was found irrespective of doping level, temperature, diamond film thickness or type of sample (annealed or unannealed). Even the undoped diamond films showed a p-type conductivity which is indicative of the absence of substantial amounts of n-type impurities or defect states. The sign of Hall voltage consistently showed this behavior over the temperature range of 77-300 K.

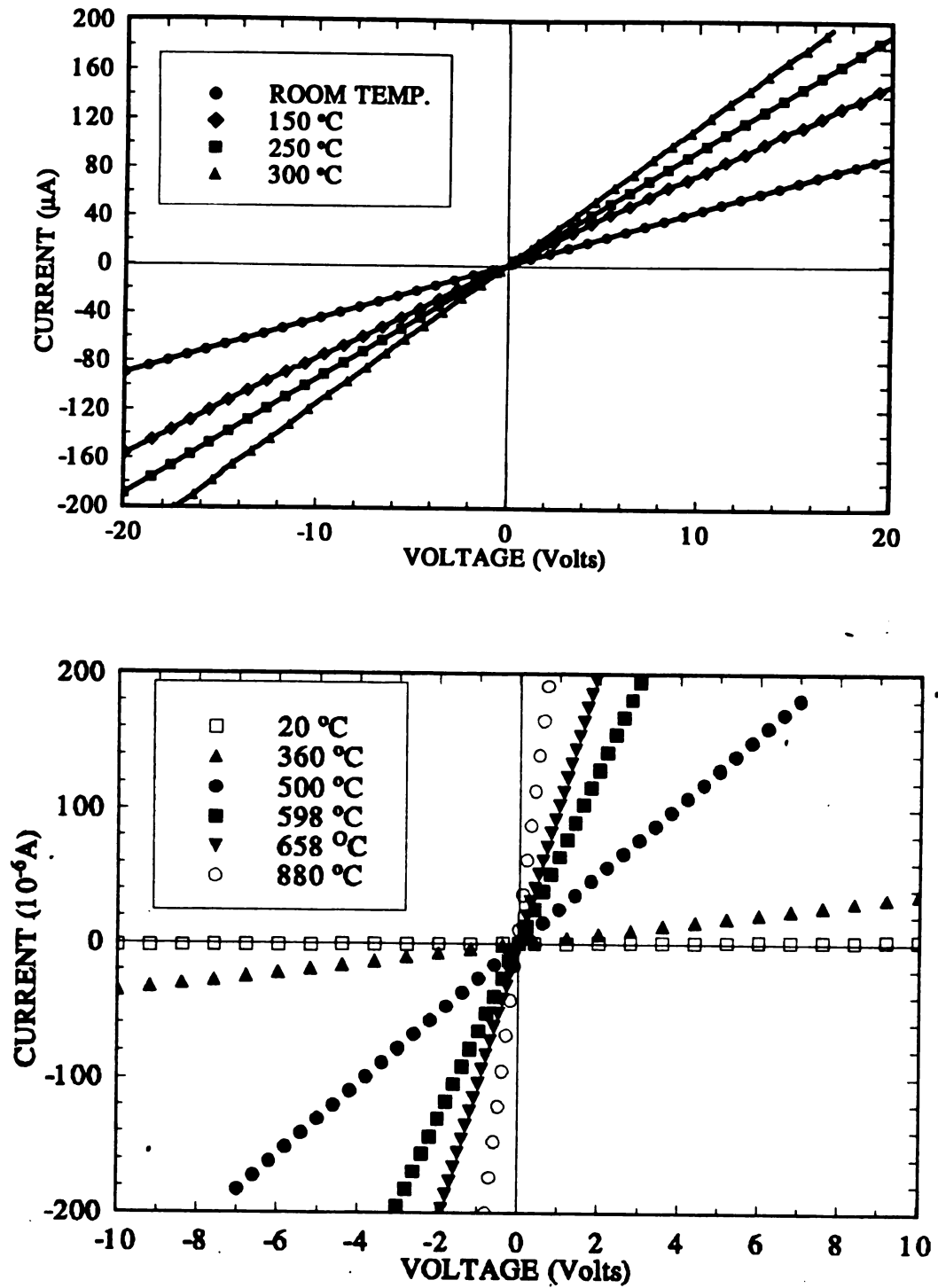


Figure 5.8 I-V characteristics of (a) discrete and (b) test chip samples over temperature range 300-573 K and 300-1273 K respectively.

5.2.4 Resistivity Measurements

The importance of resistivity, in the present case, is due to the fact that the operation of diamond sensor for thermal signals will depend on the resistivity change with temperature. The resistivity measurements were also employed to characterize the in situ annealing behavior of diamond films as well as metal contacts and doping uniformity. The resistivity ρ of the p-type diamond films was determined by two methods. First, it was computed from the two terminal resistance measurements using geometrical dimensions as follows:

$$\rho = \frac{R \times W \times D}{L} \quad (5.1)$$

where R, W, D and L are resistance, width, mean thickness and the length of the diamond film resistor respectively. This method was employed mostly for high temperature measurements using the experimental arrangement shown in Fig. 5.1.

The second method used for resistivity measurement was the Van der Pauw method [167]. It was widely used due to several distinct advantages. A single method and experimental set up is sufficient for the measurement of resistivity and Hall effect. It is particularly useful for the thin samples of arbitrary shape and size. Unlike other methods, it does not depend on various correction factors in measurements for finite sized samples. This property is especially valuable for diamond film patterns of very small dimensions. Furthermore, the contact resistance is automatically taken care of, as in the case of four point probe measurement. The Van der Pauw [167] method was mostly employed for measurements over a temperature range of 77-573 K. In this method, the resistivity ρ of sample with thickness d is expressed as follows:

$$\rho = \frac{\pi d}{2 \ln 2} (R_{AB,CD} + R_{BC,DA}) f \left[\frac{R_{AB,CD}}{R_{BC,DA}} \right] \quad (5.2)$$

where the resistance $R_{AB,CD}$ is defined as the potential difference $V_D - V_C$ between the contacts D and C per unit current through the contacts A and B as per geometry

shown in Fig. 5.9. The current enters the sample through the contact A and leaves it through the contact B. $R_{BC,DA}$ is similarly defined. As indicated in the above equation, f is a function of the ratio $R_{AB,CD}/R_{BC,DA}$ only and if this ratio is close to unity, f can be approximated by the formula

$$f = \left[\frac{R_{AB,CD} - R_{BC,DA}}{R_{AB,CD} + R_{BC,DA}} \right]^2 \frac{\ln 2}{2} - \left[\frac{R_{AB,CD} - R_{BC,DA}}{R_{AB,CD} + R_{BC,DA}} \right]^4 \left\{ \frac{(\ln 2)^2}{4} - \frac{(\ln 2)^3}{12} \right\} \quad (5.2)$$

It is a slowly varying function of the ratio $R_{AB,CD}/R_{BC,DA}$. In practical measurement, it was evaluated to better than 99% precision by the following algorithm [165].

$$f = \frac{-2 \log 2}{\log(A) - \log(1-A)} \quad (5.3)$$

where $A=A_{20}$ which is found by the following recursive relation

$$A_i = (1 - A_{i-1})^k \quad \text{for } i = 1..20$$

with $A_0 = 0.5$ and $k = R_{AB,CD}/R_{BC,DA}$ or $R_{BC,DA}/R_{AB,CD}$ whichever is smaller than 1.

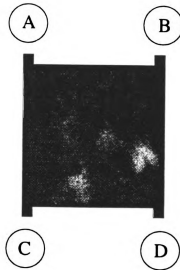


Fig. 5.9 The contact designation of the Hall Pattern on the test chip for Van der Pauw measurements.

If the contacts are placed so that they are symmetrical about a line through any pair of non-adjacent contacts, $R_{AB,CD}/R_{BC,DA} = 1$. When symmetrical contacts are used, any deviation in the ratio is a measure of homogeneity in the resistivity. This is one reason for making the contacts symmetrical on the test chip.

The room temperature resistivity of a number of test chip and discrete samples doped by using various amounts of boron powder is given in Fig. 5.10. The two separate curves in the figure correspond to test chips and discrete samples. The difference between two types of samples has been described in section 5.2.1. As expected, the resistivity decreases with increasing quantity of boron powder used to dope the films. There is an almost constant difference between the two resistivity curves. The resistivity of test chip samples vary from 64 to 0.3 $\Omega\text{-cm}$ corresponding to 0-2.6 mg of boron powder quantity used for doping these samples. In case of discrete samples, the resistivity change is in the range of 98-20 $\Omega\text{-cm}$ corresponding to 0.2-1.2 mg of boron powder. Although there is some scatter in the data, the controlling of doping through quantity of boron powder appears to hold sufficiently.

The resistivity measurements (on $\ln \rho$ scale) over the temperature range of 300-573 K (on $1000/T$ scale) for four discrete samples with different Hall concentrations are shown in Fig. 5.11. The reason for selecting a $\ln \rho$ vs $1000/T$ axis system is to be able to extract information on boron activation energy from the slope of the resistivity curves. In this figure, each resistivity curve displays a single slope over the entire temperature range. The slope of the curves decrease with increasing Hall concentration. The difference between two intermediate curves is not appreciable due to the small difference in Hall concentration. In case of the test chips, the resistivity was measured before and after annealing over a temperature range of 77-573 K and 77-1273 K respectively. Typical resistivity measurements on a test chip are shown in Fig. 5.12. The resistivity measurements corresponding to temperature range of 300-1273 K, as shown in Fig. 5.12(a), show two distinct slopes. The first slope exists from room

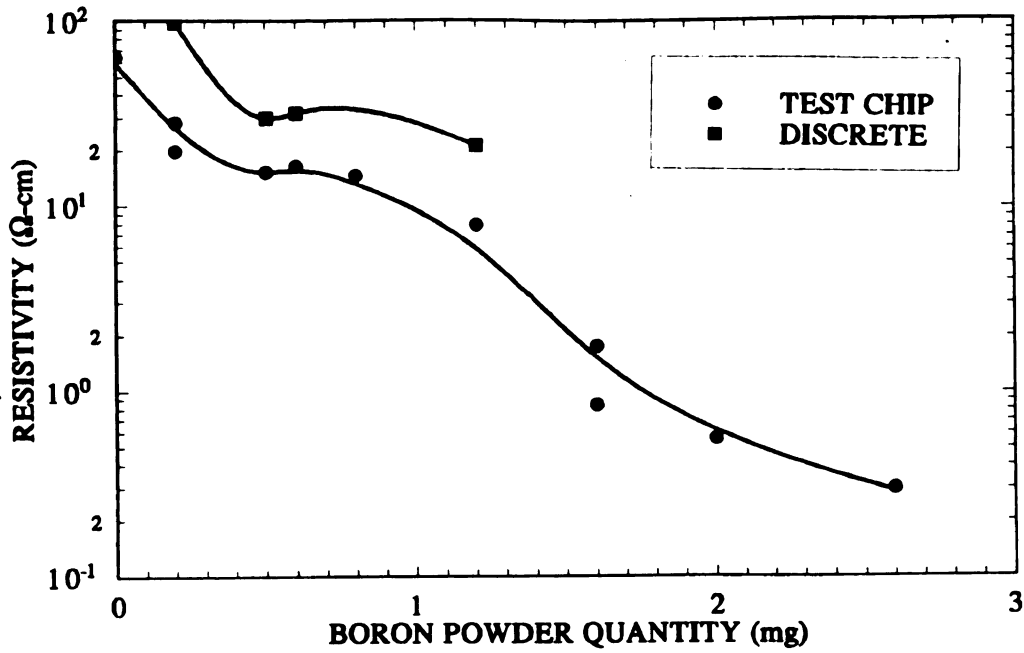


Figure 5.10 The room temperature resistivity vs quantity of boron powder used for the doping of diamond films during deposition.

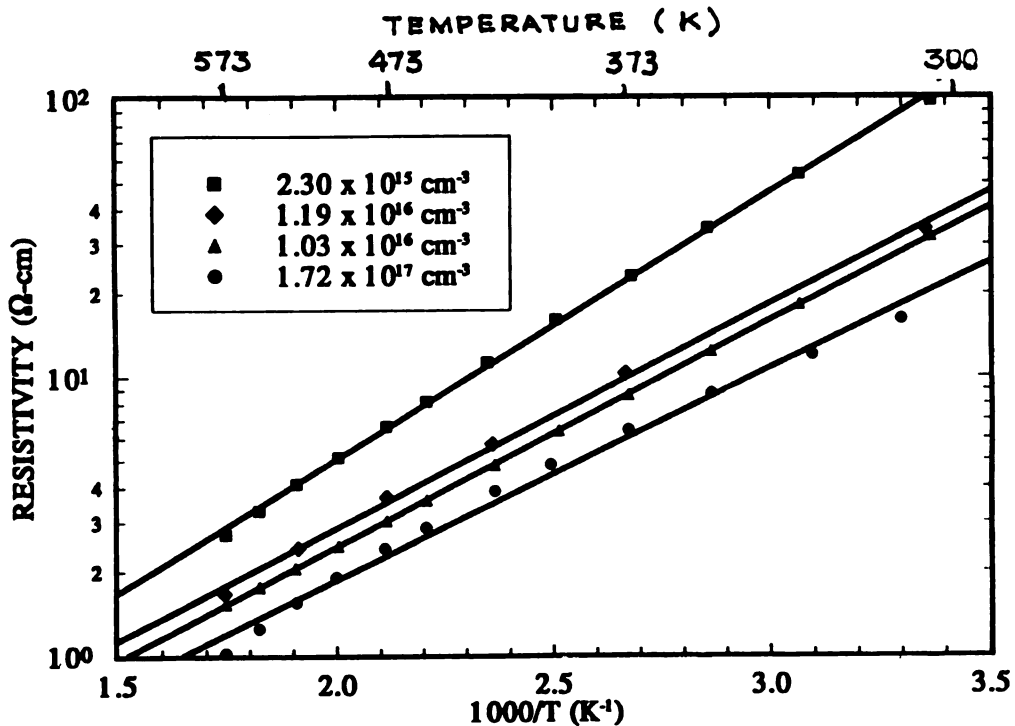


Figure 5.11 The temperature response of resistivity of discrete samples over temperature range of 300-573 K. The room temperature Hall concentration of each sample is also indicated.

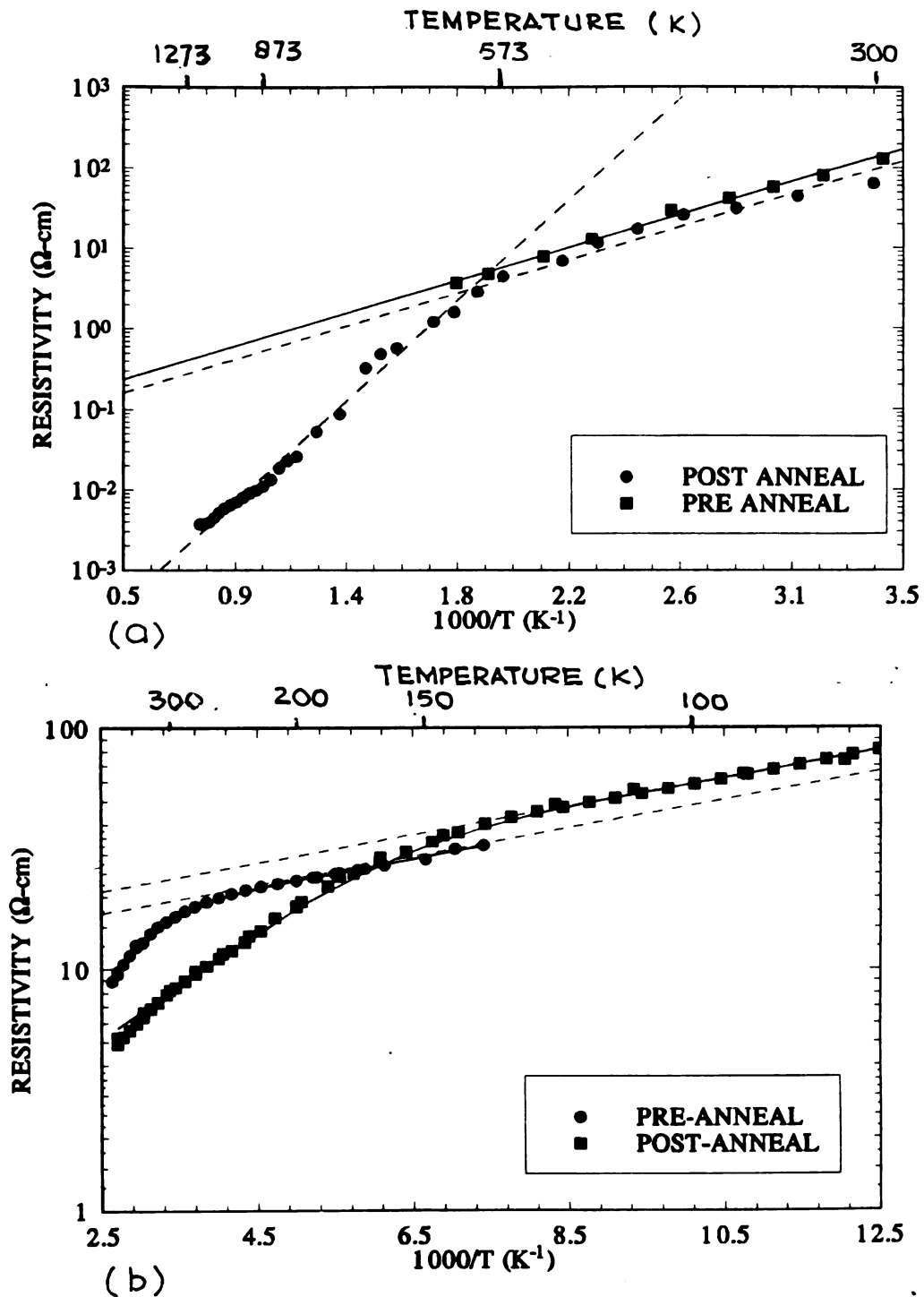


Figure 5.12 The temperature response of resistivity of test chips before and after annealing over temperature range of (a) 300-1273 K ($p=2 \times 10^{15} \text{ cm}^{-3}$) and (b) 77-300 K ($p=1.7 \times 10^{16}$). The solid and dash lines indicate the exponential curve fit for temperature response before and after annealing.

temperature to approximately 573°C and corresponds to band conduction in freeze-out region [107]. The second slope, that is for temperatures beyond 573°C, corresponds to the extrinsic and intrinsic region [8]. However, no distinction in these two regions is visible from this part of the curve. The slope of the curves in the temperature range of 300-573 K, for test chips, decrease with increasing resistivity (and Hall concentration) but the slope for temperatures beyond 573°C is largely unaffected by resistivity values. The resistivity measurements in the temperature range of 77-300 K, as shown in Fig. 5.12(b) before and after annealing, also show two slopes. The slope at temperature below approximately 160 K corresponds to hopping conduction within the freeze-out region whereas the slope at temperatures beyond approximately 160 K corresponds to band conduction within the freeze-out region [93]. This behavior is typical of all the test chip resistivity measurements. The evaluation of various activation energies will be discussed under section 5.3.

5.2.5 Hall Measurements

The Hall measurements were also made by the Van der Pauw method. The Hall mobility was determined by measuring the change in resistance $R_{BD,AC}$ namely $\Delta R_{BD,AC}$, once a magnetic field B is applied perpendicular to the sample with mean thickness d . $R_{BD,AC}$ is defined as the potential difference $V_C - V_A$ between the contacts C and A per unit current through the contacts B and D as per geometry shown in Fig. 5.9. The Hall mobility μ_H is given by [167]

$$\mu_H = \frac{d}{B} \frac{\Delta R_{BD,AC}}{\rho} \quad (5.3)$$

However, a number of spurious signals are included in this measurements. To eliminate them, a series of readings were taken with all possible combinations of current and magnetic field and $\Delta R_{BD,AC}$ was evaluated as follows:

$$\Delta R_{BD,AC} = \frac{1}{4} \frac{V_{(+B,+I)} + V_{(-I,-B)} - V_{(+B,-I)} - V_{(-B,+I)}}{I} \quad (5.4)$$

From the mobility values, the Hall concentration (free holes) was evaluated using the following relation for p-type semiconductor

$$p = \frac{1}{q \mu_c \rho} \quad \text{assuming } \mu_H = \mu_c \quad (5.5)$$

Though the two types of mobility are different by a factor of $3\pi/8$, the Hall mobility is usually approximated with conductivity mobility μ_c for perfect single crystal bulk material. By making measurements at high magnetic fields, this factor can be reduced to 1, regardless of the conduction mechanism [81]. In this research, a magnetic field of about 3kG was used which is considered high enough to allow the reduction of this factor to unity.

The Hall concentration measured against various resistivity values for two type of samples has been plotted in Fig. 5.13(a). The corresponding Hall mobilities are also shown in Fig. 5.13(b). As expected the resistivity and Hall mobility decreased with increasing carrier concentration. The range of Hall concentration i.e., 10^{15} – 10^{19} cm^{-3} covers fairly well the whole practical range of interest. Comparing the two types of samples, the resistivity of discrete samples is larger and the Hall mobility is smaller for comparable Hall concentration. The Hall mobility of the discrete samples is relatively very small especially at higher Hall concentration. Nevertheless, both of these parameters agree with values found in the literature on polycrystalline diamond films [96-98]. However, the mobility is about two orders of magnitude less than reported value of $1200 \text{ cm}^2\text{V}^{-1}\text{s}^{-1}$ for crystalline diamond [47]. This may be due to the strong influence of scattering at the grain boundaries present in the polycrystalline films. With comparable Hall concentrations, the lower Hall mobility for discrete samples can be attributed to the relatively smaller grain size (Hence more grain boundaries and carrier scattering) due to smaller thickness (2-3 μm versus 3.4-4.5 μm) or the relative purity of the film as discussed in chapter 3.

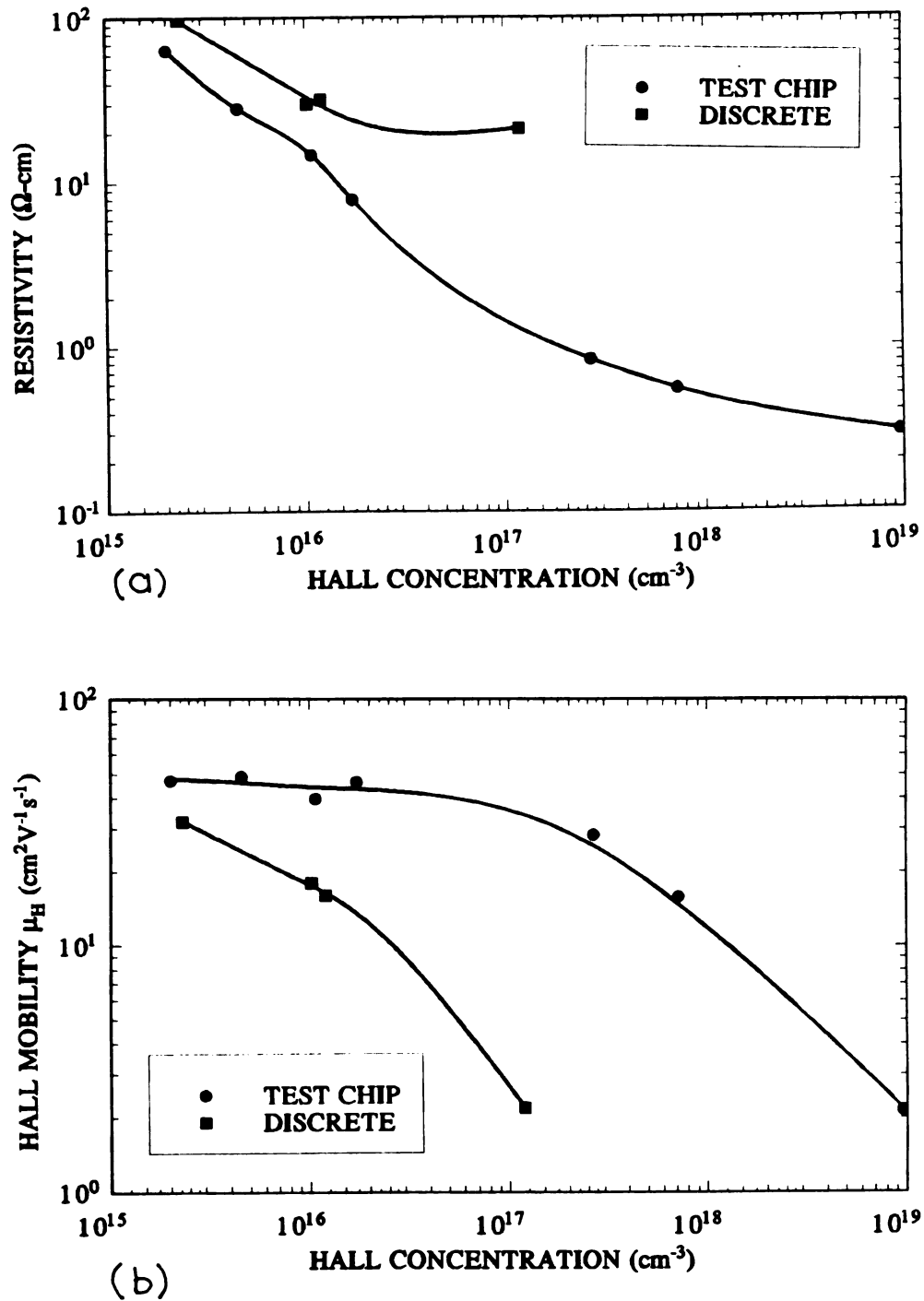


Figure 5.13 The room temperature (a) resistivity and (b) Hall mobility vs measured Hall concentration of the two types of samples.

The measurement of Hall concentration and the corresponding Hall mobilities over the temperature range 77-300 K have been shown in Fig. 5.14. The Hall concentration, as expected, increase with temperature. The Hall mobility plotted against $T^{-3/2}$, showed a maxima around 160 K. The part of the mobility curve below and above this temperature is usually controlled by lattice and impurity scattering respectively. The mobility due to lattice scattering and impurity scattering are expected to follow $\mu_L \propto T^{-3/2}$ and $\mu_I \propto T^{3/2}$ respectively in crystalline semiconductors. However, the curve in Fig. 5.14(b), plotted against $T^{-3/2}$ does not appear to follow these relations which is indicative of additional scattering mechanism.

5.3 COMPUTED PARAMETERS

For all test chips, $\ln \rho$ vs $1/T$ curves corresponding to resistivity measurements over the temperature range of 300-1273 K show two distinct slopes (see Fig. 5.12(a)). The slope in temperature range 300-573 K, corresponds to the band conduction zone of the freeze-out region of diamond where boron impurities are partially ionized [107,166]. The slope for temperature $>300^\circ\text{C}$ corresponds to the extrinsic and intrinsic regions of natural semiconducting diamonds [47,107]. However, there is a possibility that the freeze-out region extends beyond 300°C with a different boron activation energy. In the intrinsic region the resistivity usually follows the relation

$$\rho \propto \exp\left[\frac{E_g}{2kT}\right] \quad (5.6)$$

Hence the slope of $\ln \rho$ vs $1/T$ curves should be representative of $E_g/2$. Moreover, the starting point of this region is determined by impurity concentration since they equal the intrinsic carrier concentration at this temperature.

In actual measurements, the slope of the curves beyond 300°C correspond to 0.58, 0.421 and 0.375 eV for the samples with room temperature Hall concentration of 2×10^{15} , 1.07×10^{16} , and $9.8 \times 10^{18} \text{ cm}^{-3}$ respectively. Clearly, these values are much less

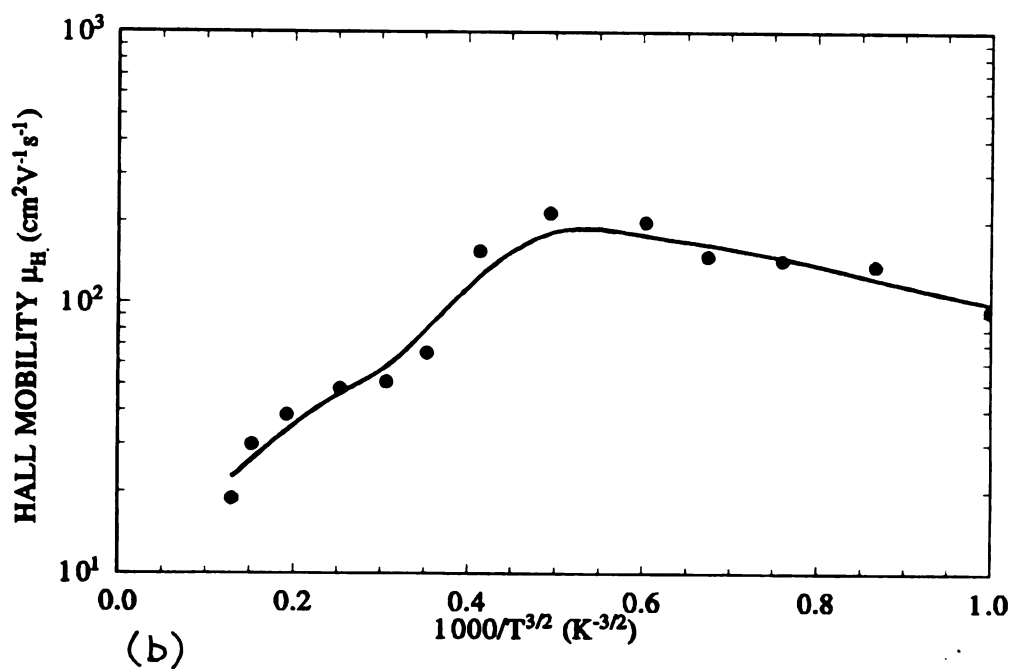
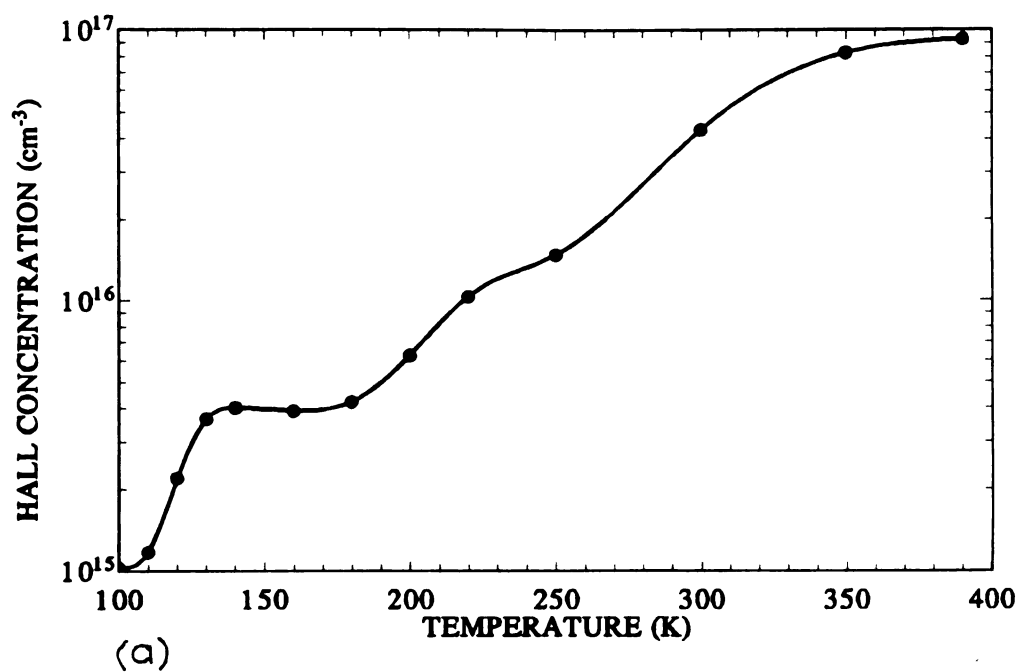


Figure 5.14 The temperature response of (a) Hall concentration and (b) Hall mobility in the temperature range of 77-300 K.

than half the band gap of diamond (that is 5.45 eV). Also, these values are somewhat impurity concentration dependent. In addition, the starting point of this slope was found to have no clear dependence on the Hall concentration. These observations suggest that the temperature response of diamond films at high temperature has no correlation with the intrinsic behavior of crystalline semiconducting diamond.

In the temperature range 77-300 K, the $\ln \rho$ vs $1/T$ curves, as shown in Fig. 5.12(b), showed two distinct slopes. The slope at temperatures beyond approximately 160 K corresponds to band conduction in freeze-out region whereas the slope at temperatures <160 K, corresponds to hopping conduction region as stated in Eq. 2.3.13. Taking \ln in this equation we obtain

$$\ln \rho = \epsilon_3/kT + \ln \rho_0 \quad (5.7)$$

where ϵ_3 is defined as the hopping conduction activation energy. The slope of resistivity curve below 160 K in Fig. 5.12(b) is essentially constant. Using Eq. 5.7, the slope of resistivity curve equals $\epsilon_3/1000 \times k$. The computed values of ϵ_3 in this case is 11.72 meV. This value of ϵ_3 , as shown in Fig. 5.12(b), did not show any sign of variation with annealing at 1000°C. Since hopping conduction takes place by jumping of charge carriers from impurity atom to impurity atom, it requires some donor states to be present. Hence, the presence of a hopping regime within freeze out region may be due to compensation of impurities.

It was stated in chapter 2 that for a partially compensated p-type semiconductor with a single impurity activation energy level at E_A in the band gap, the hole concentration can be extracted from Eq. (2.3.9). If little or no compensation is assumed, the hole concentration is given by Eq. (2.3.11). Since no donor impurities were added intentionally or found through SIMS analysis of diamond films used in this research, it can safely be assumed that little or no compensation of impurities took place. This assumption is further supported by the fact that any defect states present in the as grown diamond films are passivated by hydrogen present in the diamond films

[99,100,103,159]. This was shown on the basis of observing irreversible changes in the I-V curves of undoped diamond films annealed at various temperatures. Since no irreversible change in the temperature response of the resistivity was noticed up to 300°C, we can extend this assumption up to this temperature. Hence, all the discrete and unannealed test chip samples can be treated under this assumption. Substituting the value of p from Eq. (2.3.11) into the relation $\rho = (qp\mu_p)^{-1}$, we get

$$\rho = \frac{1}{q\mu} \left[\frac{N_v N_a}{2} \right]^{-\frac{1}{2}} \exp \left[\frac{E_a}{2kT} \right] \quad (5.8)$$

If it is assumed that $\mu \propto T^{-3/4}$, the pre-exponential factor becomes independent of temperature. In the $\ln \rho$ vs $1/T$ curves shown in Fig. 5.12(a), slope of curve for temperature below 300°C for unannealed test chip is fairly constant. Using Eq. 5.8, this slope equals $E_a/2000 \times k$. The activation energy E_a , computed by this method for a number of unannealed test chips and discrete samples, is shown against the measured Hall concentration in Fig. 5.15(a). The value of E_a decreases with increasing Hall concentration in both the discrete and the test chip samples. E_a values for the discrete samples are relatively large for comparable Hall concentration. The decrease of E_a with increasing Hall concentration may be due to formation of an impurity band within the energy gap. E_a values for most lightly doped test chips ($p=2 \times 10^{15} \text{ cm}^{-3}$) and discrete ($p=2.3 \times 10^{15} \text{ cm}^{-3}$) samples are 0.36 and 0.38 respectively which are in close agreement with the reported value 0.37 eV for single crystal diamonds [47]. Moreover, earlier measurements of E_a of CVD diamond films [97] showed values in the range of 0.26 to 0.38 eV which are consistent with E_a values given in Fig. 5.15(a).

The impurity concentration was computed by substituting values of E_a into Eq. (2.3.11) which is re-arranged as follows:

$$N_A = \frac{(2p)^2}{N_v} \exp \left[\frac{E_a}{kT} \right] \quad (5.9)$$

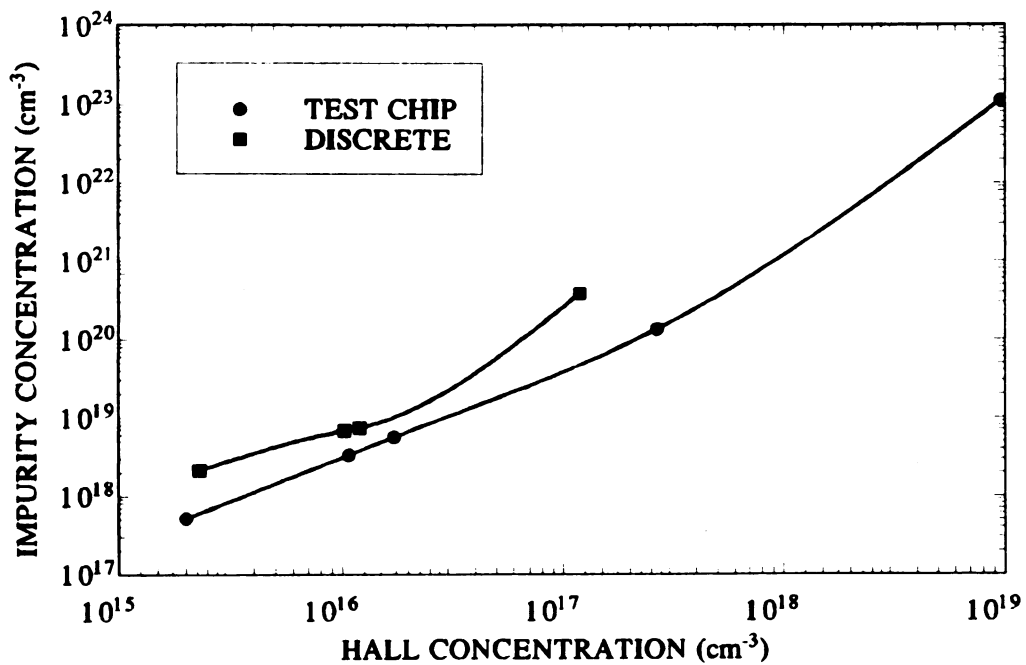
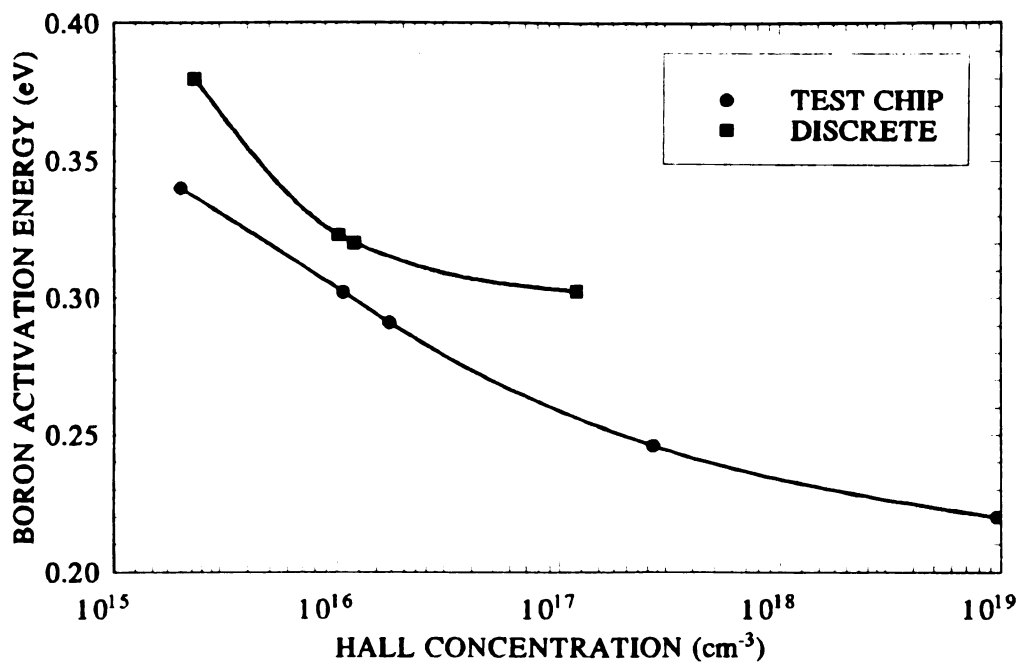


Figure 5.15 The plots of computed boron (a) activation energy and (b) concentration against measured Hall concentration for two types of samples.

N_v was computed using $m_p = m_0$ of natural semiconducting diamond [107] to yield

$$N_v = 3.137 \times 10^{15} T^{3/2} \text{ cm}^{-3} \quad (5.10)$$

At $T = 300 \text{ K}$,

$$N_v = 16.3 \times 10^{18} \text{ cm}^{-3} \quad (5.11)$$

The resulting impurity concentrations are plotted against measured Hall concentration in Fig. 5.15(b). As expected, the impurity concentration increases with Hall concentration. The fact that 0.04 to 0.75% of impurities are ionized at 300K over the whole range, agrees with the observation that at room temperature $\leq 1\%$ impurities are ionized [166]. This supports the initial assumption of little or no compensation in these films.

In the case of the annealed test chips, the assumption of passivation of the defect states is no longer valid due to dehydrogenation of diamond films during annealing [99,100,103,158]. Assuming these samples to be partially compensated and the assumption of $N_A > N_D \gg p$ holds, the hole concentration in the band conduction zone of the freeze-out region is given by Eq. (2.3.10). Substituting the value of p into the relation $\rho = (qp\mu_p)^{-1}$, we get

$$\rho = \frac{2}{q\mu N_v} \frac{K}{K-1} \exp\left(\frac{E_a}{kT}\right) \quad (5.12)$$

where $K = N_D/N_A$ is the compensation ratio. Now assuming that $\mu \propto T^{-3/2}$, the pre-exponential factor becomes independent of temperature. Using Eq. 5.12, the slope of annealed test chips in the temperature $< 300^\circ\text{C}$ equals $E_a/1000 \times k$. Note that the compensation assumption reduces the computed activation energy by one half for the same slope of $\ln \rho$ vs $1/T$ curve.

The activation energy computed by this method for a number of annealed test chip samples is shown against measured Hall concentration in Fig. 5.16. The values of E_a found earlier for the same (unannealed) samples with no compensation assumption are also included in this figure for comparison. Note that the scale on the right

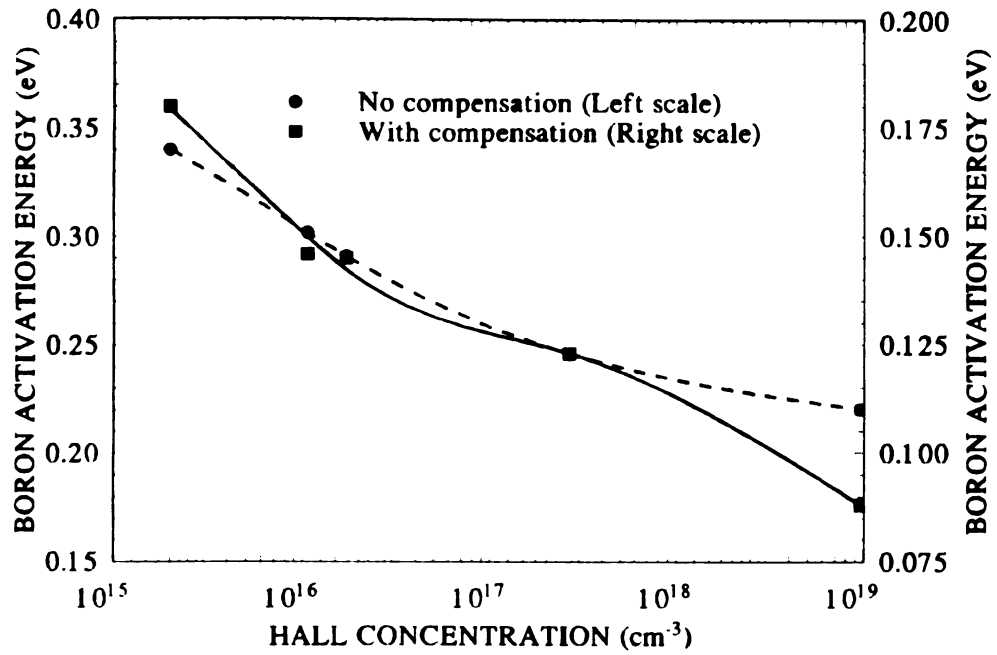


Fig. 5.16 The plots of computed boron activation energy of test chips before (assuming no compensation) and after annealing (assuming compensation) against Hall concentration measured at room temperature.

vertical axis is exactly half of what is on the left vertical axis. The present values of E_a are roughly one half of the earlier values. Beside this difference due to the computational method used, E_a increases due to annealing at lower Hall concentrations whereas this effect is reverse at higher Hall concentrations. The reason for this behavior is not understood.

The impurity concentration, in this case, can be computed by substituting the values of E_a into Eq. (2.3.10). However, in this case, N_D should be known for the evaluation of N_A . The equation can be solved for the compensation ratio K as follows:

$$K = \left[1 + \frac{2p}{N_v} \exp\left[\frac{E_a}{kT}\right] \right]^{-1} \quad (5.13)$$

The computed value of compensation ratio K is 79.6% for Hall concentration of $2 \times 10^{15} \text{ cm}^{-3}$. This value appears fairly unreasonable. This may be due to the basic assumption of $N_A > N_D \gg p$, taken for the computation of K value.

5.5 SUMMARY

In this chapter, fundamental properties such as resistivity, mobility, carrier and impurity concentration and impurity activation energy of the diamond films as a semiconductor material were acquired. The annealing behavior of diamond films was investigated. The resistivity of test chips was measured over the widest temperature range (77-1273 K) ever reported. The control of doping through the quantity of boron powder was measured. A characteristic curve of Hall concentration versus boron powder was prepared. Finally, the conduction mechanism in CVD diamond films in various regions was discussed in length. The knowledge acquired about the electrical properties of diamond films will be useful in understanding and predicting the behavior of diamond film based electronic devices in general and sensor for thermal signals in particular.

CVD DIAMOND FILM SENSORS FOR THERMAL SIGNALS

6.0 INTRODUCTION

In this chapter, the properties of diamond film sensors for temperature and heat flux will be discussed. The static temperature response over the temperature range of 77-1273 K is acquired for various doping levels. High temperature effects on the quality of diamond films are presented in section 6.2. The measurement of dynamic temperature response of the sensor and its implications on its application as a heat flux sensor is described in section 6.3. An on-chip signal processing circuit made exclusively of diamond film devices is proposed in section 6.4.

6.1 STATIC TEMPERATURE RESPONSE

The temperature response of a semiconductor is basically its resistivity change with temperature. Hence, the resistivity curves against temperature presented in the last chapter provide this information for CVD diamond films. Fig. 6.1 shows the temperature response for three doping levels (including two extreme measured values) for diamond films over the temperature range of about 77-1273 K. All the samples were

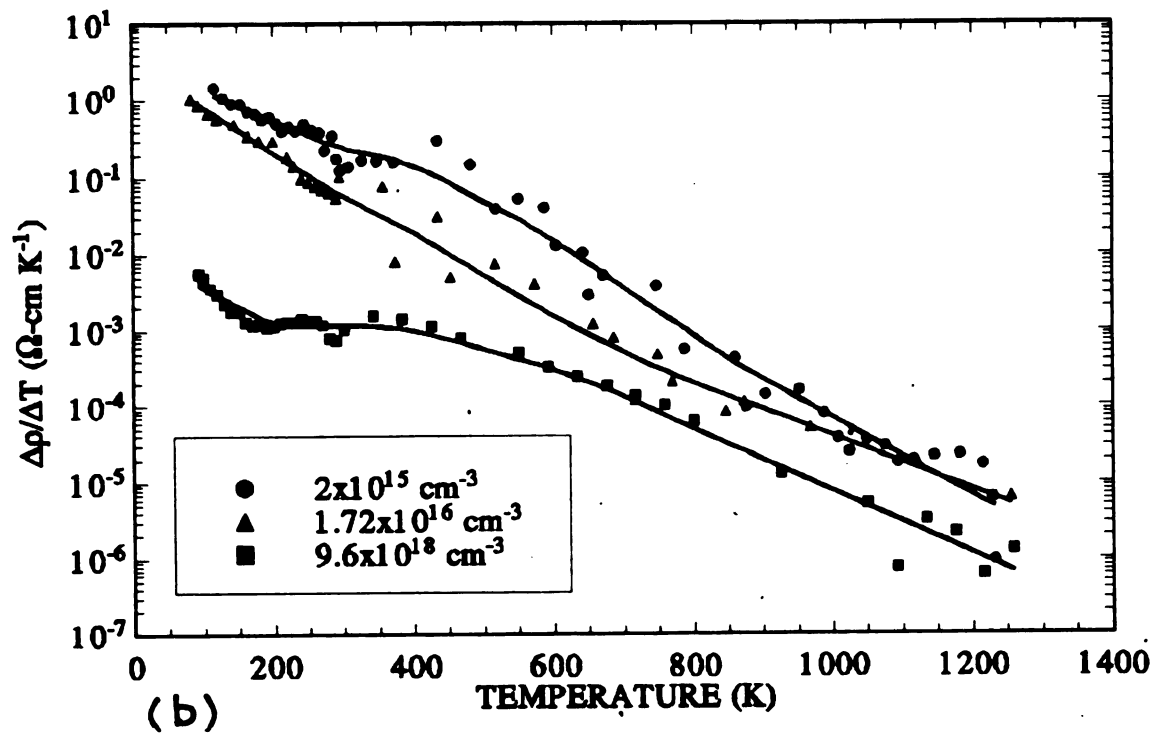
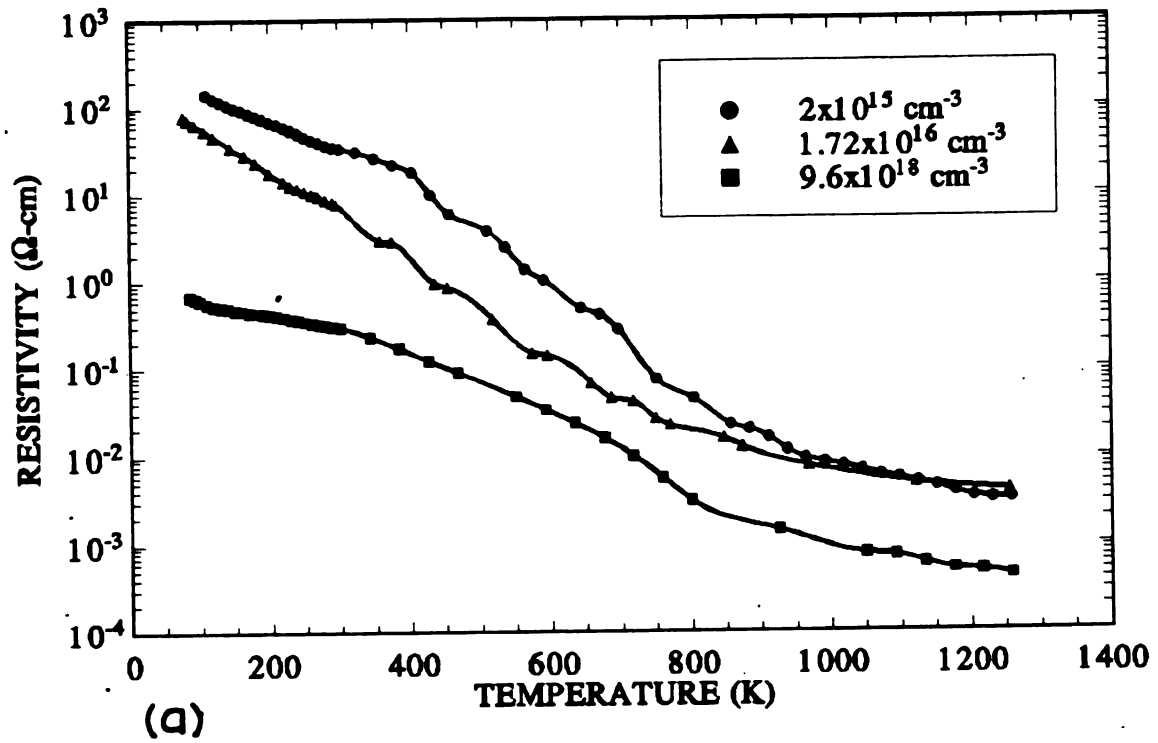


Figure 6.1 The temperature response of the (a) resistivity and (b) sensitivity in terms of $\Delta\rho/\Delta T$, of diamond film thermal sensors. The Hall concentration of each sensor is also indicated.

annealed at temperatures of 600°C and 1000°C for 35 and 8 minutes respectively at a pressure of 10^{-7} torr before taking measurements for temperature response of resistivity. It can be seen that that the sensors have a negative temperature coefficient (NTC) over the entire temperature range. This is unique to diamond films because all conventional semiconductors, monocrystalline or polycrystalline, normally exhibit a NTC only in the freeze-out and intrinsic regions and positive temperature coefficient (PTC) in the extrinsic region. This is an essential property of a sensor in order to show a monotonic change of observable with a change in measurand to avoid showing a single value of observable for multiple values of measurand. This property makes diamond films useful as a temperature sensor over a wide temperature range i.e., 77-1300 K, a range never covered by a single semiconductor temperature sensing device before.

From the curves in Fig. 6.1(a), one can see that the lower the doping level, the more rapid the change in resistivity. This effect is obvious from the plots of $\rho_{\Delta} = \Delta\rho/\Delta T$ versus temperature as shown in Fig. 6.1(b). While comparing the two extreme doping levels, the values of ρ_{Δ} are about two order of magnitude larger at the lower temperature limit and about one order of magnitude larger at higher temperature limit for the lower doping level. This observation suggests that a lower doping level is better in terms of sensitivity to the temperature changes. A criterion frequently used for comparison of sensitivity of temperature sensors is the temperature coefficient α defined as

$$\alpha = \frac{1}{\rho} \frac{\delta\rho}{\delta T} \quad (6.1)$$

The value for alpha for the same three doping levels, computed from Fig. 6.1, are shown in Fig. 6.2. The large scatter in the data resulted from the large temperature intervals between data points and the scatter in the original ρ versus temperature data. Locally weighted average curves of α show the existence of a minima and a maxima at about 200 and 600 K, respectively. Since the curves are highly non-linear and

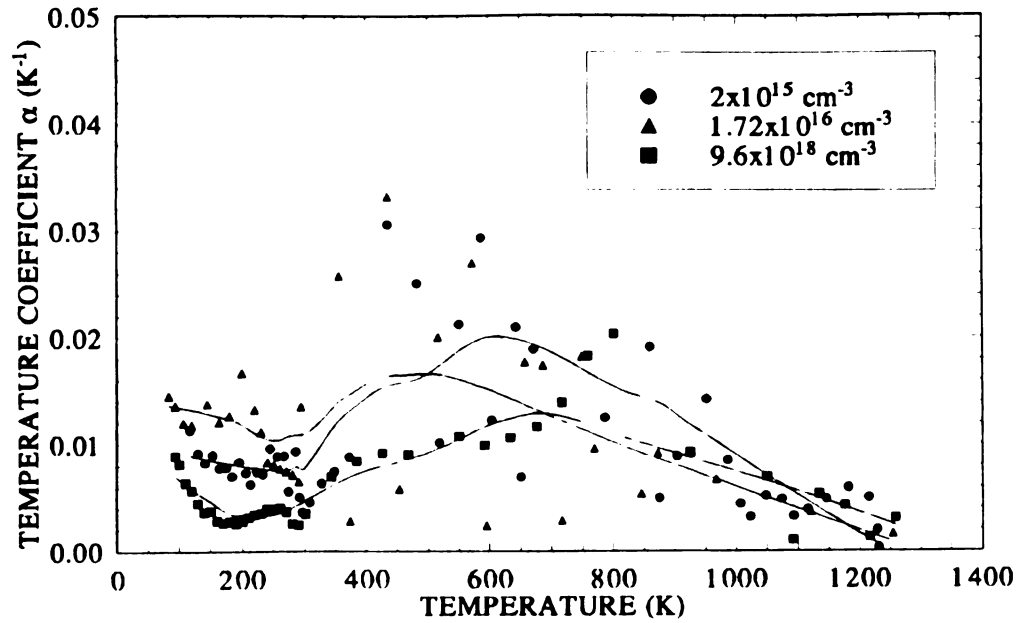


Figure 6.2 The plots of temperature coefficient α versus temperature for diamond film thermal sensors. The Hall concentration of each sensor is also indicated.

overlapping each other, it is difficult to compare the effect of doping in terms of α . The mean value of α remains about 0.006-0.008 in all cases. For comparison, the average value of α for Pt RTD is 0.00385 [9]. Hence, the sensitivity of diamond sensors is better than Pt RTD over most of the temperature range. However, the thermistors show a typical value of α in the range of 0.2-0.4 but only over a limited net temperature range i.e., typically 100 K [9].

Although α is widely used to represent the sensitivity of temperature sensors, but it was basically devised for RTDs and is not suitable for comparison of sensitivity for semiconductor sensors. To emphasize this point, a 100 k Ω thermistor and a 25 Ω RTD both with $\alpha = 0.001$ will show a resistance change of 100 Ω and 25m Ω , respectively, with a temperature change of 1 K. Though rated at the same sensitivity, the temperature measurement with the semiconducting sensor will obviously be more accurate, can achieve higher resolution and is much easier to detect. Therefore, α will not be used for comparison of semiconducting temperature sensors in this discussion anymore. Instead, another criterion, W, defined as ratio of resistance at two temperatures T_1 and T_2 is frequently used for the comparison of temperature sensors [9] has proved better for comparison of semiconducting temperature sensors.

In case of test chip, all the sensors spanned the temperature range of at least 100-1250 K, W will be defined as

$$W = \frac{\rho_{100}}{\rho_{1250}} \quad (6.2)$$

The value of W for different doping levels is shown in Fig. 6.3. It is almost linearly decreasing function of Hall concentration. From this curve it is obvious that a lower doping value will have a greater sensitivity to temperature changes.

From an application point of view, the temperature is a dependent variable which is determined from the value of resistivity (or resistance) using a calibrated curve. This calibrated curve is either incorporated into a look up table or implemented into

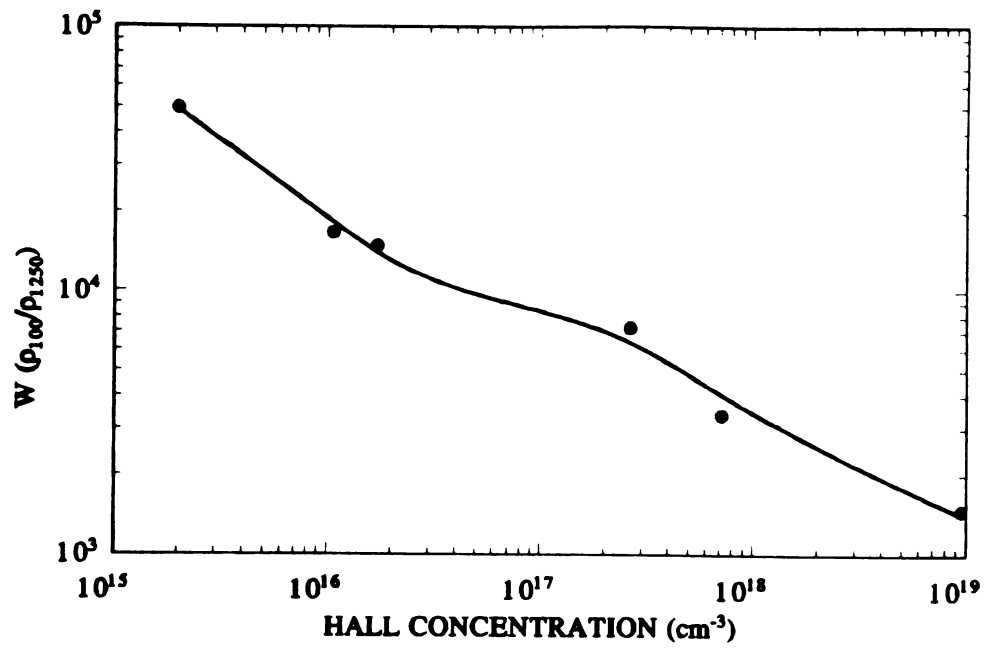


Figure 6.3 The sensitivity of diamond film thermal sensors in terms of W as defined by Eq. 6.2 against measured Hall concentration.

hardware. To estimate the diamond sensor suitability from this point of view, polynomial curve fitting was done for several sensors. In the case of a sample with Hall concentration of $2 \times 10^{15} \text{cm}^{-3}$ the following fourth order polynomial equation

$$T = 606.906 - 54.745x - 5.613x^2 - 1.633x^3 + 0.173x^4 \quad \text{with } x = \ln \rho \quad (6.3)$$

fitted the observed resistivity to the test temperature with a correlation of 99.89%. Both the measured and estimated curves are shown in Fig. 6.4(a). In spite of the large scatter in the data the maximum error of estimation was less than 9 K. It is believed that the measured data will be much smoother if it was acquired at a smaller temperature interval using a better calibrated reference than the type K thermocouple employed. In that case, a third order equation may be sufficient for good curve fitting. It is customary with manufacturers [14] to do curve fitting in terms of reciprocal temperature. It is because most thermistors show excellent linearity in the freeze-out range they are usually operated in. These curves are typically implemented in hardware using logarithmic amplifiers. Therefore, it will be suitable to do curve fitting in terms of $1/T$ for diamond sensors too. For the same sensor above (with Hall concentration of $2 \times 10^{15} \text{cm}^{-3}$) the following equation also gave a correlation of 99.88%.

$$\frac{1}{T} = 1.687 + 0.262x + 0.013x^2 - 0.019x^3 + 0.000075x^4 \quad \text{with } x = \ln \rho \quad (6.4)$$

Both the measured and estimated curves are shown in Fig. 6.4(b). Hence, an equation of same order i.e., 4, gives sufficiently close fitted curves. For conventional thermistors, which operate in a limited range, a third order polynomial equation is generally sufficient. For diamond sensors covering a total range of over 1300 K, a fourth order curve fit will give excellent performance.

Cross sensitivity to physical effects other than the primary measurand can always plague the sensor output yielding random errors. Strain in the metallic temperature sensors have shown pronounced effects on the calibration coefficients [12]. In case of diamond film temperature sensors, the change of resistivity with strain has been shown to

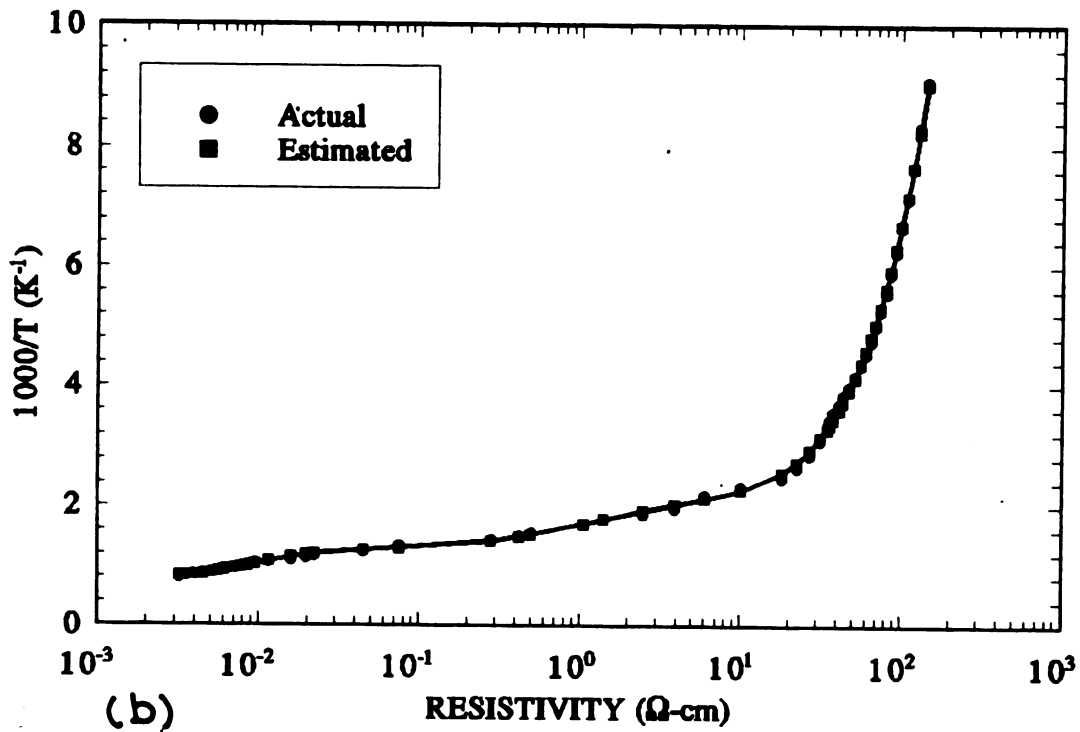
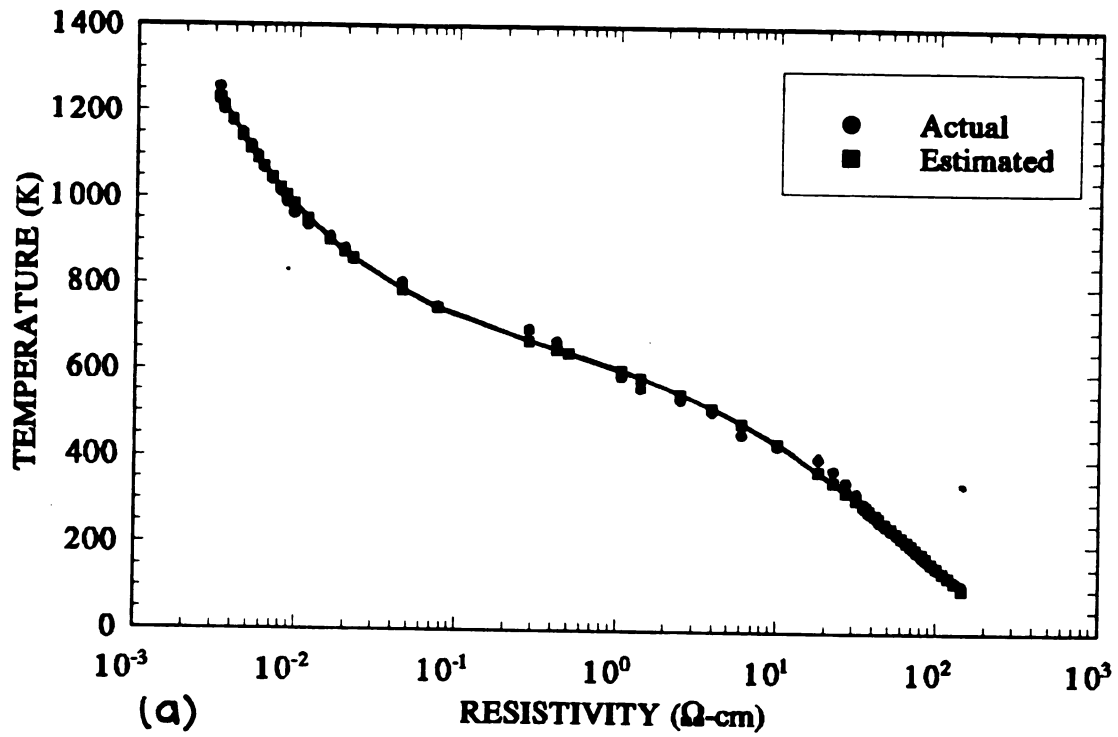


Figure 6.4 The plots of fitted curves along with measured data for (a) temperature and (b) reciprocal of temperature against \ln resistivity. ($p=2 \times 10^{15}$)

be several orders of magnitude smaller than because of temperature [168]. Hence, any effect of strain on the resistivity of diamond film temperature sensors can be neglected.

In addition to cross sensitivity, the integrity of measurements are subject to changes occurring in the properties of metal interconnects and substrate with temperature. The conductivity of the SiO₂ layer under the diamond film and the resistance of the metal conducting lines increase with temperature. These effects are shown in Fig. 6.5. The resistance of the SiO₂ was measured between two adjacent metal bonding pads (0.5 mm spacing between them) with no other conducting path between them. The resistance was beyond the measuring range of the instrument (10 MΩ) for most of the temperature range but decreased sharply after 875°C. This provides a conducting path parallel to sensors. The average SiO₂ thickness in this case was 1.129 μm. Though the oxide resistance in this case was still much higher than sensor itself (a factor of 200 at 1000°C), it should be recognized that a smaller oxide thickness may have higher conductivity than this sample.

The resistance of metal conducting lines was measured between two metal bonding pads connected with 6.75 mm long and 160 μm wide metal line. Though the resistance of the metal line, as shown in Fig. 6.5(b), increases almost linearly with temperature, it is significantly smaller than that of sensors. Hence, any effect due to variation of metal conductor resistance can be ignored.

6.2 HIGH TEMPERATURE EFFECTS

There are several effects associated with high temperature treatment of diamond films. In addition to the irreversible change in resistivity discussed in the last chapter, the oxidation of diamond is prominent. In chapter 3, diamond films were shown to oxidize in flowing oxygen at temperature >650°C. Oxidation of diamond by an oxygen plasma was observed even at lower temperatures [82]. To avoid oxidation, the diamond sensors were always tested at pressures of about 10⁻⁷ torr for the acquisition of

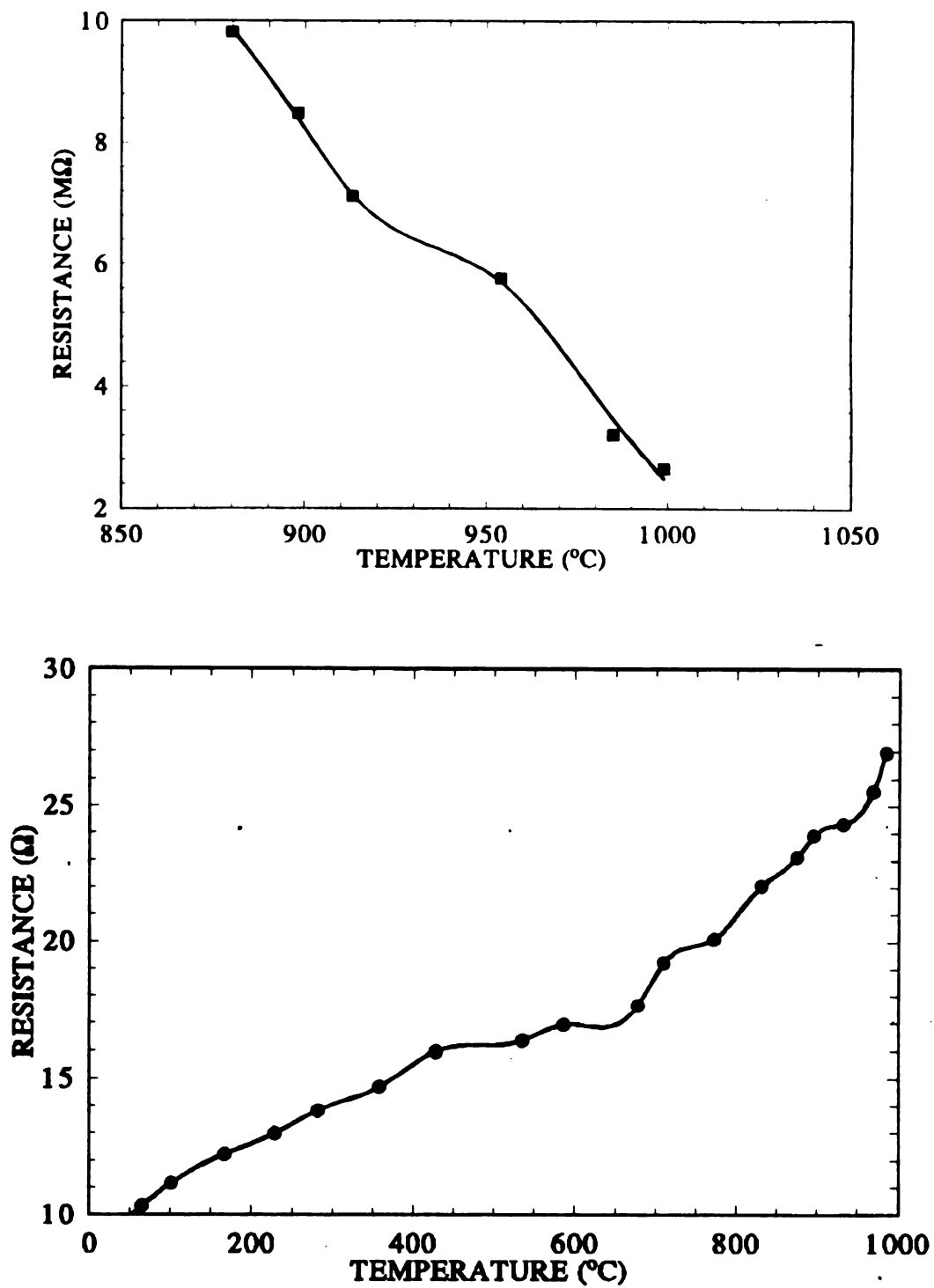


Figure 6.5 The temperature response of the resistance of (a) 1.1 μm thick thermal SiO_2 layer and (b) metal conducting lines (see text for experimental set up).

their temperature response. The similarity of Raman spectra, before and after heat treatment, as shown in Fig. 6.6(a), confirm the preservation of quality of diamond films during heat treatment. A high resolution Raman spectra shown in Fig. 6.6(b) of the same film, shows the absence of any peak at 1355 cm^{-1} corresponding to amorphous carbon. SEM micrographs of the diamond film after heat treatment at 1000°C for a total of 14 minutes in 4 cycles are shown in Fig. 6.7. Any change in the surface morphology is not visible. However, if the sample is heated at still higher temperatures, some effects start to appear. For example, a sample heated at 1249°C for 2 minutes was found to have somewhat darker grain boundaries (see Fig. 6.8(a)). However, no sign of deterioration of quality was observed from the Raman spectrum of this sample (not shown). To observe the effectiveness of high vacuum in protecting the diamond film, a sample was heat treated at 1000°C for 2 minutes at a pressure of 100 mtorr. SEM micrograph of this sample is shown in Fig. 6.8(b). Here a significant amount of erosion is clearly visible. From these SEM micrographs and Raman spectra, it may be assume that no structural change in the diamond film occurred during the high treatment of diamond films at pressure of 10^{-7} torr. However, there is a clear need to protect the diamond films in the oxidizing ambient while at temperatures $> 650^\circ\text{C}$ if this high temperature should persist beyond a few seconds. Possible protection layers are undoped diamond, SiO_2 or Si_3N_4 .

6.3 DYNAMIC TEMPERATURE RESPONSE

The dynamic thermal response time constant is defined as the time required by the sensor to reach 63.2% of a step change in temperature under a specific set of conditions (pressure, humidity, air flow, etc.,). However, generating a true step function of temperature is quite complex. Therefore, a gradual change in temperature faster than the sensor's expected time constant is usually considered an acceptable step function. Due to the small thermal time constant expected with diamond film sensors,

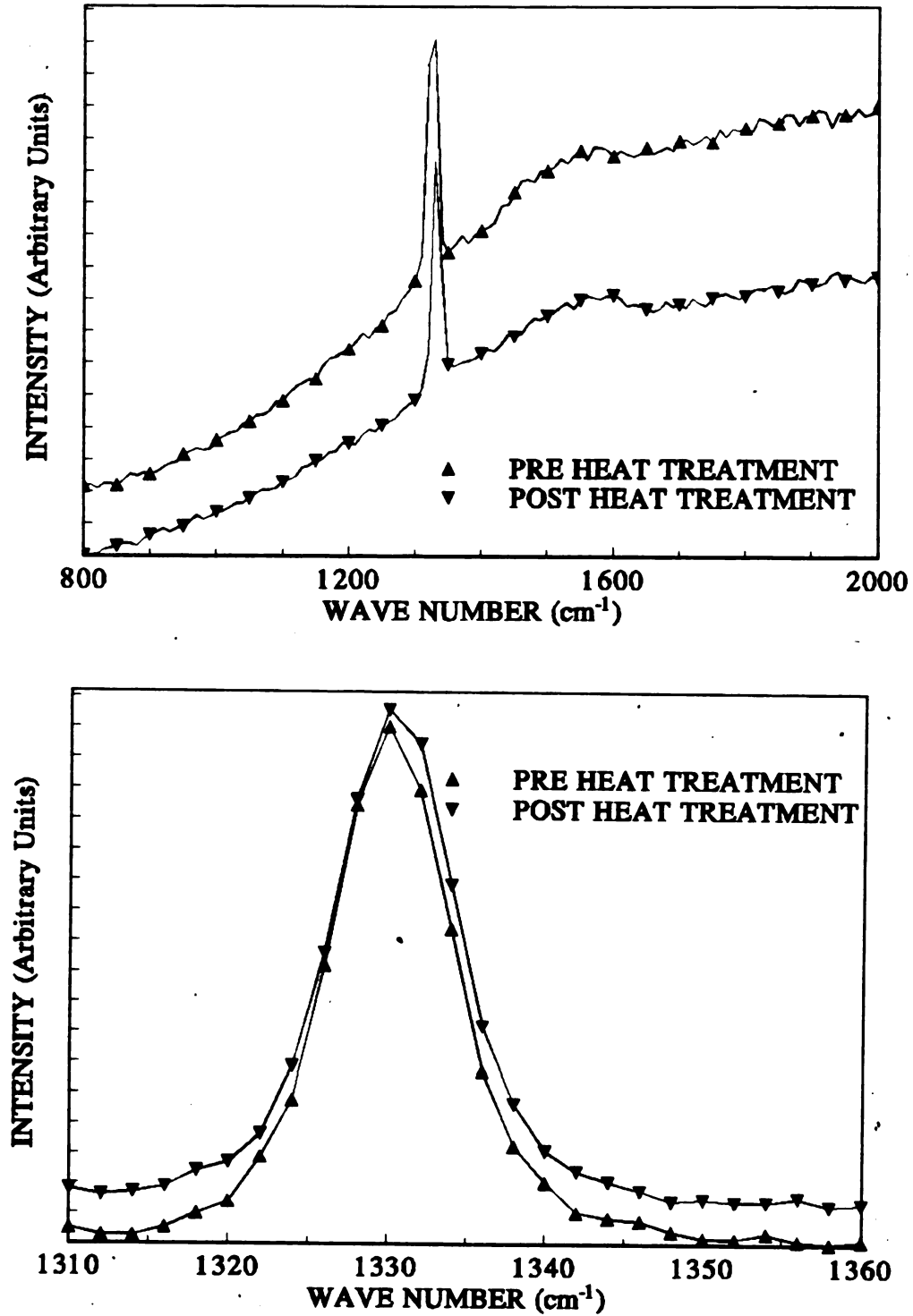


Figure 6.6. Raman spectra of diamond film thermal sensors before and after heat treatment at 1000°C for a total of 14 minutes in four cycles at a pressure of 10^{-7} torr at two scan ranges.

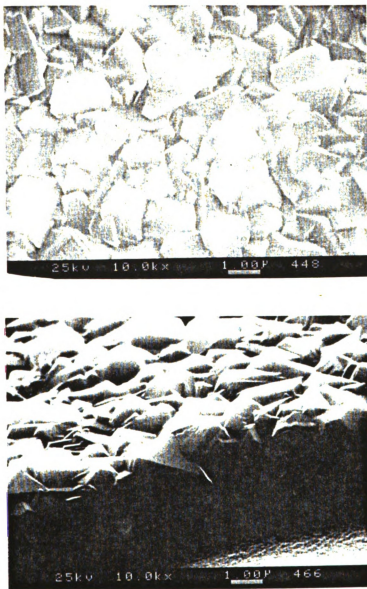
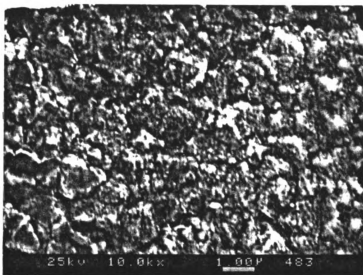


Figure 6.7 SEM micrographs of diamond film thermal sensor after heat treatment at 1000°C for a total of 14 minutes in four cycles at a pressure of 10^{-7} torr. (a) normal view and (b) view at 60° angle.



(a)

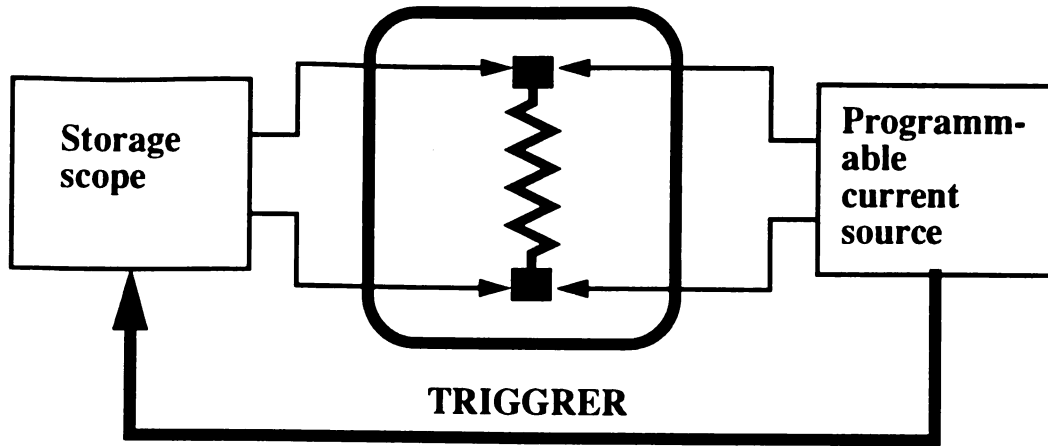


(b)

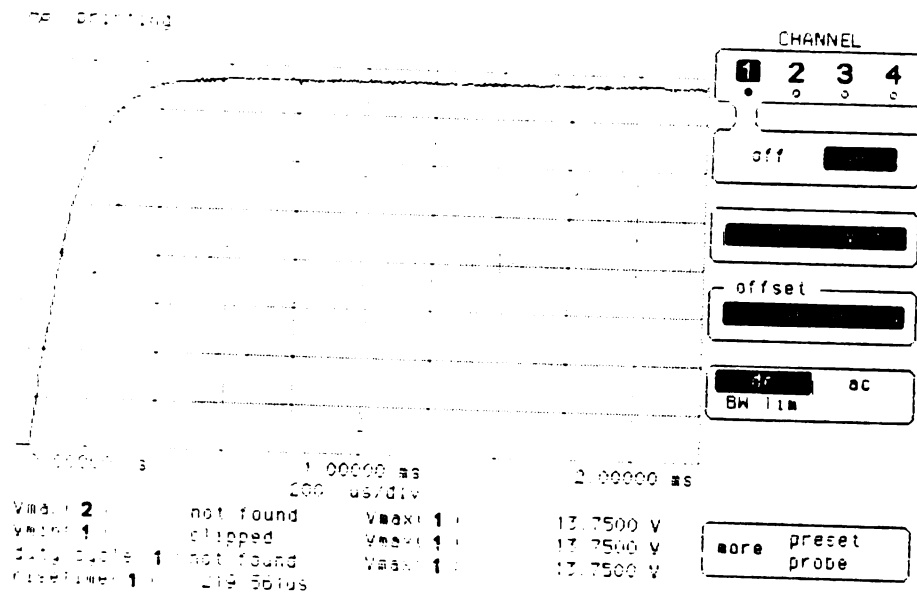
Figure 6.8 SEM micrographs of diamond film thermal sensors after two minutes of heat treatment at (a) 1249°C at 10^{-7} torr and (b) 1000°C at 100 mtorr.

conventional method of generating a temperature step function by physically moving the sensor from a cold medium to hot medium or vice versa are unsuitable. Hence, it was decided to generate a temperature step by a step of electric current through the sensor. For this purpose, the experimental set up shown in Fig. 6.9(a) was used. The voltage across the sensor (IR voltage drop) was used as a trigger for the storage scope to start its scan in a single trace mode.

In order to establish the validity of these measurements, a number of commercial resistors ranging from 15 Ω to 1 M Ω in value were tested for their response time. They exhibited a response time in the range of 0.2-1.1 ms without any clear dependence on excitation current. The important observation was that these measurements were not accompanied with any resistance change with current, hence, indicating that voltage response time measurements across resistors are not dependent on the level of excitation current. Once diamond sensors were connected in the circuit, a change in resistance with excitation current was observed. A typical trace of storage scope, when a current step function of 100 μ A was passed through the sensor, is shown in Fig. 6.9(b). The voltage across the sensor changes at the beginning of the scan and stabilizes after some time. The rise time, as measured by the system shown at the bottom of Fig. 6.9(b) (219 μ s) is representative of the time required for the current source to apply the programmed current value and for the sensor to heat up and reach a steady state value of resistance. The stabilized resistance (137.5 k Ω) is less than the room temperature resistance (165.5 k Ω in this case). From the static temperature response of the sensor ($\Delta R/\Delta T = 5663\Omega/^{\circ}\text{C}$ at room temperature) a change in temperature of 5.23 $^{\circ}\text{C}$ was computed. The rise time in this case was 219.56 μ s and was found to be independent of excitation current. As shown in Fig. 6.10, the rise time was between 200-300 μ s for all of excitation current steps considered. The steady state resistance of the sensor versus excitation current is also shown in Fig. 6.10. A decrease in resistance with increasing current indicates an increasing heating effect. It can be assumed



(a)



(b)

Fig. 6.9 (a) The experimental set up for dynamic response measurement of diamond film temperature sensors and (b) Storage scope trace of voltage once a current step of $100 \mu\text{A}$ was applied to the diamond film temperature sensor with room temperature resistance of $165.5 \text{ k}\Omega$.

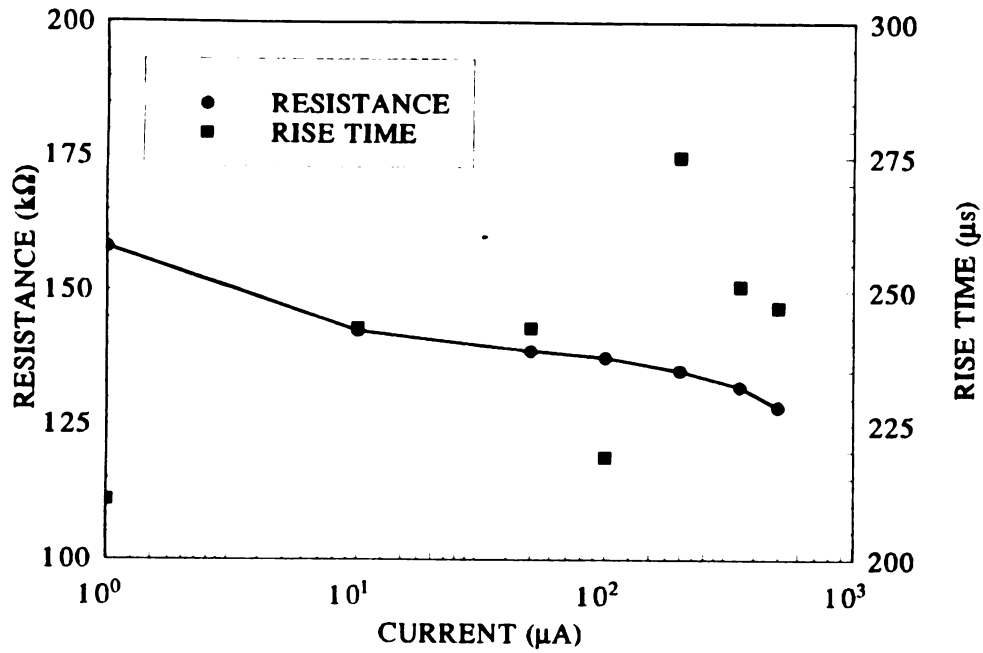


Figure 6.10 The steady state resistance of diamond film thermal sensor against current flowing through it. The rise time of the voltage across the respective sensor with the applied current step is also shown.

that the resistance change in the case of diamond sensors is due to the Joule's heating effect.

The time constant can be considered as 1/5 of the rise time. Thus, for a rise time of 219 μs , the time constant will be 43.8 μs . Some part of this time constant is due to the measurement system itself. The sensor and the measurement system are in parallel and both the measurement system and the diamond sensor are considered parallel combination of a resistor and a capacitor individually. The time constant for the diamond sensors was evaluated from the relation

$$\tau_t = (C_s + C_d)(R_s^{-1} + R_d^{-1})^{-1} \quad (6.5)$$

where R, C and τ stand for resistance, capacitance and time constant whereas subscripts s, d and t stand for measurement system only, diamond sensor only and total system including sensor respectively. For this purpose, the time constant of the measurement system was determined first. The mean value of this time constant was 135 μs . After measuring the resistance of measurement system to be 985 $\text{k}\Omega$, the value of C_s was computed to be 137 pF using the relation $\tau_s = R_s C_s$. Once the diamond sensor was connected in the system, the value of R_d was obtained from the storage scope trace (137.5 $\text{k}\Omega$). Substituting these values into Eq. (6.5), the value of C_d was computed to be 182 pF. Using the relation $\tau_d = R_d C_d$, the adjusted time constant of diamond was found to be about 25 μs . This is fairly small time constant as compared to commercial temperature sensing devices [14,9,8] which is in the range of ms to several tens of seconds.

The response time measured in the present case is for the complete device including the substrate. Hence, the thermal properties of the substrate material also contribute to the overall dynamic response of the sensor. To achieve high sensitivity to heat transfer rate, the sensors are usually mounted on thermal insulators such as Al_2O_3 [14] and fused quartz [169]. This prevents the heat from escaping from the sensing element. Quantitatively, the sensitivity ratio of two sensors with exactly similar sensing

elements but mounted on different substrate materials is given by [169]

$$S = \sqrt{\frac{(k \rho_M C_p)_{\text{substrate1}}}{(k \rho_M C_p)_{\text{substrate2}}}} \quad (6.6)$$

where

k = thermal conductivity ($\text{Wm}^{-1}\text{K}^{-1}$)

ρ_M = density (kg m^{-3})

C_p = specific heat ($\text{J-kg}^{-1}\text{K}^{-1}$)

Table 6.1. Thermal properties of Si, SiO₂, diamond, Pt and Cu [160,47,169]

Material	Thermal Conductivity, k W/m-K	Density, ρ_M kg/m ³	Specific thermal capacity, C_p J/kg-K	Thermal diffusivity, K m ² /s	$\sqrt{k\rho_M C_p}$ J ² /m ⁴ K ² s
Si	157	2328	752	89.7×10^{-6}	2.74×10^8
SiO ₂	12.7 (max.)	2653	100	61.67×10^{-6}	3.178×10^6
Diamond	2000 (max.)	3515	442+1.07 (T-25 C)	1.28×10^{-3}	3.11×10^9
Pt	73	21450	135.6 at 18-100 C	25.1×10^{-6}	2.12×10^8
Cu	385	8960	380	11.3×10^{-5}	1.31×10^8

The value of these parameters for various materials of interest are given in Table 6.1. Considering SiO₂ and pure Si as two substrates, $S = 86.22$. Hence, a sensing element

placed on SiO₂ will respond 86.22 times faster than the one on Si substrate. In case of the test chips, although the sensing elements are placed on SiO₂, they can be considered on Si due to small (~1 μm) thickness of SiO₂. The dynamic heat calculations show that such a thin SiO₂ layer only retards the heat flow marginally in flowing from diamond into the Si substrate. If it were placed on bulk SiO₂, the mean time constant of diamond sensors would reduce to about 290 ns. However, for temperature sensors requiring only fractional ms response times, there is no need to increase the thickness of SiO₂ layer.

As a heat flux sensor, the temperature sensor measures the surface temperature of the body on which it is placed. The theory of transient heat conduction in a non-homogeneous body is used to relate the surface temperature history to the rate of heat transfer. In this way, it is possible to measure the surface temperature history of the body and calculate the heat transfer rate. The present interest in diamond film sensors as heat flux sensors is to compare their performance with conventional heat flux sensors made of Pt or Cu.

The heat conduction analysis of a heterogeneous sensor body of test chip or rod can be modeled as a one dimensional problem as shown in Figure 6.11. Regions 1 and 2 represent the sensor and substrate materials with dissimilar thermal and physical properties. It will be assumed that lateral heat flow is relatively much smaller compared to the vertical heat flow in Fig. 6.11 and can be neglected because of the extremely small thickness of region 1 in comparison with region 2.

Considering this model, the surface temperature is given approximately by the relation [169]

$$T(t) = 2q \sqrt{\frac{t}{\pi k_2 \rho_{M,2} C_{p2}}} - q \frac{l}{k_1} \left[\frac{k_1 \rho_{M,1} C_{p1}}{k_2 \rho_{M,2} C_{p2}} - 1 \right] \quad \text{with } q = \text{constant} \quad (6.7)$$

where

T = temperature increment above T(t≤0) °C

t = time (seconds)

l = thickness of sensor film (m)

q = rate of heat transfer to the surface

and subscripts 1 and 2 refer to the conditions in region 1 and 2 from the Fig. 6.11

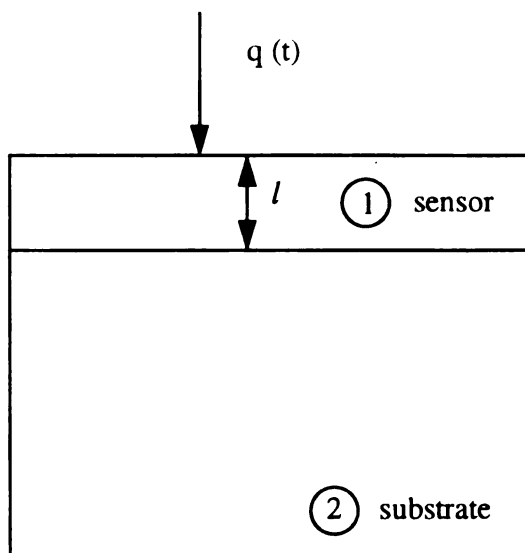


Figure 6.11 The one-dimensional heat conduction model for thin film heat flux sensors on thermal insulator [124].

respectively. In this equation, the first term correspond to the temperature of the substrate material if the sensor was not present, whereas the second term corresponds to a temperature offset because of the presence of sensor. Hence, the temperature measured by the sensor is actually the substrate temperature but offset by the second term in the equation. At a given time, the temperature measured is less than the temperature of

the substrate (the measurement of which is actually desired) if the sensor was not present. Therefore, second term should be as small as possible. In addition to decreasing the sensor thickness, a material of high thermal conductivity can help reduce the second term. Several materials such as Al, Cu, Au, Ni and Ag were tried as heat flux sensing materials [14]. However, no significant improvement could be achieved. In case of diamond film sensor, its high thermal conductivity along with its other thermal properties, as mentioned in Table 6.1, can reduce this temperature lag by a factor of more than 2 for same size sensor made of Pt.

The characteristic time defined as l^2/K (seconds), is another criterion for comparing heat flux sensors. For the same thickness of sensors, diamond film sensor will be 51 and 11.3 times faster than Pt and Cu sensors respectively. Comparing diamond with other sensing materials such as Ni, Ag, and Fe, the characteristic time of diamond film sensors is at least 20 times smaller. Thus, it can be concluded that diamond heat flux sensor with their added advantage in terms of temperature range of sensing and resistance to harsh environment, are much superior to any other known sensor.

6.4 ON-CHIP SIGNAL PROCESSING

The concept of integration of sensors and signal processing circuit on a single chip can enhance the system reliability, automation, precision and interface simplification. This is now routinely done for pressure sensors [2] but is rarely found for temperature sensors [9]. The reason is that unlike pressure sensor, the complete chip is exposed to the temperature being measured. This poses the demand of an extensive temperature compensation schemes for on-chip signal processing circuit. In the present case, this problem becomes even harder due to the wide temperature range. The diamond film technology is still in infancy. Currently, no active device with stable operation over even part of this temperature range is available. The non-availability of a suitable n-type dopant is another issue. The diamond based components currently

available are MOSFET [58,153], MESFET [131], Schottky diodes [155,148,154] and resistors [124]. The operation of all of these devices is highly temperature dependent. In addition, most of these devices are fabricated on homoepitaxial diamond films. Nevertheless, the availability of "almost crystalline" diamond film synthesis technology [66] on silicon substrates has made the fabrication of these devices possible on substrate other than diamond.

From the foregoing description of the present state of diamond technology the design of diamond signal processing circuit is precluded, at least in analog mode. However, the inherent noise immunity encourages the design of digital circuits. For a digital system, an electronic switch is the key element. From the available diamond devices, the p-channel depletion-mode MESFET [131] is the only device which can perform this role. It has been characterized as completely cut off under reverse bias condition. A circuit using this device, as shown in Fig. 6.12(a), is proposed for implementing NAND logic. For proper operation of the circuit R_{OFF}/R_{ON} should be a large. Since this ratio is not available for this device, a typical number of 10^5 is assumed. Since any logic system can be built using a NAND gate, this circuit can act as building block for the proposed thermistor array multiplexer circuit shown in Fig. 6.12(c). It is assumed that the counter and decoder circuits will be fabricated by using NAND gates only. Due to device characteristics, logic 0 and 1 correspond to V^+ and V^- volts. In absolute terms, these voltages are depend on the device behavior.

The primary function of this circuit is to reduce the output connections from the sensor chip. The operation of the circuit is based on turning the MESFETs 'ON' sequentially and making the current through the sensor, available at the output line for read out by an ammeter. The following assumptions are made for the operation of this circuit.

- (1) $R_S/R_{ON} \geq 100$ and $R_S/R_{OFF} \leq 10^{-3}$ (R_S : sensor resistance at reference temperature).

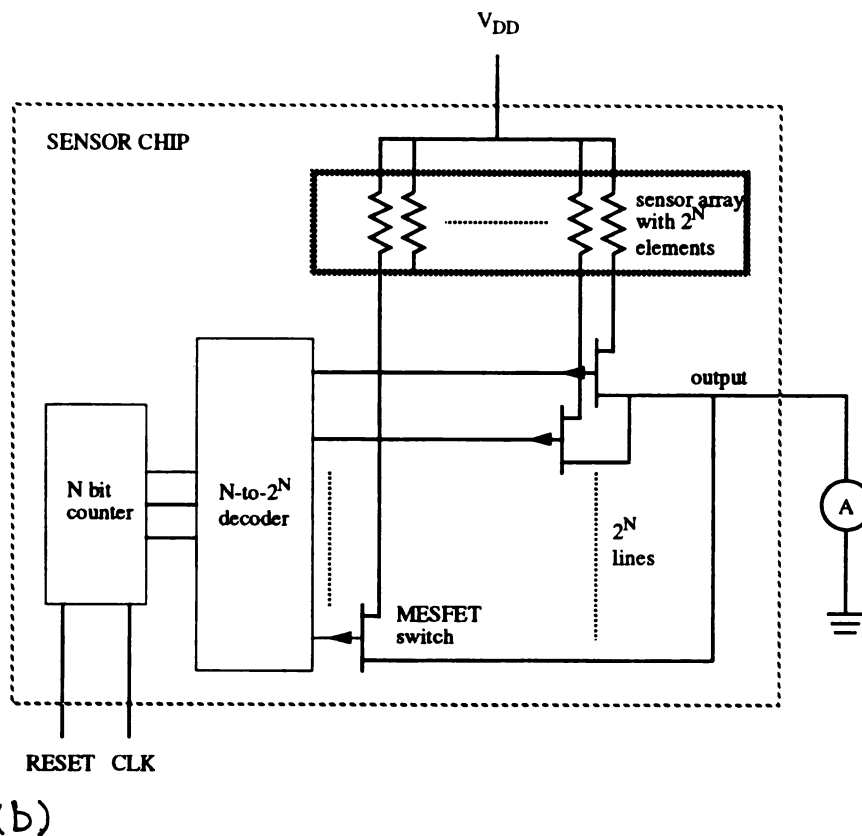
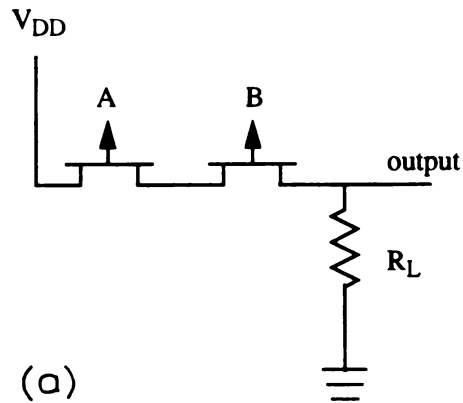


Fig. 6.12 (a) The implementation of NAND logic with two p-channel depletion mode diamond MESFETs and a diamond resistor. (b) The block diagram of the proposed analog multiplexer circuit using all diamond based NAND gates shown in (a).

- (2) The doping level is the same for the sensor and the MESFET channel, thereby both follow the same temperature dependence.
- (3) All the MESFETs and sensors are identical respectively in terms of physical structure e.g., size, doping, etc.
- (4) The whole chip is subject to almost the same temperature such that assumption (1) holds at all times.

The whole circuit is primarily a bank of parallel circuits, each of which consists of a MESFET switch and a sensor in series. At one time only one of the switches will be ON (low resistance). The resistance of the circuit is equivalent to the resistance of all parallel branches. Since only one of the switches will be ON (low resistance) at one time, the resistance of the circuit seen at the output line at any given time will be

$$\frac{V_{DD}}{I_{OUT}} = \left[\frac{1}{R_S + R_{ON}} + \sum_{i=1}^{2^N-1} \frac{1}{R_{S,i} + R_{OFF,i}} \right]^{-1} \quad (6.8)$$

where I_{OUT} is the measured current at the output. By giving an allowance for finite leakage current during the OFF state (typically 10 nA), the error in the measured resistance and true R_S will be less than 1%. Even this error can be taken care of by calibrating individual sensors.

6.5 SUMMARY

In this chapter the temperature response of the diamond microsensor is discussed. This class of sensor is shown to have reasonable ($\alpha = 0.006-0.008$) sensitivity over a temperature range of 77-1300 K. At this time, no other single temperature measuring device is known to operate over this temperature range either in absolute or relative terms. By exhibiting a monotonic change of resistivity with temperature over the entire range, the polycrystalline diamond film thermistors have outperformed even natural semiconducting diamond thermistors. Moreover, the dynamic temperature response time constant for the diamond film sensor has been measured to be about 25 μ s. This

is smaller than any known solid state temperature sensor. As a heat flux sensor, diamond film thermistor is shown qualitatively to outperform conventional Pt sensors for shock tunnel applications. Finally a digital circuit made exclusively of diamond devices has been proposed to function as a multiplexer to cut down the number of output connection from the chip.

SUMMARY & CONCLUSIONS

The primary objective of this research was to develop CVD diamond film based microsensors for thermal signals in the range of from approximately 77 K to 1273 K. To achieve this objective new techniques for boron doping, nucleation, patterning and metallization of diamond films were developed. The electrical characterization of the diamond films as a semiconductor was carried out on a specially designed and fabricated test microchip. Static temperature response of the sensors was acquired over a temperature range of 77-1273 K for the first time. The dynamic temperature response of temperature sensors was also measured.

7.1 SUMMARY AND CONTRIBUTION

7.1.1 Synthesis of p-type Diamond Films

Using hot filament chemical vapor deposition (HFCVD) experimental parameters such as reactant gases, gas flow rates, pressure and substrate and filament temperatures were optimized to achieve high quality diamond films. In situ boron doping was implemented using an accurately measured quantity (0.1-2.6 mg) of high purity

amorphous boron powder (5N8) through a specially designed holder placed near the substrate. The quality of the diamond films as determined from Raman spectroscopy and SEM was not affected by boron doping in the useful range of boron concentration (up to 10^{19} cm^{-3}). SIMS depth profile and Hall concentration measurements showed uniform boron concentration throughout the thickness of the films. Significant amounts of impurities which might act as donor or compensators (such as P or N) were not found. The SIMS data also confirm the increase in boron incorporation with the weight of powder in the evaporator. The measured resistivity and Hall concentration of diamond films doped by using 0.1-2.6 mg of boron powder were in the range of 0.3-64 $\Omega\text{-cm}$ and 2×10^{15} – $9 \times 10^{18} \text{ cm}^{-3}$, respectively.

7.1.2 Patterning and Metallization

A test microchip was designed and fabricated. For the fabrication of the devices the diamond film patterning and metallization were two crucial processes. Three IC compatible techniques for diamond film patterning based on selective deposition and selective etching were developed. Patterning of diamond films on non-diamond substrates through selective etching was achieved for the first time. The diamond photoresist (DPR) patterning technique based on mixing diamond powder in photoresist is especially advantageous in terms of selectivity, resolution and ease and flexibility of implementation. This method was developed to achieve optimum grain size (nucleation density $\sim 10^8 \text{ cm}^{-2}$, film thickness uniformity and surface smoothness. In case of metallization, the stringent requirement of providing ohmic contacts on diamond films, and of stability and good adhesion on diamond as well as SiO_2 surfaces simultaneously was extremely demanding. This task was best accomplished by a two layer structure of Pt(8000 $^\circ\text{A}$)/Ti(100 $^\circ\text{A}$) based on experimental results of this research and previous work on high temperature metallization of Si ICs using silicide.

7.1.3 Electrical Characterization

Resistivity (77-1273 K), Current-voltage measurement, carrier type (77-300 K), Hall concentration (77-300 K) and Hall mobility (77-300 K) were directly measured. The resistivity and Hall mobility were in the range of 0.3-64 $\Omega\text{-cm}$ and 2-48 $\text{cm}^2\text{V}^{-1}\text{s}^{-1}$ respectively. These parameters provided informations to evaluate the impurity concentration and various activation energies such as corresponding to dopant (boron) and hopping conduction. The dopant activation energies, as computed from the resistivity versus temperature curves (up to 300°C), were in the range of 0.38-0.11 eV corresponding to Hall concentration in the range of 2×10^{15} - $9\times 10^{18}\text{cm}^{-3}$ and boron concentration in the range of 10^{17} - 10^{23}cm^{-3} . The compensation of impurities was estimated to be in the range of 0.2 to 80% over the entire range of measured Hall concentration. The activation energies corresponding to high temperature conduction and low temperature hopping conduction was computed to be 0.375-0.58 eV and 11.72 meV respectively. Due to the change of properties of diamond during heating at high temperature, the annealing behavior of doped diamond films was investigated for the first time and an optimum annealing schedule (1000°C for 8 minutes) was acquired.

7.1.4 Diamond Film Sensor for Thermal Signals

The characterization of diamond film thermal sensors was carried out over the temperature range of 77-1273 K. The change in resistivity with temperature is monotonic with reasonable sensitivity (temperature coefficient $\sim 0.07\text{ K}^{-1}$) at all doping levels over the entire temperature range. At this time, no other single temperature measuring device is known to operate over this temperature range either in absolute or relative terms. In this range, the polycrystalline diamond film have outperformed even natural semiconducting diamond since natural semiconducting diamonds show a negative temperature coefficient (NTC) of resistivity in the freeze-out and intrinsic region and positive temperature coefficient (PTC) of resistivity in the extrinsic region. This

behavior presents multiple values of temperatures for a single value of resistivity and, hence, make them unsuitable for temperature measuring application over more than one temperature region.

The dynamic temperature response of the temperature sensors was measured experimentally. The typical response time of diamond temperature sensor on oxidized silicon substrate was about 25 μ s, which is smaller than any known temperature sensing device (for comparison a Pt RTD has a response time of 115 ms). An analytical comparative analysis proved that diamond sensors will give better performance than conventional Pt sensors. As a heat flux sensor, the characteristic response time of diamond sensor was estimated to be 51 and 11.3 times smaller than Pt and Cu sensors respectively. Comparing with other sensing materials such as Ag, Ni, Fe and certain alloys, the characteristic time of diamond film sensors is at least 20 times smaller. The success in fabrication of an array of sensors on the cylindrical surface of substrate brings this application closer to practical realization. To minimize the number of pin out connections from the sensing device, an on-chip analog multiplexer circuit designed exclusively with diamond devices has also been suggested.

7.2 FUTURE RESEARCH

Since the diamond microelectronics is in its infancy, there is an abundance of research work ahead in this area. Some of the key topics which need immediate attention for continuation of the present research are described as follows.

- (a) The temperature response of resistivity of temperature sensors at the extremes of the temperature range of 77-1273 K showed good sensitivity. This is an indication that their operational temperature range can be extended on both sides. An immediate area of interest could be to procure an appropriate apparatus and characterize them below 77 K (to possibly 10 K) and beyond 1273 K (to possibly 1900 K).

- (b) At present, the biggest obstacle in the operation of diamond sensors at high temperature is its oxidation. Passivation of diamond sensors with other materials such as SiO_2 and Si_3N_4 tend to degrade their dynamic temperature response. A quantitative analysis to this effect can give accurate informations about the suitability of a particular material for specific applications. A natural choice of passivation layer material for response time sensitive applications such as heat flux measurement in shock tunnels would be diamond itself. These sensors will be disposable since they will last until the passivation layer oxidizes completely.
- (c) The feasibility of homoepitaxial diamond film temperature sensors should be investigated for potential improvement in the temperature sensor parameters.
- (d) All the diamond film based active devices developed so far are highly temperature sensitive. This is understandable because they are operating in the freeze-out region (up to approximately 700 K). An immediate application of the temperature response characterization of the diamond films is to design a temperature compensation scheme so that these devices could exhibit stable performance over a wide temperature range. This will also help towards integration of signal processing circuit on the sensor chips.
- (e) Since the properties of polycrystalline diamond films on non-diamond substrates are dependent on deposition conditions, an effort to optimize the growth parameters, especially the nucleation method, can improve the electrical properties significantly and create an opportunity for their application in high performance electronic devices.
- (f) For the application of diamond films in active electronic devices, knowledge of additional electronic properties beyond what were obtained during this research can supply crucial information. Specifically, an investigation into the extent of impurity compensation present and the thickness dependence of the mobility are very important.

APPENDICES

DIAMOND FILM DEPOSITIONS

This appendix is a collection of information regarding the diamond depositions made during the course of this research. A number of abbreviations and acronyms are used in the tabulated format and are explained first.

A.1 Process

The number appearing in this correspond to the sequence of the log book entries. The numbers missing in the sequence correspond to the depositions made by others or for other experiments.

A.2 Sample Description

This column describes the type of substrate, its pre-treatment and type of pattern (if any). The substrate material is oxidized p-type doped silicon (100) polished wafer unless otherwise mentioned. Following acronyms have been used to specify the nucleation method:

UT(*) - Ultrasonic treatment

DPR(*) - Diamond photoresist seeding

where * describes the pattern type as follows:

- U - No pattern
- D - Diffusion mask from MSU device fabrication lab.
- L - Parallel lines, the width ranging from 75 μ m to 575 μ m. The length of all the lines is 5 mm.
- S - Square pattern (7.5 mm \times 7.5 mm for Hall measurement)
- TC4 - Test chip (4 patterns)
- TC1 - Test chip (1 pattern)
- O - Others (unspecified)

A.3 Deposition Conditions

Following standard deposition conditions abbreviated as std has been used unless otherwise indicated.

- Gas Flow Rates - $C_2H_2 : H_2 : CO$ 0.5 : 100 : 12 sccm
- Pressure - 50 torr
- Filament Temperature (f. t.) - 2400 $^{\circ}C$
- Substrate Temperature (s. t.) - 890 $^{\circ}C$
- Boron powder quantity has been shown either by weight (for example B = 0.4 mg) or by number of holes filled in the boron holder (for example Bx4 to indicate 4 holes filled). The weight of boron powder in each hole has been measured to about 0.2 mg.
- std* stands for standard deposition conditions except the substrate temperature was held at 850 $^{\circ}C$ for first 15 minutes of the deposition.

Process #	Samples	Deposition Conditions	Time (Hrs.)
016	2xSi(micromachined), 1x Ni/Si, 1xUT(U)	s.t.=890	2.0
017	same as #016	s.t.=910	1.5
018	same as #016	s.t.=870	1.75
019	same as #016 (UT)	s.t.=830	1.75
025	same as #016	s.t.=860	1.25
026	1 sample on Mo plate	s.t.=830, Bias=60V	2.0
027	same as #106, Ni film (annealed) on Si	f.t.=2200	2.0
031	4xUT(U)	s.t.=870, f.t.=2475	1.5
053	same as #031	s.t.=830, f.t.= 2300, Bias=15V(0.12A)	1.5
057	4xDPR(D), 1xUT(D)	std	1.0
058	6xDPR(D), 1xUT(D)	std	3.0
060	1xDPR(D), 3xUT(D)	std	1.0
061	3xDPR(D), 1xUT(U), 1xDPR(D) on Ni/Si	std	2.5
062	3xDPR(D), 1xUT(D), 1xUT(U)	std	2.0
063	3x DPR(D), 1xUT(D)	std	1.5
065	3xUT(D), 1xUT(O)	std	2.0
073	2xUT(O)	std	1.5
078	1xDPR(O)	std	1.75
082	1xDPR(U), 1xUT(U)	std*	4.0
083	4xDPR(D), 2xUT(D)	std*	2.25
084	2xDPR(D), 2xUT(D)	std*	3.0
088	2xDPR(D), 2xUT(D)	std*	4.0
089	2xDPR(D), 2xUT(D)	std*	4.0

Process #	Samples	Deposition Conditions	Time (Hrs.)
091	2x #089, 1x #088	std*	6.25
092	2x #89	std*	7.5
094	2xDPR(L), 1xUT(L)	std*	3.25
095	1xPPR(L), 1xUT(L)	std*	3.25
102	1xUT(U)	H ₂ =98, H ₂ (bubbler)=5.0 CO=0.0, std*, bubbler (Methanol) t.=23.9	1.5
103	1xUT(U)	H ₂ =95, H ₂ (bubbler)=5.0 CO=10, std*, Bubbler temp.=23.4	1.5
104	1x UT(U)	H ₂ =92, H ₂ (bubbler)=2.0 CO=0.0, std*, Bubbler temp.=23.8	1.5
105	1xUT(U)	H ₂ =95, H ₂ (bubbler)=0, Bubbler line openCO=0.0, std*, Bubbler temp.=23.4	2.0
110	1x UT(U)	H ₂ =95, H ₂ (bubbler)=2.0, CO=0.0, std*, Bubbler temp.=-78.2	2.0
115	1x UT(U)	std*, B=13 mg	2.25
116	1xUT(D)	std*, B=2 mg	3.5
123	1xDPR(U), 1xDPR(L), 1x UT(U)	std*, B=1 mg	3.0
131	1x DPR(S), 1x DPR(L) 1x DPR(U)	std*, B=14.5 mg	6.0
132	1x DPR(S), 1x DPR(L) 1x DPR(U)	std*, pre-cleaning run without sample = 4 hrs	6.0
138	1xDPR(L), 1xUT(U)	std*, b= 0.7 mg	6.0
142	1x DPR(S), 1x DPR(L) 1x DPR(U)	std*, B= 0.1 mg	6.0
143	1x DPR(S), 1x DPR(L) 1x DPR(U), 1x Si ₃ N ₄	std, B=0	6.0

Process #	Samples	Deposition Conditions	Time (Hrs.)
144	1x DPR(S), 1x DPR(L) 1x DPR(U), 1x Si ₃ N ₄	std, B=0.2 mg	4
145	1xPR(L), 1x UT(U)	CO=0.0, B= 0.5 mg	3
146	1x DPR(S), 1x DPR(L) 1x DPR(U), 1x Si(ch.)	s.t.= 950, CO=0.0, B= 0.6 mg	8
154	1x DPR(S), 1x DPR(L) 2x DPR(U),	std, B= 1 mg	6
156	1x DPR(S), 1x DPR(L) 2x DPR(U),	std, B= 1.2 mg	6
158	same as #156	std, B= 0.7 mg	6
162	5x DPR(U)	std	6
164	Cu plate with diamond grit sprayed	std	1
165	1xSi ₃ N ₄ /Si, 1x SiO ₂ /Si	std	1
166	1xSi ₃ N ₄ /Si x #165 1x SiO ₂ /Si x #165 1xSi ₃ N ₄ /Si, 1x SiO ₂ /Si	std	2
167	Si with diamond grit sprayed	std	4
168	1x UT(U), 1x DPR(U)	No carbon gases, bubbler with Acetone	3.5
169	1x #158, 1x DPR(L) on Ni coated oxidized Si	std, B=1.1 mg	4.5
170	2x UT(U)	Methanol = 0.5, No carbon gases	1
171	1x UT(U), 1x Si	filmant distance = 5/32", Cu tube (1") installed	1
172	1x UT(U)	std	1
173	same as #172	f.t.= 2348	1
174	same as #172	Cu tube distance=1.25" from the flange plane, std	2.0
175	same as #172	f.t. 2475	2.0
176	same as #172	Pressure = 60 torr	3.0

Process #	Samples	Deposition Conditions	Time (Hrs.)
177	1x UT(U), 1x DPR(U)	Pressure = 70 torr	3.0
178	same as #177	Pressure = 100 torr	3.0
179	1x DPR(U)	CH ₄ = 0.5, Cu tube 1.6" from the flange plane.	3.0
180	3x DPR(U)	CH ₄ = 0.5,	3.0
181	same as # 180	CH ₄ = 0.5,	3.0
182	4x DPR(U)	CH ₄ = 0.5,	0.25
183	2x DPR(U)	CH ₄ = 0.5,	0.25
184	2x DPR(U) x #182 2x DPR(U) x #183	CH ₄ = 0.5,	3
185	4x DPR(L)	CH ₄ = 0.75	3
186	2x #185	CH ₄ = 0.75	4
187	2x PR(S)	CH ₄ = 0.75	0.25
188	2x DPR(L)	CH ₄ = 0.75	3
189	1x DPR(L)	CH ₄ = 0.75	3
190	1x DPR(L)	CH ₄ = 1.0	3
191	1x DPR(L), 1x DPR(S)	CH ₄ = 0.5	4
192	1x DPR(TC4)	CH ₄ = 0.5	4
193	1x DPR(TC4)	CH ₄ = 0.5	4
194	1x DPR(TC4)	CH ₄ = 0.5	4
195	1x DPR(TC1) x #194	CH ₄ = 0.5, B= 0.6 mg	4
196	1x DPR(TC4)	std	4
197	1x DPR(TC1) x #196	std, B= 0.6 mg	4
198	1x DPR(TC4)	std	4
199	1x quartz rod UT(U), 1x quartz rod DPR(P)	std	4
200	1x DPR(TC1) x #196	std, Bx3	4
203	1x DPR(TC1) x #196	std, Bx4	4

Process #	Samples	Deposition Conditions	Time (Hrs.)
204	1x DPR(TC1) x #198, 2x crystalline (100) and (110) diamonds	std, Bx5	4
206	quartz rod DPR(A)	std	4
208	quartz rod x #206	std, Bx3	4
209	1x DPR(TC1) x #198	std, Bx1	4
210	1x DPR(TC1) x #198	std, Bx1	5
214	flat quartz plate	std	6
216	1x UT(U), 1x (U), 1x DPR(U)	std, substrate=polysilicon	3
219	1x DPR(TC1)x #198 1x crystalline (100) diamond, 4x DPR(U)	std, Bx3	6
221	Alumina rod DPR(A)	std, Bx2.5	5
225	4x DPR(U) x #219	std, Bx3	3
226	Vycor glass rod DPR(A)	std	4
227	oxidized polysilicon rod DPR(A)	std, Bx6	5
228	1x DPR(TC4)	std	4
229	1x DPR(TC4)	std	4
230	DPR(TC1) x #229	std, Bx8	4
231	DPR(TC1) x #229	std, Bx13	4
232	2x DPR(TC1) x #229	std, Bx10	3.5
233	Si rod DPR(A)	std	4.0
234A	1x #233	s.t.=865	1.0
234B	1x DPR(TC1) x #228	std, Bx8	4.0
235A	1x DPR(TC1) x #228	s.t.=850, Bx6	4.0
235B	1x Si rod DPR(A)	std	4.0
236	1x #235B	std, s.t.=870	4.0

Process #	Samples	Deposition Conditions	Time (Hrs.)
237	1x PMMA(U)	std	3.5
238	2x Si rod DPR(A)	std	4.0
239	2x Si rod DPR(A)	std, Bx8	4.0
240	1x DPR(TC2) x MM2, 1x MDPR(O)	std, Bx8	4.0
242	1x MDPR(TC4)	std	4.0

BIBIOGRAPHY

BIBLIOGRAPHY

- [1] S. Middelhoek, P. J. French, J. H. Huijsing and W. J. Lian, "Sensors with Digital or Frequency Output", *Sensors and Actuators*, 15, 119-133 (1988).
- [2] K. D. Wise and N. Najafi, "The Coming Opportunities in Microsensor Systems", *Transducers '91: The Next Decade*, Tokyo, June 24, 1991.
- [3] W. J. Tompkins and J. G. Webster, "Interfacing Sensors to the IBM PC", *Prentice Hall, Englewood Cliffs, NJ* (1988).
- [4] S. Middelhoek and S. A. Audit, "Silicon Sensors", *Academic Press, London*, 1989.
- [5] J. B. Huang and Q. Y. Tong, "Integrated Multi-Function Sensor for Flow Velocity, Temperature, and Vacuum Measurement", *Sensors and Actuators*, 19, 3-11 (1989).
- [6] A. Boyer, E. Cisse, Y. Azzouz and J. P. Cheron, "Narrow-bandgap Semiconductors Based Thermal Sensors", *Sensors and Actuators A*, 25-27, 637-640 (1991).
- [7] B. Xie and S. Ren, "A Versatile Thermal Biosensor", *Sensors and Actuators*, 19, 53-59 (1989).
- [8] H. B. Sachse, "Semiconductor Temperature Sensors and Their Applications", *John Wiley and Co.* (1975).
- [9] T. D. McGee, "Principles and Methods of Temperature Measurements", *John Wiley & Sons*, 1988.
- [10] O. Zucker, W. Langheinrich and J. Mayer, "Investigation of Polysilicon for its Applications to Multi-function Sensors", *Sensors and Actuators A*, 25-27, 647-651 (1991).
- [11] B. W. Van Oudheusden and J. H. Huijsing, "Integrated Flow Friction Sensor", *Sensors and Actuators*, 15, 135-144 (1988).
- [12] S. Middelhoek, P. J. French, J. H. Huijsing and W. J. Lian, "Sensors with Digital or Frequency Output", *Sensors and Actuators*, 15, 119-133 (1988).
- [13] K. Nelson, " Calibration of Sensor Resistance by Laser Trimming", *Transducers '91: The Next Decade*, Tokyo, June 24, 1991.

- [14] "The Temperature Handbook", *Omega Engineering Inc., Stamford CA* (1992).
- [15] J. M. Swartz and D. L. Swartz, "Recent Advances in Resistance, Diode and Capacitance Thermometry for Use at Cryogenic Temperatures", *Advances in Cryogenic Engineering*, 20, 389-401 (1975).
- [16] M. P. Timpo, "A two Terminal IC Temperature Transducer", *IEEE J. Solid State Circuits*, SC-11, 784-788 (1976).
- [17] W. Schafer, "Temperature Sensors: New Technologies on Their Way to Industrial Applications", *Sensors and Actuators*, 17, 27-37 (1989).
- [18] D. G. Blair, C. C. Matheson and B. J. Saunders, *Cryogenics*, 12, 561 (1972).
- [19] D. Hibberson, "Modern Thermistors Meet Rugged Demands", *Machine Design*, 66-67, July 1990.
- [20] E. D. Macklin, "Thermistors", *Electrochem. Publications, Ltd., Ayn, Scotland*, (1979).
- [21] C. E. Woodhouse, "High Precision Rapid Readout of Cryogenic Temperature Sensors in the Space Shuttle Environment", *IEEE Trans. Instrum. and Meas.*, 39(1), 279-284 (1990).
- [22] H. V. Estrade, "Linearization of the Temperature Dependence of the Silicon Resistivity for its use as a Thermistor", *Proc. SOUTHEASTCON '90*, New Orleans, 3, 1095-1099, 1-4 Apr. 1990.
- [23] D. S. Schwartz, "Narrow Range High Output Temperature Sensors Based on Combined PTC/NTC Schemes", *Proc. 37th Intl. Instrum. Symp.*, CA, 581-601, 5-9 May 1991.
- [24] H. W. Trolander, D. A. Case and R. W. Harrugg, "Reproducibility, Stability and Linearization of Thermistor Resistance Thermometers", *Temperature*, 4 part 2, 997-1009 (1972).
- [25] K. Ohe and Y. Naito, "A new resistor having an anomalously large positive temperature coefficient", *Jpn. J. Appl. Phys.*, 10(1), 99-107 (1971).
- [26] E. Ling, H. S. Gamble, B. M. Armstrong and J. Wakefield, "A Novel Polycrystalline Silicon Temperature Sensor", *Sensors and Actuators*, 16, 225-234 (1989).
- [27] T. Nugai and M. Itoh, "SiC thin film thermistors", *IEEE Trans. Industry Applications*, 26(6), 1139-1143 (1990).
- [28] E. W. Kiewra and P. C. Wayner Jr., "The Development of a Thin Film Silicon Carbide Thermistors Array for Determining Temperature Profile in an Evaporating Liquid Film", *J. Electrochem. Soc.*, 136(3), 740-744 (1989).

- [29] N. O. Ivanova, A. I. Chalyi, "Thin Film Bismuth Thermistors", *Instrum. Exp. Tech.*, 33(5) part 2, 1236-1237 (1990).
- [30] R. M. Nigamatullin, M. G. Shibanov and A. A. Kumanbeava, "Bismuth Based Thin Film Thermistors", *Instrum. Exp. Tech.*, 33(5) part 2, 1444-1446 (1990).
- [31] R. Dambra, G. Gallinaro, F. Gatti and S. Vitale, "Properties of Ruthenium Oxide Resistor Elements of Composite Bolometers", *Nucl. Instrum. Methods Phys. Res. A*, 302(1), 83-88 (1991).
- [32] E. Roess, "Ceramic Electronic Components", *Siemens Components*, 25(6), 213-216 (1990).
- [33] S. A. Obukhov, B. S. Neganov, Y. F. Kiselov, A. N. Chernikov, V. S. Vekshina and N. I. Pepkik and A. N. Popkov, "Low temperature Resistance of p-InSb(Mn)", *Cryogenics (UK)*, 31(10), 874-877 (1991).
- [34] T. Yamamoto and S. Takao, "Complex Impedance Analysis of Nb-doped (Ba, Sr)TiO₃ PTC Thermistors", *Sumitomo Search*, 45, 56-64 (1991).
- [35] C. J. Murray, "Design Cuts Sensor's Response Time of Resistance Temperature Detectors for Supersonic Fighter Aircrafts", *Design News*, 47(6), 176-177 (1991).
- [36] C. Jessen and H. Gronig, "A New Method of Manufacture of Thin Film Heat Flux Gauges", *Schock Waves*, 1, 161-164 (1991).
- [37] G. B. Rogers and F. A. Raal, "Semiconducting Diamonds as Thermistors", *Rev. Sci. Inst.*, 31, 663-664 (1960).
- [38] U.S. Patent, 3,435,399, 25 March 1969.
- [39] N. Fujimori and H. Nakahata, "Thermistor made of CVD Diamond Films" *New Diamonds*, 98-101 (1990).
- [40] "Diamond Thin Films: Hot New Material for the 90's", *Design News*, 70-75, Apr. 1989.
- [41] K. Tankala, T. DebRoy and M. Alam, "Oxidation of Diamond Films Synthesized by Hot-Filament Assisted Chemical Vapor Deposition", *J. Mat. Res.*, 5(11), 2483-2489 (1990).
- [42] S. M. Sze, "Physics of Semiconductor Devices", 2nd ed., *John Wiley & Sons*, (1981).
- [43] A. T. Collin, "Diamond Electronic Devices --- A Critical Appraisal", *Semicond. Sci. Technol.*, 4, 605-611 (1989).
- [44] J. S. Blackmore, "Design of Germanium Resistance Thermometers for Thermometric Applications", *Rev. Sci. Instrum.*, 33, 106-112 (1962).

- [45] L. C. Conner, "CVD Diamond: Beyond the Laboratory", *Gorham Advanced Materials Institute at the Global Business and Technical Outlook for High Performance Inorganic Thin Film Coatings*, (1988).
- [46] J. C. Angus, Y. Wang and M. Sunkara, "Metastable Growth of Diamond and Diamond-like Phases", *Annual Rev. Mat. Sci.*, (1990); J. C. Angus, and C. C. Hayman, "Low-Pressure, Metastable Growth of Diamond and Diamond-like Phases", *Science*, 241, 913 (1988).
- [47] J. E. Field, *The Properties of Diamond*, Academic Press, (1971).
- [48] J. C. Angus, H. A. Will and W. S. Stanko, "Growth of Diamond Seed Crystals by Vapor Deposition", *J. Appl. Phys.*, 39, 2915 (1968).
- [49] F. P. Bundy, H. T. Hall, H. M. Strong and R. H. Wentroff, *Nature*, 176, 51-55 (1955).
- [50] J. C. Angus, H. A. Will and W. S. Stanko, "Growth of Diamond Seed Crystals by Vapor Deposition", *J. Appl. Phys.*, 39, 2915 (1968).
- [51] B. V. Spitsyn, L. L. Bouilov and B. V. Deryagin, *J. Crystal Growth*, 52, 219-226 (1981).
- [52] S. Matsumoto, Y. Sato, M. Kamo and N. Setaka, "Vapor Deposition of Diamond Particles from Methane", *Jpn. J. Appl. Phys.*, 21, L183 (1982); S. Matsumoto, *J. Mat. Sci. Lett.*, 4, 600 (1985).
- [53] Okano *et. al.*, *Jpn. J. Appl. Phys.*, 27, L173 (1988);
- [54] K. Suzuki, "Growth of Diamond Thin Films by DC Plasma Chemical Vapor Deposition", *Appl. Phys. Lett.*, 50 (12), 728-729 (1987).
- [55] K. Suzuki, "Characterization of the DC Discharge Plasma During Chemical Vapor Deposition of Diamond Growth", *Appl. Phys. Lett.*, 53 (19), 1818-1819, Nov. 1988.
- [56] D. E. Meyer *et. al.*, *J. Vac. Sci. Technol. A7* (3), 2325-2327 (1989).
- [57] S. Matsumoto *et. al.*, *MRS Symposia Proceedings*, EA-15, 119-122 (1988).
- [58] G. S. Goldenblat, S. A. Grot, C. W. Hatfield, and A. R. Badzian, "High Temperature Thin Film Diamond Field-Effect Transistor Fabricated using a Selected Growth Method", *IEEE Electron. Dev. Lett.*, EDL-12 (2), Feb. 1991.
- [59] M. Kamo, Y. Sato, S. Matsumoto and N. Setaka, "Diamond Synthesis from Gas Phase in Microwave Plasma", *J. Crystal Growth*, 62(3), 642 (1983).
- [60] Y. Mitsuda *et. al.*, *Rev. Sci. Instrum.*, 60 (2), 249-252 (1989); Y. Mitsuda, Y. Kojima, T. Yoshida, and K. Akashi, "The Growth of Diamond in Microwave Plasma Under Low Pressure", *J. Mat. Sci.*, 22, 1557-1562 (1987).

- [61] Y. Liou, A. Inspeckton, R. Weimer and R. Messier, "Low Temperature Diamond Deposition by Microwave Plasma Enhanced Chemical Vapor Deposition", *Appl. Phys. Lett.*, 55(7), 631-633, Aug. 1989.
- [62] K. Kurihara, K. Sasaki, M. Kawarada and N. Koshino, "High Rate Synthesis of Diamond by DC Plasma Jet CVD", *Appl. Phys. Lett.*, 52(6), 437-438 (1988).
- [63] Y. Tzang, C. Cutshaw, R. Phillip, T. Srivinyunon, A. Ibrahim and B. H. Loo, "Growth of Diamond Films on Silicon from an Oxygen-Acetylene Flame", *Appl. Phys. Lett.*, 53(19), 1818-1819, Nov. 1988.
- [64] W. A. Yarbough and R. Messier, "Current Issues and Problems in the Chemical Vapor Deposition of Diamond", *Science*, 247, 688-695 (1990).
- [65] S. Koizumi, T. Murakami, T. Inuzuka and K. Suzuki, "Epitaxial Growth of Diamond Thin Films on Cubic Boron Nitride {111} Surfaces by DC Plasma Chemical Vapor Deposition", *Appl. Phys. Lett.*, 57 (6), Aug. 1990.
- [66] M. W. Gies, H. I. Smith, A. Argoit, J. Angus, G. H. M. Ma, J. T. Glass, J. Butler, C. T. Robinsin, and R. Proyer, "Large Area Mosaic Diamond Films Approaching Single Crystal Quality",
- [67] D. G. Jeng and H. S. Tuan, "Oriented Cubic Nucleations and Local Epitaxy During Diamond Growth on Silicon {100} Substrates", *Appl. Phys. Lett.*, 56 (20), May 1990.
- [68] Y. Hirose and Y. Terasawa, "Synthesis of Diamond Thin Films by Thermal CVD Using Organic Compounds", *Jpn. J. Appl. Phys.*, 25(6), L519-L521, June 1986.
- [69] F. P. Doty and W. A. Jesser, "Investigation of the Role of Charged Species in Hot Filament Assisted CVD of Diamond", *J. Electron. Mat.*, 20(2), (1991).
- [70] S. J. Harris and L. R. Martin "Methyl Versus Acetylene as Diamond Growth Species", *J. Mat. Res.*, 5(11), 2313-1319 (1990).
- [71] *Diamond Deposition: Science and Technology*, 2(6), 12-13, Aug. 1991.
- [72] P. K. Bachmann, D. Leers and H. Lydtin, " Towards a general concept of Diamond Chemical Vapor Deposition", *Diamond and Related Materials*, 1(1), 1-12 (1991).
- [73] S. J. Harris and A. M. Weiner, "Effect of Oxygen on Diamond Growth", *Appl. Phys. Lett.*, 55(21), 2179-2181, Nov. 1989.
- [74] J. A. Mucha, D. L. Flamm and D. E. Ibbotson, "On the Role of Oxygen in Diamond Forming Discharges", *J. Appl. Phys.*, 65(9), 3448-3452, May 1989.

- [75] Y. Liou, R. Weimer, D. Knight and R. Messier, "Effects of Oxygen in Diamond Deposition at Low Substrate Temperature", *Appl. Phys. Lett.*, 56(5),
- [76] S. A. Solin and A. K. Ramdas, "Raman Spectrum of Diamond", *Phys. Rev. B*, 1, 1687-1698 (1970).
- [77] M. Yoshikawa, G. Katagiri, H. Ishida and A. Ishitani, "Resonant Raman Scattering of Diamond-like Amorphous Carbon Films", *Appl. Phys. Lett.*, 52(19), May 1988.
- [78] M. Yoshikawa, G. Katagiri, H. Ishida, A. Ishitani and T. Akamatsu, "Raman Spectra of Diamond-like Amorphous Carbon Films", *J. Appl. Phys.*, 64(11), 6464, Dec. 1988.
- [79] D. S. Knight and W. B. White, "Characterization of Diamond Films by Raman Spectroscopy", *J. Mat. Res.*, 4, 385-393 (1989).
- [80] L. H. Robins, E. N. Farabangh and A. Feldman, "Line Shape Analysis of Raman Spectrum of Diamond Films Grown by Hot-Filament and Microwave Chemical Vapor Deposition", *J. Mat. Res.*, 5(11), 2456-2468 (1990).
- [81] W. R. Runyan, "Semiconductor Measurements and Instrumentation", *McGraw Hill Book Co.*, 1975.
- [82] H. Chiemi and Y. Sato, "Plasma Etching of Diamond Films", *New Diamond*, 6, 32 (1990).
- [83] G. E. Anner, "Planar Processing Primer", *Van Nostrand Reinhold, New York*, 110 (1990).
- [84] J. F. H. Clusters, *Nature*, 176, 360 (1955).
- [85] J. J. Brophy, *Phys. Rev.*, 99, 1336 (1955).
- [86] I. M. Buckley *et. al.*, *Diamond and Related Materials*, 1(1), 43 (1991).
- [87] M. W. Gies, N. N. Efremow, and D. P. Rathman, "Summary Abstract: Device Applications of Diamonds", *J. Vac. Sci Technol. A*, 6(3), 1953-1954, May/June 1989.
- [88] A. Nishikawa, "Measurement of Thermal Conductivity of Diamond Films", *New Diamond*, 6, 70-72 (1990).
- [89] "AT&T Reports Progress in Their Thermal Conductivity Studies", *Diamond Deposition: Science and Technology*, 3(1), 1 (1992).
- [90] R. H. Wentrof and H. P. Bovenkerk, *J. Chem. Phys.* 36, 1987 (1962).
- [91] W. B. Wilson, *Phy. Rev.*, 127, 1549 (1962).

- [92] N. F. Mott, and W. D. Twose, *Adv. Phys.*, 10, 107 (1961).
- [93] Y. F. Tsay *et al.*, *J. Appl. Phys.*, 43(9), 3677 (1972).
- [94] B. Massarani and J. C. Bourgoin "Hopping Conduction in Semiconducting diamond",
Phys. Rev. B., 17(4), 1758-1769 (1978).
- [95] I. A. Parfianovich, Y. S. Mukhachev and S. Y. Borzenko, "Electrical Conductivity and Thermoelectric Power of natural diamonds",
- [96] K. Nishimura, K. Das and J. T. Glass, "Material and Electrical Characterization of Polycrystalline Boron-doped Diamond Films Grown by Microwave Plasma Chemical Vapor Deposition", *J. Appl. Phys.*, 69 (5), Mar. 1991.
- [97] K. Okano, H. Naruka, Y. Akiba, T. Kurosu, M. Iida, Y. Hirise, and T. Nahamura, "Characterization of Boron-Doped Diamond Films", *Jpn. J. Appl. Phys.*, vol. 28, no. 6, pp. 1066-1071, June 1989.
- [98] R. Ramesham, T. Roppel, C. Ellis, B. H. Loo, "Electrical Characterization of Undoped and Boron Doped Polycrystalline Diamond Thin Films", *J. Electrochem. Soc.*, 138 (10), Oct. 1991.
- [99] L. S. Pan, D. R. Kania, S. Han, J. W. Ager III, M. Landstrass, O. L. Landen and P. Pianetta, "Electrical transport Properties of Undoped CVD Diamond Films", *Science*, 255, 830-833 (1992).
- [100] Y. Muto, T. Sugino, J. Shirafugi and K. Kobashi, "Electrical Conduction in Undoped Diamond Films Prepared by Chemical Vapor deposition", *Appl. Phys. Lett.*, 59(7), 843-845 (1991).
- [101] G. H. Glover, "The C-V Characteristics of Schottkey Barrier on Laboratory Grown Semiconducting Diamonds", *Solid State Electron.*, 16, 973-983 (1973).
- [102] B. Huang and D. K. Reinhard, "Electric Field-dependent Conductivity of Polycrystalline Diamond Thin Films" *Appl. Phys. Lett.*, 59 (12), Sep. 1991.
- [103] M. I. Landstrass and K. V. Ravi, "Hydrogen Passivation of Electrically Active Defects in Diamond", *Appl. Phys. Lett.*, 55 (14), May 1990.
- [104] G. A. Sokolina, A. A. Botev, S. V. Bantsekov, O. I. Lazareva and A. F. Belyamin, "temperature and Frequency Dependence of the Electrical Conductivity of Diamond Films", *Sov. Phys. Semicond.*, 24(1), 105-108 (1990).
- [105] G. S. Gildenblat, A. Grot and A. Badzian, "The Electrical Properties and Device Applications of Homoepitaxial and Polycrystalline Diamond Films", *IEEE Proc.*,
- [106] A. S. Vishnevskil, A. G. Gontar, V. I. Torishnil, and A. A. Shul'zhenko, "Electrical Conductivity of Heavily Doped P-Type Diamonds",

- [107] A. W. S. Williams, E. C. Lightowers, A. T. Collins, "Impurity Conduction in Synthetic Semiconducting Diamond," *J. Phys, C: Solid St. Phys.*, vol. 3, 1727-1735 (1970).
- [108] S. Amelinckx, *The Direct Observation of Dislocations*, Academic Press, New York, (1964).
- [109] J. L. Shay *et. al.*, *Appl. Phys. Lett.*, 28, 31 (1976).
- [110] S. Wagner, "Epitaxy in Solar Cells", *J. Crystal Growth*, 31, 113 (1975).
- [111] P. Choudhari, *J. Vac. Sci. Technol.*, 9, 520 (1972).
- [112] N. F. Mott and E. A. Davis, "Electronic Processes in non-crystalline materials", *John Wiley & Sons*, (1971).
- [113] L. L. Kazmerski, "Polycrystalline and Amorphous Thin Films and Devices",
- [114] R. F. Greene, *Phys. Rev.*, 141, 687 (1966).
- [115] A. Amith, *J. Phys. Chem. Solids*, 14, 271 (1960).
- [116] H. H. Weilder, *Thin Solid Films*, 31, 123 (1976).
- [117] M. E. Crowder and T. O. Sedgewick, *J. Electrochem. Soc.*, 119, 1565 (1972).
- [118] A. L. Flipp, "Dependence of Resistivity on the Doping Level of Polycrystalline Silicon", *J. Appl. Phys.*, 46, 1240 (1975).
- [119] T. I. Kamins, "Hall Mobility in Chemically Deposited Polycrystalline Silicon" *J. Appl. Phys.*, 42(11), 4357-4365 (1971).
- [120] J. Y. W. Seto, *J. Electrochem. Soc.*, 122, 701 (1975).
- [121] J. Y. W. Seto, "The Electrical Properties of Polycrystalline Silicon", *J. Appl. Phys.*, 46(12), 5247-5254 (1975).
- [122] G. Baccarani *et. al.*, *J. Appl. Phys.*, 49, 5565 (1978).
- [123] C. H. Seager and T. G. Castner, "Zero Bias Resistance of Graon Boundaries in Neutron Transmutation Doped Polycrystalline Silicon", *J. Appl. Phys.*, 49(7), 3879-3889 (1978).
- [124] L. M. Edwards and J. L. Davidson, "Fabrication Technology Development of Polycrystalline Diamond Resistors", *Abstract accepted to Intl. Symposium on Microelectronics*, 19-21 Oct. 1992.
- [125] J. Mort, D. Kuhman, M. Machonikin, M. Morgan, F. Jansen, K. Okumura, Y. M. LeGrice and R. J. Nemanich, "Boron Doping of Diamond Thin Films",

Appl. Phys. Lett., 55(11), 1121-1123, Sep 1989.

- [126] K. Okano, Y. Akiba, T. Kurosu, M. Iida and T. Nakamura, "Synthesis of B Doped Diamond Films", *J. Crystal Growth*, 99, 1192-1195 (1990).
- [127] V. S. Vavilov, M. A. Gukasyan, M. I. Guseva and E. A. Konorova, "Conductivity of Diamond Doped by Implantation of Phosphorous Ions", *Sov. Phys. Semicond.*, 9(8), 962-964 (1976).
- [128] R. H. Wentrof and K. A. Darrow, *Phy. Rev.*, 137, 1614 (1965).
- [129] V. V. Vavilov, G. E. A. Konorova, V. F. Sergienko and M. I. Guseva, *Sov. Phys. Semicond.*, 4(1), 12-16 (1970).
- [130] P. A. Sullivan, J. W. Boring, and R. A. Baragiola, "Iono-luminescence of Diamond and Ion Implanted Light Emitting Diodes", *Proc. 1991 Intl. Semicond. Device Res. Symp., Charlottesville, Dec. 1991*.
- [131] "Varian: Diamond Circuits are Feasible", *Diamond Deposition: Science and Technology*, 2(5), 6, Aug. 1991.
- [132] K. Okano, H. Kiyota, T. Iwasaki, Y. Nakamura, Y. Akiba, T. Kurosu, M. Iida and T. Nakamura, "Synthesis of N-Type Semiconducting Diamond Films Using Diphosphorous Pentoxide as the Doping Source", *J. Appl. Phys.*, A 51, 344-346 (1990).
- [133] K. Hirabayashi and Y. Taniguchi, "Selective Deposition of Diamond Crystals by Chemical Vapor Deposition using a Tungsten-filament Method", *Appl. Phys. Lett.*, 53, 19 (1988).
- [134] J. S. Ma, H. Kawarada, T. Yonehara, J. Suzuki, J. Wei, Y. Yokota, and A. Hiraki, "Selective Nucleation and Growth of Diamond Particles by Plasma-assisted Chemical Vapor Deposition", *Appl. Phys. Lett.*, 55, 1071 (1989).
- [135] Moeljanto W. Leksono, and H. R. Shanks, "Patterning of Microwave Plasma Deposited Diamond Films", to be published in *Microwave Processing of Materials II* (MRS 1990).
- [136] A. R. Kirkpatrick, B. W. Ward, and N. P. Economou, "Focused Ion-beam Crater Array for Induced Nucleation of Diamond Films", *J. Vac. Sci. Technol.*, 7, 60 (1989).
- [137] N. N. Efremow, M. W. Geis, D. C. Flanders, G. A. Lincoln, and N. P. Economou, "Ion beam assisted etching of diamond", *J. Vac. Sci. Technol. B*, 3 (1), 416-418 (1985).
- [138] J. L. Davison, C. Ellis and Ramesham, "Selective Deposition of Diamond Films", *J. Electron. Mater.*, 18, 711-715 (1985).

- [139] S. S. Grot, C. W. Hatfield, G. S. Gildenblat, A. R. Badzian, and T. Badzian, "Selective deposition of Homoepitaxial diamond Films",
- [140] J. L. Valdes, J. W. Mitchel, J. A. Mucha, L. Seibles and H. Huggins, "Selected-Area Nucleation and Patterning of Diamond Thin Films by Electro-phoretic Seeding",
- [141] L. M. Edwards and J. L. Davidson, "Delineation Methods of Polycrystalline Diamond Films", *Abstract accepted to 6th Intl. Electronic Materials and Processing Conf, Baltimore MD, 23-24 June 1992.*
- [142] J. F. Prins, "Bipolar Transistor Action in Ion-Implantation Diamond", *Appl. Phys. Lett.*, 41(10), 950-952 (1982).
- [143] K. L. Moazed, R. Ngyen and J. R. Zeidler, "Ohmic Contacts to Semiconducting Diamonds", *IEEE Trans. Electron Devices*, 9, 350-351 (1988).
- [144] M. W. Geis, "Diamond Transistor Performance and Fabrication", *IEEE Proceedings*, 79(5), 669-675 (1991).
- [145] J. Engermann, H. Keller, D. K. Reinhard, B. Huang, and J. Assmussen, "Dual-side Contact Formation on Isolated Diamond Films",
- [146] F. Fang, C. A. Hewett, M. G. Fernandes and S. S. Lau, "Ohmic Contacts Formed by Ion Mixing in Si-Diamond System", *IEEE Trans. Electron Devices*, 36, 1783-1786 (1989).
- [147] A. T. Collins, E. C. Lightowers, and A. W. S. Williams, "Electrical Contacts to Semiconducting Diamonds," *Diamond Res.*, pp. 19-22, (Suppl. Ind. Diamond Rev.) (1970).
- [148] M. C. Hicks, C. R. Wronski, S. A. Grot and G. S. Gildenblat, "The Barrier Height of Schottky Diodes with a Chemical Vapor Deposited Diamond Base", *J. Appl. Phys.*, 65(5), 2139-2141 (1989).
- [149] S. A. Grot, G. S. Gildenblat, C. W. Hatfield, C. R. Wronski, A. R. Badzian, T. Badzian and R. Messier, "The Effect of Surface Treatment on the Electrical Properties of Metal Contacts to the Boron Doped Homo-epitaxial Diamond Films", *IEEE Electro. Dev. Lett.*, EDL-11, 100-102 (1990).
- [150] L. R. Zhang, L. S. Hung, S. Q. Feng, P. Revesz and J. W. Mayer, "Interaction of TiSi₂ layer with Polycrystalline Si", *Appl. Phys. Lett.*, 48(12), 767-769 (1986).
- [151] S. P. Murarka, "Refractory Silicides for Integrated Circuits", *J. Vac. Sci. Technol.*, 17(4), (1980)
- [152] J. F. Prins, "Bipolar Transistor Action in Ion-Implantation Diamond", *Appl. Phys. Lett.*, 41(10), 950-952 (1982).

- [153] H. Shiomi, Y. N. Yashi, and N. Fujimori, "Field Effect Transistors Using Boron Doped Diamond Epitaxial Films", *Jpn. J. Appl. Phys.*, 28, L2153-2154, 1989.
- [154] M. W. Geis, D. D. Rathman, D. J. Ehrlich, R. A. Murphy and W. T. Lindley, "High Temperature Point Contact Transistors and Schottky Diodes Formed on Synthetic Boron Doped Diamonds", *IEEE Trans. Electron Device Lett.*, ELD-8(8), 341-343 (1987).
- [155] G. S. Gildenblat "High Temperature Schottky Diodes with Thin Film Diamond Base", *IEEE Electron. Dev. Lett.*, EDL-11, 371-372, Sep. 1990.
- [156] B. I. Shklovskii and A. L. Efros, "Electronic Properties of Doped Semiconductors", *Springer-Verlag*, (1984).
- [157] L. L. Kazmerski, P. J. Ireland and T. F. Ciszek, "Summary Abstract: Electrical and Compositional Properties of Grain Boundaries in Multigrain Silicon Using Surface Analysis Techniques", *J. Vac. Sci. Technol.*, 17(1), (1980).
- [158] S. A. Grot, G. S. Gildenblat, C. W. Hatfield, C. R. Wronski, A. R. Badzian, T. Badzian and R. Messier, "The Effect of Surface Treatment on the Electrical Properties of Metal Contacts to Boron-Doped Homoepitaxial Diamond Films", *IEEE Electron Dev. Lett.*, EDL-11(2), 100-102 (1990).
- [159] S. Albin and L. Watkins, "Electrical Properties of Hydrogenated Diamond", *Appl. Phys. Lett.*, 56(15), 1454-1456 (1990).
- [160] J. W. Mayer and S. S. Lau, "Electronic Materials Science: For Integrated Circuits in Si and GaAs", *Macmillan Publishing Company, New York*, 1990.
- [161] S. P. Mrarka and M. C. Peckerar, "Electronic Materials: Science and Technology", *Academic Press Inc.* 1989.
- [162] B. Huang, "Electrical Properties and Physical Characterization of Polycrystalline Diamond Films Deposited in Microwave Plasma Disk Reactor", *PhD Dissertation, Michigan State University*, 1992.
- [163] M. Hansen, "Constitution of Binary Alloys, First Supplement", *McGraw-Hill, New York*, 1965.
- [164] L. S. Pan, D. K. Kania, S. Han, J. W. Ager III, M. Landstrass, O. L. Landen and P. Piaetta, "Electrical Transport Properties of Undoped CVD Diamond Films", *Science*, 255, 830-833 (1992).
- [165] "H-50 Hall and Van der Pauw Controller", *MMR Technologies Inc.*, 4 (1986).
- [166] A. T. Collins, *Mater. Res. Soc. Symp. Proc.*, 162, 3 (1989).
- [167] L. J. Van der PAuw, "A method of Measuring Specific Resistivity and Hall Effect of Discs of Arbitrary Shapes", *Philips Res. Repts.*, 13, 1-9 (1958).

- [168] M. Aslam, I. Taher, A. Masood, "Piezoresistivity in Vapor-deposited Diamond Films", *Appl. Phys. Lett.*, 60(23), 2923-2925 (1992).
- [169] R. J. Vidal, "Model Instrumentation Techniques for Heat transfer and Force Measurements in a Hypersonic Schock Tunnels", *Cornell Aeronautical Laboratory Buffalo NY rept.*, AD-917-A-1, (1956).

MICHIGAN STATE UNIV. LIBRARIES



31293007937653